

Collaborative Locomotion of Quadrupedal Robots: From Centralized Predictive Control to Distributed Control

Jeeseop Kim

Dissertation submitted to the Faculty of the
Virginia Polytechnic Institute and State University
in partial fulfillment of the requirements for the degree of

Doctor of Philosophy
in
Mechanical Engineering

Kaveh Akbari Hamed, Chair
Corina Sandu
Alexander Leonessa
Alan Asbeck
Craig Woolsey

August 5, 2022
Blacksburg, Virginia

Keywords: Cooperative Locomotion, Legged Locomotion, Nonlinear Control, Model
Predictive Control, Distributed Control

Copyright 2022, Jeeseop Kim

Collaborative Locomotion of Quadrupedal Robots: From Centralized Predictive Control to Distributed Control

Jeeseop Kim

(ABSTRACT)

This dissertation aims to realize the goal of deploying legged robots that cooperatively walk to transport objects in complex environments. More than half of the Earth’s continent is unreachable to wheeled vehicles—this motivates the deployment of collaborative legged robots to enable the accessibility of these environments and thus bring robots into the real world. Although significant theoretical and technological advances have allowed the development of distributed controllers for complex robot systems, existing approaches are tailored to the modeling and control of multi-agent systems composed of collaborative robotic arms, multi-fingered robot hands, aerial vehicles, and ground vehicles, but not collaborative legged agents. Legged robots are inherently unstable, unlike most of the systems where these algorithms have been deployed. Models of cooperative legged robots are further described by high-dimensional, underactuated, and complex hybrid dynamical systems, which complicate the design of control algorithms for coordination and motion control. There is a fundamental gap in knowledge of control algorithms for safe motion control of these inherently unstable hybrid dynamical systems, especially in the context of collaborative work. The overarching goal of this dissertation is to create a formal foundation based on scalable optimization and robust and nonlinear control to develop distributed and hierarchical feedback control algorithms for cooperative legged robots to transport objects in complex environments.

We first develop a hierarchical nonlinear control algorithm, based on model predictive control (MPC), quadratic programming (QP), and virtual constraints, to generate and stabilize locomotion patterns in a real-time manner for dynamical models of single-agent quadrupedal robots. The higher level of the proposed control scheme is developed based on an event-based MPC that computes the optimal center of mass (COM) trajectories for a reduced-order linear inverted pendulum (LIP) model subject to the feasibility of the net ground reaction force (GRF). QP-based virtual constraint controllers are developed at the lower level of the proposed control scheme to impose the full-order dynamics to track the optimal trajectories while having all individual GRFs in the friction cone. The analytical results are numerically verified to demonstrate stable and robust locomotion of a 22 degree of freedom (DOF) quadrupedal robot, in the presence of payloads, external disturbances, and ground height variations.

We then present a hierarchical nonlinear control algorithm for the real-time planning and control of cooperative locomotion of legged robots that collaboratively carry objects. An innovative network of reduced-order models subject to holonomic constraints, referred to as

interconnected LIP dynamics, is presented to study quasi-statically stable cooperative locomotion. The higher level of the proposed algorithm employs a supervisory controller, based on event-based MPC, to effectively compute the optimal reduced-order trajectories for the interconnected LIP dynamics. The lower level of the proposed algorithm employs distributed nonlinear controllers to reduce the gap between reduced- and full-order complex models of cooperative locomotion. We numerically investigate the effectiveness of the proposed control algorithm via full-order simulations of a team of collaborative quadrupedal robots, each with a total of 22 DOFs. The dissertation also investigates the robustness of the proposed control algorithm against uncertainties in the payload mass and changes in the ground height profile.

Finally, we present a layered control approach for real-time trajectory planning and control of dynamically stable cooperative locomotion by two holonomically constrained quadrupedal robots. An innovative and interconnected network of reduced-order models, based on the single rigid body (SRB) dynamics, is developed for trajectory planning purposes. At the higher level of the control scheme, two different MPC algorithms are proposed to address the optimal control problem of the interconnected SRB dynamics: centralized and distributed MPCs. The MPCs compute the reduced-order states, GRFs, and interaction wrenches between the agents. The distributed MPC assumes two local QPs that share their optimal solutions according to a one-step communication delay and an agreement protocol. At the lower level of the control scheme, distributed nonlinear controllers are employed to impose the full-order dynamics to track the prescribed and optimal reduced-order trajectories and GRFs. The effectiveness of the proposed layered control approach is verified with extensive numerical simulations and experiments for the blind, robust, and cooperative locomotion of two holonomically constrained A1 robots with different payloads on different terrains and in the presence of external disturbances. It is shown that the distributed MPC has a performance similar to that of the centralized MPC, while the computation time is reduced significantly.

Collaborative Locomotion of Quadrupedal Robots: From Centralized Predictive Control to Distributed Control

Jeeseop Kim

(GENERAL AUDIENCE ABSTRACT)

Future cities will include a complex and interconnected network of collaborative robots that cooperatively work with each other and people to support human societies. Human-centered communities, including factories, offices, and homes, are developed for humans who are bipedal walkers capable of stepping over gaps, walking up/down stairs, and climbing ladders. One of the most challenging problems in deploying the next generation of collaborative robots is maneuvering in those complex environments. Although significant theoretical and technological advances have allowed the development of distributed controllers for motion control of multi-agent robotic systems, existing approaches do not address the collaborative locomotion problem of legged robots. Legged robots are inherently unstable with nonlinear and hybrid natures, unlike most systems where these algorithms have been deployed. Furthermore, the evolution of legged collaborative robot teams that cooperatively manipulate objects can be represented by high-dimensional and complex dynamical systems, complicating the design of control algorithms for coordination and motion control.

This dissertation aims to establish a formal foundation based on nonlinear control and optimization theory to develop hierarchical feedback control algorithms for effective motion control of legged robots. The proposed layered control algorithms are developed based on interconnected reduced-order models. At the high level, we formulate cooperative locomotion as an optimal control problem of the reduced-order models to generate optimal trajectories. To realize the generated optimal trajectories, nonlinear controllers at the low level of the hierarchy impose the full-order models to track the trajectories while sustaining stability. The effectiveness of the proposed layered control approach is verified with extensive numerical simulations and experiments for the blind and stable cooperative locomotion of legged robots with different payloads on different terrains and subject to external disturbances. The proposed architecture's robustness is shown under various indoor and outdoor conditions, including landscapes with randomly placed wood blocks, slippery surfaces, gravel, grass, and mulch.

Dedication

To my parents and my wife.

Acknowledgments

At the end of this journey, I would like to express my gratitude to everyone who helped and encouraged me to reach here. First of all, my deepest gratitude and respect go first to my advisor, Dr. Kaveh Akbari Hamed. I am extremely grateful for the invaluable knowledge you have passed down to me and all your support. This most rewarding journey that you've made was full of pleasure. Your professional guidance and support have taught me how to live an authentic life with a passionate attitude, which will always serve as a beacon in my life.

I would also like to thank my Ph.D. committee for their times and valuable comments. Dr. Corina Sandu, Dr. Alexander Leonessa, Dr. Alan Asbeck, and Dr. Craig Woolsey gave me valuable advice so that this dissertation could achieve decent level of completion.

My appreciation also extends to all my colleagues in the Hybrid Dynamics Systems and Robot Locomotion (HDSRL) Lab. It has been a great pleasure for me to work with gifted and warmhearted people, Dr. Vinay R. Kamidi, Mr. Abhishek Pandala, and Mr. Randy Fawcett. I would also express my sincere gratitude to Mr. Basit Muhammad Imran, Ms. Leila Amanzadeh, and Mr. Taizoon Chunawala for the many hours of conversation and inspiration that made this journey possible.

This long journey could not have been completed without unconditional support, encouragement, and love from my parents, Dr. Youngkag Kim, Mrs. Kyunghwa Shin. I would like to express my deep gratitude to my parents for their lifelong commitment and faith in my abilities and plans. Lastly, I truly appreciate all my family and family in-laws whose names may not be enumerated here. I can accomplish this journey because of your support and encouragement.

Last but not least, I sincerely appreciate my beloved wife, Dr. Myongjin Shin, for her limitless love and support. I could stay on track because of her thoughtful consideration and warm encouragement. I will never forget her dedication in this journey and always remember our beautiful memories in Blacksburg, where our marriage started.

Contents

List of Figures	xi
List of Tables	xx
1 Introduction	1
1.1 Motivation, Related Work, and Challenges	2
1.2 Scope, Goals, and Specific Objectives	4
1.2.1 Event-based MPC and QP-based low-level nonlinear controllers for single-agent legged robots	5
1.2.2 Hierarchical control algorithms with supervisory MPC for multi-agent legged robots	6
1.2.3 Layered control algorithm with centralized and distributed MPC based on interconnected SRB model for multi-agent legged robots	7
1.2.4 Structure of the Dissertation	8
1.3 Significance and Importance	8
1.4 Literature Review: Modeling, Planning, and Control of Legged Robots	8
1.4.1 Full-Order Lagrangian Models	9
1.4.2 Full-Order Hybrid Dynamical Models	10
1.4.3 Reduced-Order Models	10
1.4.4 Trajectory Optimization	12
1.4.5 Existing Control Techniques for Legged Robots	13
1.5 Relevant Publications	14
1.6 Outline	15

I	Event-Based MPC and Nonlinear Controllers for Locomotion of Single-Agent Legged Robots	17
2	Legged Locomotion via Event-Based MPC and Virtual Constraints	18
2.1	Introduction	18
2.2	Hybrid Models of Locomotion	18
2.3	QP-Based Virtual Constraint Controllers	21
2.3.1	Virtual Constraints	22
2.3.2	QP-Based I-O Linearization	22
2.4	Event-Based Predictive Control	24
2.4.1	Reduced-Order LIP Model	24
2.4.2	Steering Problem	25
2.4.3	Event-Based MPC	26
2.5	Numerical Simulations	27
2.6	Summary	32
II	Cooperative Locomotion via Supervisory MPC and Distributed Nonlinear Controllers	33
3	Collaborative Locomotion with Supervisory MPC	34
3.1	Introduction	34
3.2	Interconnected LIP Dynamics	35
3.3	Supervisory Predictive Control	39
3.4	Distributed Virtual Constraint Controllers	42
3.5	Numerical Simulations	46
3.6	Discussion	51
3.6.1	Robustness against Uncertainties	52
3.6.2	Limitations and Analysis of Results	55
3.7	Summary	57

III Cooperative Locomotion via Centralized and Distributed MPCs	58
4 Centralized and Distributed MPCs of Cooperative Locomotion	59
4.1 Introduction	59
4.1.1 Motivation and Goal	59
4.1.2 Related Work	61
4.1.3 Objectives and Contributions	64
4.1.4 Outline	65
4.2 Reduced-Order Model of Cooperative Legged Locomotion	65
4.3 MPC-Based Trajectory Planning	69
4.3.1 Centralized MPC	69
4.3.2 Distributed MPC	71
4.4 Distributed Nonlinear Controllers for Full-Order Models	73
4.5 Numerical and Experimental Validations	75
4.5.1 Closed-Loop System	75
4.5.2 Numerical Validation	79
4.5.3 Experimental Validation and Robustness Analysis	82
4.6 Discussion and Comparison	87
4.6.1 Comparison of the Centralized and Distributed MPCs	88
4.6.2 Evolution of the Lagrange Multiplier in Distributed MPC	91
4.6.3 Synchronization and Asynchronization	91
4.6.4 Robustness Against Unknown Holonomic Constraints	92
4.6.5 Limitations and Future Study	93
4.7 Summary	95
5 Conclusions and Future Works	96
5.1 Summary of the Contributions	96
5.1.1 Event-based MPC and QP-based low-level nonlinear controllers for single-agent legged robots	96

5.1.2	Hierarchical control algorithms with supervisory MPC for multi-agent legged robots	96
5.1.3	Layered control architecture with centralized and distributed approaches for cooperative locomotion of legged robots	97
5.2	Directions of Future Work	97
5.3	Conclusion	99
	Bibliography	100

List of Figures

1.1	(a) Vision 60 robot. (b) Illustration of the system under investigation in this thesis. Commercially available Kinova arms are affixed on existing Vision 60s to form the legged co-robot team. (c) and (d) Examples of legged co-robot teams that cooperatively work with each other and people for construction, manufacturing, and assembly.	1
1.2	Examples of state-of-the-art quadrupedal robots: (a) Vision60 (Ghost Robotics) [167] augmented with Kinova arm, (b) collaborative Vision60s (c) Spot (Boston Dynamics) with a robotic arm [64], (d) ANYmal (ANYbotics) [22] with a Kinova arm, (e) ANYmal-C (ANYbotics) [22], (f) MIT mini cheetah [40], and (g) A1 (Unitree Robotics) [194].	2
1.3	Event-based MPC and QP-based low-level controller for single-agent legged robots.	5
1.4	Hierarchical control algorithm with supervisory MPC for collaborative locomotion of legged-robot teams.	6
1.5	Layered control algorithm with centralized and distributed MPC for cooperative locomotion.	7
1.6	Full-order modeling accounts for all links and DOFs in the model.	9
1.7	SRB model.	11
1.8	LIP model.	11
1.9	Centroidal dynamics.	12
2.1	Illustration of a locomotion pattern with the corresponding graph $\mathcal{G} = (\mathcal{V}, \mathcal{E})$. Each continuous-time domain shows the support polygon as convex hull.	19
2.2	Illustration of 22 DOFs for the full-order model of the composite robot. The robot is composed of the 18-DOF Vision 60 plus the 4-DOF Kinova arm. Six unactuated DOFs are associated with the absolute position and orientation of the torso frame with respect to an inertial world frame. Each leg of the robot then consists of three actuated joints as hip roll, hip pitch, and knee joints. The arm is finally composed of four actuated joints. The axis of actuation for actuated joints are shown with dashed lines, where the axes with circle ends, axes with square ends, and axes with triangle ends represent the x, y, and z directions, respectively.	20

2.3	Illustration of the proposed hierarchical control algorithm based on nonlinear control, QP, and event-based MPC.	21
2.4	Illustration of the reduced-order model of locomotion (i.e., LIP dynamics) over different continuous-time domains. The figure also depicts the time-varying support polygon used for the ZMP condition.	24
2.5	Illustration of a locomotion pattern with the corresponding graph $\mathcal{G} = (\mathcal{V}, \mathcal{E})$ and event-based MPC law.	26
2.6	Plot of the COM and COP trajectories for the forward and diagonal trot gaits of the reduced-order system. Convergence to the target points (0.82, 0) and (0.58, 0.34) is clear.	28
2.7	Plot of the virtual constraints and torque inputs in RaiSim for (a) forward trot, (b) diagonal trot, and (c) forward trot with payloads. Here, $y_x, y_y, y_z, y_{\text{roll}}, y_{\text{pitch}}, y_{\text{yaw}}$ denote the first six components of the virtual constraints that relate to the absolute position and orientation of the body. In addition, FH, FK, RH, and RK stand for the front hip, front knee, rear hip, and rear knee of the left-hand-side of the robot, respectively. The subscripts “roll” and “pitch” for the torque plots also denote the roll and pitch motions of the hip joints. (d) Plot of the virtual constraints and torques for trot gait subject to the LuGre contact model in MATLAB/Simulink when the control frequency is reduced to 500 Hz with a delay of 2 (ms) in solving QPs.	29
2.8	Snapshots of (a) the forward trot gait and (b) the diagonal trot gait with the proposed event-based MPC and QP-based virtual constraint controller.	29
2.9	Snapshots of the forward trot gait with an unknown payload of 12 (kg) on the robot’s torso and an unknown payload of 1.4 (kg) at the robot’s EE.	30
2.10	(a) Snapshots of the unstable locomotion with an MPC that is only solved once at the beginning of the gait. (b) Snapshots of the robustly stable locomotion with the proposed event-based MPC in the presence of unknown disturbances.	30
2.11	Plot of the virtual constraints and torque inputs of the full-order closed-loop system in RaiSim for forward trot with (a) and (b) external disturbances, (c) external push, and (d) ground height variations.	31
2.12	(a) Snapshots of the unstable locomotion with an MPC that is only solved once at the beginning of the gait. (b) Snapshots of the robustly stable locomotion with the proposed event-based MPC in the presence of ground height variations.	31

3.1	Overview of the proposed hierarchical nonlinear control algorithm for collaborative locomotion of legged robots subject to holonomic constraints. The figure also illustrates the concept of the interconnected LIP dynamics.	35
3.2	(a) Illustration of the proposed supervisory predictive control. Here, agents share their actual and reduced-order states with the higher-level supervisory control. The supervisory control then optimizes for the COM motions subject to the interconnected LIP dynamics and feasibility conditions. (b) Illustration of the directed cycle to represent the locomotion pattern of each agent with different continuous-time domains. Snapshot of the cooperative locomotion highlights different domains for each agent.	39
3.3	Illustration of 22 DOFs for the full-order model of each robotic agent. The agents are composed of the 18-DOF quadrupedal robot Vision 60 plus the 4-DOF Kinova arm.	42
3.4	COM and COP trajectories of the individual agents in the interconnected LIP dynamics (3.9) during forward trot gaits with $N = 2$ agents ((a) and (b)) and $N = 3$ agents ((c)-(e)). Here, the optimal control inputs (i.e., COPs) are computed via the supervisory predictive control (3.15). The sampling time for the supervisory predictive control in (a)-(e) are assumed to be $T_s = 80$ (ms).	47
3.5	Evolution of the virtual constraints and torque inputs in RaiSim for stable forward trot gait with $N = 2$ agents. Subplots (a) and (c) illustrate the evolution of outputs whereas subplots (b) and (d) depict the evolution of torque inputs. Here, y_x, y_y, y_z denote the virtual constraints corresponding to the absolute position (i.e., $x, y,$ and z) of the agent. In addition, the subscript “rFHip”, “pFHip”, and “FKnee” in the torque plots represent the roll torque of the front hip, pitch torque of the front hip, and pitch torque of the front knee for the left side of the robot, respectively.	48
3.6	Plot of the virtual constraints and torque inputs in RaiSim for stable forward trot gait with $N = 3$ agents. Subplots (a), (b), and (c) correspond to the agents 1, 2, and 3, respectively. Subplots in the first and second rows correspond to the virtual constraints and torque inputs of each agent, respectively.	49
3.7	Evolution of the 2-norm of the defect variable δ in RaiSim for $N = 2$ agents. Subplots illustrate the evolution for each agent.	49
3.8	Evolution of the virtual constraints and torque inputs in RaiSim for robust trot gait subject to a payload with $N = 2$ agents. Subplots (a) and (c) illustrate the evolution of outputs whereas subplots (b) and (d) depict the evolution of torque inputs.	50

3.9	Plot of the virtual constraints and torque inputs in RaiSim for robust forward trot gait subject to a payload with $N = 3$ agents. Subplots (a), (b), and (c) correspond to the agents 1, 2, and 3, respectively. Subplots in the first and second rows correspond to the virtual constraints and torque inputs of each agent, respectively.	50
3.10	Plot of the virtual constraints and torque inputs in RaiSim for robust trot gait subject to a payload with $N = 4$ agents. Subplots (a), (b), (c), and (d) correspond to the agent 1, 2, 3, and 4, respectively. Subplots in the first and second rows correspond to the virtual constraints and torque inputs of each agent, respectively.	51
3.11	(a) Snapshots of the unstable cooperative locomotion of 2 agents with the individual predictive control of Chapter 2 for agents in RaiSim. Here, each agent makes use of MPC for its own LIP dynamics without considering the interaction forces. (b) Snapshots of the robustly stable cooperative locomotion of 2 agents with the proposed supervisory predictive control of this chapter in the presence of a 20 (kg) payload.	52
3.12	(a) Snapshots of the unstable cooperative locomotion of 3 agents in RaiSim, in which each agent makes use of its own MPC without considering the interaction forces between agents in the interconnected LIP dynamics. (b) Snapshots of the robustly stable cooperative locomotion of 3 agents with the proposed supervisory predictive control in the presence of a 32 (kg) payload.	52
3.13	(a) Snapshots of the unstable cooperative locomotion of 4 agents in RaiSim, in which each agent makes use of its own MPC without considering the interaction forces in the interconnected LIP dynamics. (b) Snapshots of the robustly stable cooperative locomotion of 4 agents with the proposed supervisory predictive control in the presence of a 48 (kg) payload.	53
3.14	Evolution of virtual constraints and control inputs for locomotion of $N = 2$ agents over an unknown terrain. Plots show the inputs and outputs for individual agents.	53
3.15	Evolution of virtual constraints and control inputs for locomotion of $N = 3$ agents over an unknown terrain.	54
3.16	(a) Snapshots of the unstable cooperative locomotion of 2 agents over an unknown terrain, where each agent makes use of its own MPC algorithm without considering the interaction forces. (b) Snapshots of the robustly stable cooperative locomotion of 2 agents over the same terrain with the proposed supervisory predictive control based on the interconnected LIP dynamics.	54

3.17	(a) Snapshots of the unstable cooperative locomotion of 3 agents, where each agent makes use of its own MPC algorithm without considering the interaction forces. (b) Snapshots of the robustly stable cooperative locomotion of 3 agents over an unknown terrain with the proposed supervisory predictive control.	55
4.1	Snapshot illustrating holonomically constrained quadrupedal robots locomoting on gravel while carrying a payload of 4.53 (kg).	60
4.2	Overview of the proposed layered control approach with the centralized MPC algorithm at the high level and distributed nonlinear controllers at the low level for cooperative locomotion.	60
4.3	Overview of the proposed layered control approach with the distributed MPC algorithms at the high level and distributed nonlinear controllers at the low level for cooperative locomotion.	62
4.4	Illustration of the interconnected SRB models for the cooperative locomotion of two quadrupedal robots.	66
4.5	Illustration of the mechanisms designed to be mounted on the torso of each robot to holonimally constrain the motion of agents. The mechanism in (a) can implement the holonomic constraint (4.2) with free ball joints. The mechanisms in (b), (c), and (d) implement the constraint (4.2) while also restricting the roll, yaw, and pitch motions, respectively. The mechanism implemented on top of the robots is illustrated in (e).	76
4.6	Numerical and experimental validation system setup. Here, the joystick commands the desired velocity trajectories to the trajectory planner of each agent. Both agents are controlled by one joystick. Joystick sends out the desired trajectories on both numerical simulations and experimental validations. The network switch is used to build the connection between the computer and two agents without IP address collision. UDP communication protocol through Ethernet cables is used in experimental validations.	77
4.7	Snapshots demonstrating the performance of the proposed control approach in numerical simulations. The left plot shows the snapshot of the numerical simulation with the interconnected reduced-order model (torso dynamics) and subject to a 5 (kg) payload (40% uncertainty in one robot's mass) between the agents. The right plot shows the snapshot of the numerical simulation with the full-order model and subject to a 5 (kg) payload between agents and unknown time-varying external disturbances applied to the robots. Arrows at the leg ends describe the GRFs, and the ones on the torso represent the external disturbance forces. The payload is illustrated with a box.	78

4.8	Plots of the desired and actual velocities of the closed-loop interconnected reduced-order model for two agents in the numerical simulation. Here, two nominal MPCs are applied to the reduced-order models of agents to generate optimal GRFs <i>without</i> considering the holonomic constraints between them. The joystick provides desired trajectories. The instability of the cooperative gait is evident.	79
4.9	Plots of the desired and actual velocities of the closed-loop interconnected reduced-order model for two agents in the numerical simulation. Here, the optimal GRFs are generated by the centralized MPC (4.16) and are applied to the reduced-order models subject to an unknown payload of 5 (kg) between agents. A joystick provides desired trajectories. The robust tracking is evident.	80
4.10	Plots of the desired and actual velocities of the closed-loop interconnected reduced-order model for two agents in the numerical simulation. Here, the optimal GRFs are generated by the distributed MPCs (4.22) and are applied to the reduced-order models subject to an unknown payload of 5 (kg) between agents. A joystick provides desired trajectories. The robust tracking is evident.	80
4.11	Comparison between the desired velocities and optimal velocities, generated with the high-level centralized and distributed MPCs, for the closed-loop interconnected full-order model in RaiSim. The joystick provides time-varying reference trajectories. The figure depicts the optimal trajectories generated by (a) the centralized MPC (4.16) and (b) the distributed MPC (4.22) for agent 1. Here, we consider a trot gait over rough terrain with an unknown payload of 5 (kg) between the agents and subject to unknown, time-varying, and external disturbance forces applied to the robots.	81
4.12	Snapshots demonstrating the performance of the proposed layered control algorithm for a series of cooperative locomotion experiments. Indoor experiments: (a) rough terrain with the agents traversing arbitrarily displaced wooden blocks, (b) asymmetrical terrain with one agent being on a compliant surface and elevated by 10 (cm), (c) slippery surface covered by a cooking spray, and (d) tethered pulling. The robots are loaded with a payload of 4.53 (kg) (36% uncertainty in one robot's mass) in (a), (c), and (d). The friction coefficient is taken as $\mu = 0.3$ in (c) and $\mu = 0.6$ in (a), (b), and (d). Here, (a) and (b) show the snapshots where the centralized MPC is applied, while (c) and (d) show the snapshots where the distributed MPC is employed. Videos of all experiments are available online [https://youtu.be/mzAFemO0XeI]. . .	82
4.13	Comparison between the desired and optimal velocities of the robots for the nominal trot experiment on flat ground. Optimal velocities are provided from the high-level centralized MPC. Time-varying desired trajectories are provided by the joystick to coordinate the robots' motions. It is observed that the centralized MPC's outputs can successfully track the desired trajectories.	83

4.14	Plots of the optimal GRFs generated from the centralized MPC for agents 1 and 2 during the nominal trot experiment on flat ground. The figure depicts the z components of the optimal GRFs for the left front leg of each agent. We remark that the GRFs in the z -direction are close to 60 (N) since the trot gait is adopted and the total mass of the robot is 12.45 (kg).	84
4.15	Plots of the desired and optimal velocities for cooperative locomotion experiments on (a) rough terrain, (b) a slippery surface, and (c) subject to external disturbances with the centralized MPC. Time-varying desired trajectories are provided by the joystick. It is clear that the centralized MPC's outputs can robustly track the desired trajectories in the presence of uncertainties and disturbances.	84
4.16	Plots of the optimal GRFs, generated by the centralized MPC, for cooperative locomotion experiments on (a) rough terrain, (b) a slippery surface, and (c) subject to external disturbances. The figure depicts the optimal GRFs for the left front leg of agent 1 along the z -direction.	85
4.17	Phase portraits for (a) the body roll and (b) the body pitch of agent 1 with the centralized MPC and (c) the body roll and (d) the body pitch of agent 1 with the distributed MPCs during different experiments. The plots show the robustness of the cooperative locomotion over rough terrain covered with randomly dispersed wooden blocks, the slippery surface, and subject to unknown external disturbances.	86
4.18	Plots of the desired and optimal velocities for cooperative locomotion experiments on (a) rough terrain, (b) a slippery surface, and (c) subject to external disturbances with the distributed MPC. Time-varying desired trajectories are provided by the joystick. It is clear that the distributed MPC's outputs can robustly track the desired trajectories in the presence of uncertainties and disturbances.	87
4.19	Plots of the optimal GRFs, generated by the distributed MPC, for cooperative locomotion experiments on (a) rough terrain, (b) a slippery surface, and (c) subject to external disturbances. The figure depicts the optimal GRFs for the left front leg of agent 1 along the z -direction.	87
4.20	Snapshots demonstrate the proposed layered controller's performance for a series of cooperative locomotion experiments. Outdoor experiments: (a) cooperative locomotion on gravel, (b) transitioning from concrete surface to grass, (c) cooperative locomotion on mulch, and (d) cooperative locomotion on grass. The robots cooperatively transport a payload of 4.53 (kg) (36% uncertainty) in (b) and (c) and 6.80 (kg) (55% uncertainty) in (a) and (d). Here, (a) and (c) show the snapshots where the distributed MPC is adopted, while (b) and (d) show the snapshots where the centralized MPC is employed.	88

4.21	Plots of the virtual constraints of agent 1 during cooperative locomotion with unknown payloads and on various outdoor terrains, including (a) locomotion on gravel, (b) transitioning from concrete to grass, (c) locomotion on mulch, and (d) locomotion on grass. The payload is 4.53 (kg) in (b) and (c) and 6.80 (kg) in (a) and (d). Here, (a) and (c) depict the evolution of virtual constraints with the distributed MPC at the high level. In addition, (b) and (d) illustrate the evolution of the virtual constraints with the centralized MPC at the high level. Here, we plot the components of virtual constraints in (4.24) that correspond to the COM position along the x and y axes (m) (i.e., COM position tracking) and the body’s roll and pitch angles (rad) (i.e., angle tracking). It is clear that the full-order system tracks the prescribed optimal and reduced-order trajectories generated by the MPCs.	89
4.22	Illustration of the comparison results between the nominal, centralized, and distributed MPCs. (a) The snapshot shows the RaiSim simulation environment with one of the randomly generated rough terrains. The maximum height of the generated terrains is 12 (cm) (46% uncertainty in robots’ height). (b) The plot describes the success rate of the proposed trajectory planners over 1500 randomly generated rough terrains in numerical simulations. The overall success rate of the nominal, centralized, and distributed MPCs over randomly generated rough terrain is 0%, 54.2%, and 53.8%, respectively. (c) The snapshot shows the RaiSim simulation environment with one of the randomly generated external forces and a randomly generated payload. The arrows illustrate the applied external forces on each agent. The maximum external force is 80 (N) (65% of one robot’s weight) on the x -, y -, and z -directions. The evolution of the forces in each direction is sinusoidal with a maximum random period of 4 (s). External forces are applied from 1 (s) to 60 (s). The maximum payload mass is 5 (kg). (d) The plot describes the success rate of the proposed trajectory planners with 1200 randomly applied external forces and payloads in numerical simulations. The overall success rate of the nominal, centralized, and distributed MPCs subject to unknown external forces and payloads is 0%, 55.6%, and 53.9%, respectively.	90
4.23	Plots of the locally estimated Lagrange multiplier λ by two agents using the distributed MPC algorithm. It is clear that the local values reach an agreement and stay close to each other.	91
4.24	Plots of the estimated height of agents’ front right legs. Initial locomotion has complete synchrony before encountering the rough terrain described in the gray area in the plot. After engaging the rough terrain, it is clear that asynchrony happens between agents. However, the layered control approach robustly stabilizes the cooperative gait.	92

4.25 Phase portraits for (a) the body roll and (b) the body pitch of agent 1 with the centralized MPC and (c) the body roll and (d) the body pitch of agent 1 with the distributed MPC during different experiments. The plots show the robustness of the cooperative locomotion over rough terrain with fixed DOFs in holonomic constraints on the roll, pitch, and yaw directions. 93

List of Tables

List of Abbreviations

COM	Center of Mass
COP	Center of Pressure
DCM	Divergent Component of Motion
DMPC	Distributed Model Predictive Control
DOF	Degrees of Freedom
EE	End Effector
GRF	Ground Reaction Forces
HZD	Hybrid Zero Dynamics
LIP	Linear Inverted Pendulum
LP	Linear Programming
MPC	Model Predictive Control
MRS	Multi Robot System
NLP	Nonlinear Programming
ODE	Ordinary Differential Equation
QP	Quadratic Programming
SLIP	Spring Loaded Inverted Pendulum
SRB	Single Rigid Body
ZMP	Zero Moment Point

Chapter 1

Introduction

Future cities will include a complex and interconnected network of *collaborative robots (co-robots)* that cooperatively work with each other and people to support human societies. Human-centered communities, including factories, offices, and homes, are developed for humans who are bipedal walkers capable of stepping over gaps, walking up/down stairs, and climbing ladders. One of the most challenging problems in deploying the next generation of co-robots is *mobility* in complex environments. More than half of the Earth’s landmass is inaccessible to wheeled vehicles —this motivates the deployment of *legged co-robots* to access these environments and thus bring robots into the real world. Legged robots that are augmented with manipulators can form *co-robot teams* that assist humans in different aspects of their life such as labor-intensive tasks, construction, manufacturing, assembly, and disaster response (see Fig. 1.1). In recent years, there have been important advances in the construction of legged robots (see Fig. 1.2). While Boston Dynamics’ Spot and ETH Zurich’s ANYmal make use of robotic arms to demonstrate an outstanding level of locomotion and manipulation, existing techniques are tailored to the motion planning and control of one legged agent, but *not* collaborative teams of legged robots. Although important theoretical and technological advances have allowed the development of distributed controllers for motion control of complex robot systems, state-of-the-art approaches address the control of multiagent systems composed of collaborative robotic arms, multifingered robot hands, aerial vehicles, and ground vehicles, but *not* cooperative legged agents. Legged robots are *inherently unstable*, unlike most of the systems where these algorithms have been deployed. Furthermore, the evolution of legged co-robot teams that cooperatively manipulate objects can be represented by high-dimensional and *complex hybrid dynamical systems* which com-

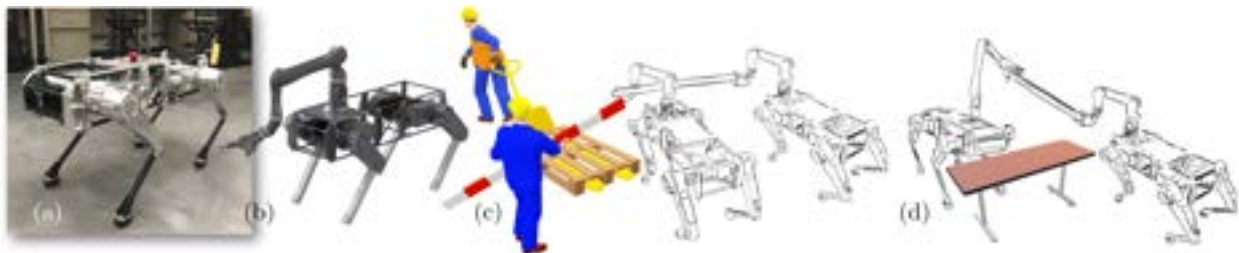


Figure 1.1: (a) Vision 60 robot. (b) Illustration of the system under investigation in this thesis. Commercially available Kinova arms are affixed on existing Vision 60s to form the legged co-robot team. (c) and (d) Examples of legged co-robot teams that cooperatively work with each other and people for construction, manufacturing, and assembly.



Figure 1.2: Examples of state-of-the-art quadrupedal robots: (a) Vision60 (Ghost Robotics) [167] augmented with Kinova arm, (b) collaborative Vision60s (c) Spot (Boston Dynamics) with a robotic arm [64], (d) ANYmal (ANYbotics) [22] with a Kinova arm, (e) ANYmal-C (ANYbotics) [22], (f) MIT mini cheetah [40], and (g) A1 (Unitree Robotics) [194].

PLICATE the design of distributed control algorithms for coordination and motion control. In particular, there is a *fundamental gap in knowledge* of distributed control algorithms for motion control of these inherently unstable, underactuated, and complex hybrid dynamical systems.

1.1 Motivation, Related Work, and Challenges

The necessity of scalable and distributed control algorithms for collaborative locomotion: Existing control approaches for legged robots are tailored to the path planning and stabilization of dynamic gaits for single agent legged machines, but *not* complex hybrid dynamical models that describe the evolution of multiagent legged robotic systems. This is mainly due to the fact that state-of-the-art techniques for dynamic locomotion are centralized approaches that *cannot* be easily transferred to legged co-robot teams. Centralized controllers interpret data from all joints of the robot and then relays decisions back to all actuators. A legged co-robot team that manipulates an object can be modeled as a set of legged robots which are coupled to each other and the object by a set of holonomic constraints. The **significant challenge** is to construct controllers for such a complex robotic system that control locomotion and manipulation with many **Degrees of Freedom (DOFs)** and large amounts of sensory data. Computing the control torques for such a composite system in 1kHz is often impossible—*this underlines the importance of developing scalable*

distributed and decentralized controllers.

In decentralized schemes, the control problem defines lower-dimensional subsystems (e.g., each co-robot) that use only sensory feedback local to each subsystem. Each subsystem has its own controller to make its own decisions based on its own measurements. The absence of communication between controllers in decentralized strategies, however, may limit the achievable performance. This issue can be fixed through designing distributed control schemes in which decentralized controllers can communicate as well. Furthermore, a substantial body of research in biological motor control [60, 143, 181] suggests that the human/animal movement and locomotion control can be achieved through *distributed and hierarchical schemes*. Although important theoretical and technological advances have allowed the development of distributed controllers for motion control of **multi robot system (MRS)** (e.g., [33, 133, 138, 191, 209]), existing approaches are tailored to the control of multiagent systems composed of collaborative robotic arms [142], multifingered robot hands [143], aerial vehicles [69, 136, 139, 148, 173, 174, 184, 192, 193], and ground vehicles [33, 50, 136, 138, 148, 149, 191, 209], but *not* cooperative legged agents.

The necessity of innovative optimal control algorithms for real-time planning of collaborative locomotion: Gait planning for complex dynamical models of collaborative locomotion is a **significant challenge** arising from the hybrid nature of models, nonlinearities, high dimensionality, and strong interactions amongst the agents. Hybrid systems theory has provided powerful techniques for modeling and analyzing dynamic locomotion of single legged machines [4, 6, 7, 8, 9, 10, 16, 17, 19, 21, 24, 34, 35, 36, 37, 42, 43, 46, 52, 53, 84, 89, 91, 92, 98, 99, 104, 107, 117, 130, 141, 152, 153, 158, 159, 161, 163, 168, 169, 170, 172, 177, 179, 180, 182, 183, 188, 196, 203, 206, 212]. Models of legged locomotion are hybrid with continuous-time domains representing the Lagrangian dynamics and discrete-time transitions representing the change of contact points with the environment. Advanced nonlinear control algorithms have been developed to address the hybrid nature of locomotion such as hybrid reduction [18, 20, 21, 87], controlled symmetries [179], transverse linearization [130, 176], and **hybrid zero dynamics (HZD)** [19, 205]. The HZD approach considers a set of kinematic constraints, referred to as virtual constraints, to coordinate the links of the robots during locomotion. Virtual constraints are asymptotically imposed by the action of a feedback control law (e.g., input-output (I-O) linearization [106]) and have been validated for stable locomotion of bipedal robots [19, 43, 103, 132, 166, 183] and powered prosthetic legs [88, 214]. The full-order gait planning in the HZD approach is typically formulated as a **nonlinear programming (NLP)** problem. Reference [103] developed a scalable gait planning approach based on HZD and direct collocation [39, 102, 113, 153, 157] that can be effectively solved with existing NLP tools. Although the direct-collocation-based HZD approach generates optimal trajectories for full-order models of legged robots in a fast manner, it *cannot* address real-time trajectory optimization for collaborative locomotion.

Collaborative manipulation of objects by legged robot teams is a **significant challenge**, mainly due to the uncertainty and multi-faceted nature of interaction problems, which can affect the stability of each agent and whole interconnected system. Interaction models typi-

cally deal with intent detection, arbitration, and feedback [123] but make broad assumptions about the operating environments. One approach to address *uncertainties* arising from collaborative manipulation/locomotion, interaction with objects, payloads, terrain structures, and environmental conditions can be through the development of *robust optimal control algorithms*. Robustness of control systems to uncertainties and disturbances has always been a central issue in feedback control. Developing multi-variable robust control methods has been the focal point of the control community in the last decades. The $\mathcal{H}_2/\mathcal{H}_\infty$ robust control theory is the result of this effort, e.g., [23, 26, 31, 32, 45, 61, 62, 79, 81, 82, 195, 215, 216]. State-of-the-art $\mathcal{H}_2/\mathcal{H}_\infty$ controllers are tailored to the stabilization of equilibrium points for **ordinary differential equations (ODEs)** and *not* hybrid trajectories for sophisticated dynamical systems arising from legged agents. This *underlines* the importance of the development of **Model Predictive Control (MPC)** and robust optimal control approaches that allow real-time planning and dynamic coordination of autonomous quadrupedal robots to effectively and safely interact with other agents in the presence of uncertainties and disturbances.

A variety of powerful MPC-based approaches have been introduced for the real-time planning and robust control of solitary legged machines including the **Linear Inverted Pendulum (LIP)**-based approach [14, 66, 94, 109, 162, 208], **single rigid body (SRB)** dynamics approach [56, 57, 198], nonlinear MPC [145], policy-regularized MPC [27], and **Quadratic Programming (QP)**-based whole-body control [70, 118]. Quadrupedal robots that cooperatively transport an object can be described by a set of legged robots that are coupled to each other and the object via a set of holonomic constraints. The *challenge* is to develop real-time optimal control algorithms for such a complex and inherently unstable robotic system that controls locomotion with many DOFs. Existing MPC approaches for legged robots are typically formulated as QPs to be solved every time sample—this makes the extension of these MPC-based techniques for composite mechanical systems arising from collaborative locomotion of quadrupedal robots *computationally intensive*. We aim to deploy innovative MPC techniques in the context of *networked systems* that can reduce the computational burden to allow real-time planning and coordination of sophisticated co-robot teams. One approach to tackle this challenge is through the development of *event-based* MPC techniques [121], in which MPC problems are solved at particular time samples, referred to as events (e.g., beginning of each gait), rather than every time sample.

1.2 Scope, Goals, and Specific Objectives

The evolution of legged robotic teams that cooperatively manipulate objects can be represented by *high-dimensional* and *highly-coupled hybrid dynamical systems* that complicate the design of coordination and control algorithms. Section 1.1 emphasized that existing control architectures for legged robots are not suitable for collaborative locomotion due to the lack of scalability and efficiency. Existing literature on **MRS** is also primarily tailored to weakly coupled unmanned ground vehicles (UGV) and unmanned aerial vehicles (UAV), and hence,

they are outside the scope of collaborative legged locomotion. *The overarching goal of this thesis is to establish a formal foundation based on nonlinear systems and optimization theory to develop scalable and hierarchical feedback control algorithms for effective motion control of interconnected cooperative legged robots.* The thesis aims to establish an innovative control paradigm, based on MPC and nonlinear control, in the context of interconnected systems that allow supervisory and distributed control of collaborative legged machines.

The specific objectives and key innovations of the dissertation include:

- (1) Creation of nonlinear feedback control algorithms for full-order dynamical models of single-agent legged robots based on virtual constraints and event-based MPC to reduce the computational burden for path planning and motion control;
- (2) Creation of hierarchical control algorithms, based on supervisory and event-based MPC, for collaborative locomotion of multi-agent legged robots;
- (3) Creation of layered control algorithms, based on centralized and distributed MPC, for planning and motion control of dynamic cooperative locomotion of multi-agent legged robots; and
- (4) Transferring the theoretical contributions and layered control algorithms into numerical simulations and practice through experiments on a team of quadrupedal robots.

These objectives will be achieved through the following research aims.

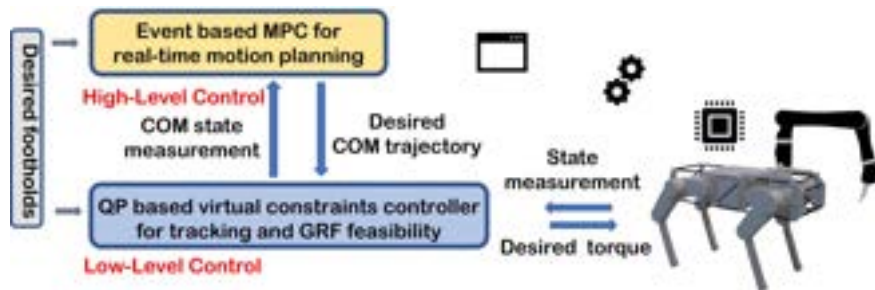


Figure 1.3: Event-based MPC and QP-based low-level controller for single-agent legged robots.

1.2.1 Event-based MPC and QP-based low-level nonlinear controllers for single-agent legged robots

In this research aim, we develop a hierarchical nonlinear control algorithm, based on MPC, QP, and virtual constraints, to generate and stabilize locomotion patterns in a real-time manner for dynamical models of single-agent quadrupedal robots (see Fig. 1.3). The higher level of the proposed control scheme is developed based on an event-based MPC that computes the optimal **center of mass (COM)** trajectories for a reduced-order LIP model subject

to the feasibility of the net [ground reaction force \(GRF\)](#). It is shown that the event-based nature of the proposed MPC approach can significantly reduce the computational burden associated with the real-time implementation of MPC techniques. To bridge the gap between reduced- and full-order models, QP-based virtual constraint controllers are developed at the lower level of the proposed control scheme to impose the full-order dynamics to track the optimal trajectories while having all individual GRFs in the friction cone. The analytical results are numerically verified to demonstrate stable and robust locomotion of a 22 DOF quadrupedal robot, in the presence of payloads, external disturbances, and ground height variations.

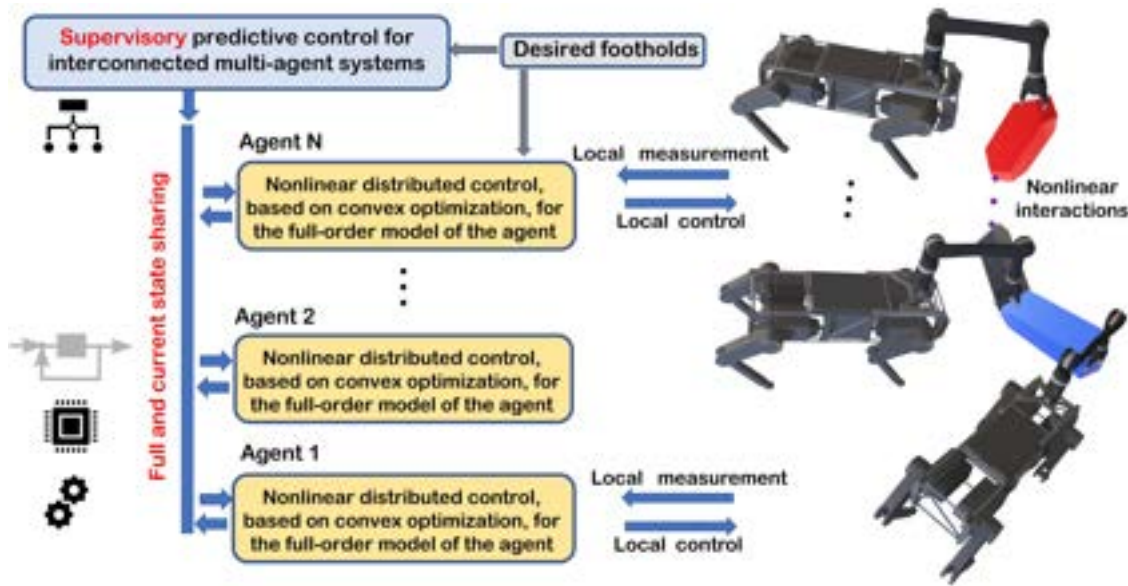


Figure 1.4: Hierarchical control algorithm with supervisory MPC for collaborative locomotion of legged-robot teams.

1.2.2 Hierarchical control algorithms with supervisory MPC for multi-agent legged robots

In this research aim, we develop a hierarchical nonlinear control algorithm for the real-time planning and control of cooperative locomotion of legged robots that collaboratively carry objects (see Fig. 1.4). An innovative network of reduced-order models subject to holonomic constraints, referred to as interconnected LIP dynamics, is presented to study cooperative locomotion. The higher-level of the proposed algorithm employs a supervisory controller, based on event-based MPC introduced in Section 1.2.1, to effectively compute the optimal reduced-order trajectories for the interconnected LIP dynamics. The lower-level of the proposed algorithm employs distributed nonlinear controllers to reduce the gap between reduced- and full-order complex models of cooperative locomotion. In particular, the distributed controllers are developed based on QP and virtual constraints to impose

the full-order dynamical models of each agent to asymptotically track the reduced-order trajectories while having feasible contact forces at the leg ends. We numerically investigate the power of the proposed control algorithm via full-order simulations of a team of two, three, and four collaborative quadrupedal robots, each with a total of 22 DOFs. We also investigate the robustness of the proposed control algorithm against uncertainties in the payload mass and changes in the ground height profile.

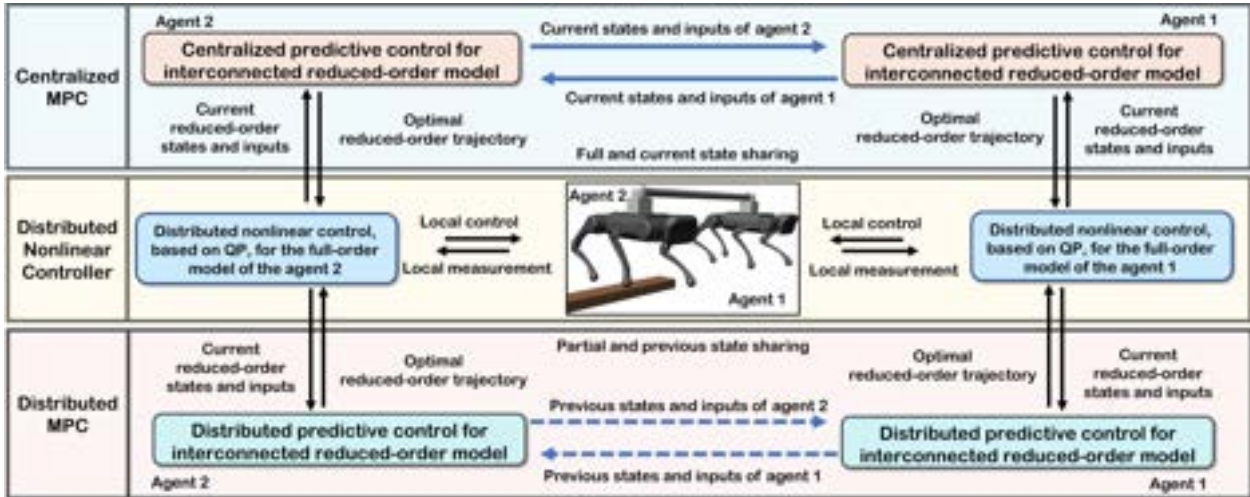


Figure 1.5: Layered control algorithm with centralized and distributed MPC for cooperative locomotion.

1.2.3 Layered control algorithm with centralized and distributed MPC based on interconnected SRB model for multi-agent legged robots

The framework of Section 1.2.2 assumes that all agents instantaneously share their reduced-order states at the beginning of continuous-time domains to formulate the optimal control problem for the interconnected LIP dynamics. To address the dynamic cooperative locomotion and inherent communication delays in practice, we develop a centralized MPC based on interconnected SRB model, which can capture the interaction wrenches without losing the dynamic richness. Furthermore, distributed network of MPC algorithms developed based on centralized MPC allow communication delays while guaranteeing the stability of the interconnected reduced-order model (see Fig. 1.5). More specifically, we alter the hierarchical control scheme of Section 1.2.2 by replacing the higher-level supervisory MPC with centralized and distributed MPC. The low-level nonlinear whole body motion controllers are also re-developed for generating the whole-body motion on the A1 robot. We numerically and experimentally investigate the effectiveness of the proposed layered control algorithm for cooperative locomotion of a team of multi-agent legged robots subject to uncertainties and disturbances in indoor and outdoor environments.

1.2.4 Structure of the Dissertation

We address the above-mentioned specific objectives in three parts. Part I focuses on addressing the development of event-based MPC and QP-based low-level nonlinear controllers. Part II addresses the development of a hierarchical control algorithm consisting of the supervisory MPC and distributed low-level controllers. Part III presents the layered control architecture with centralized and distributed MPCs as trajectory planner and QP-based low-level nonlinear controller. The detailed numerical and experimental validations are also discussed in Part III.

1.3 Significance and Importance

This dissertation aims to address the largely unexplored field of distributed control of large-scale and inherently unstable hybrid systems of legged co-robots. The innovative proposed algorithms are theoretically significant as 1) they *scalably* plan and systematically synthesize distributed feedback controllers for complex hybrid models of legged co-robot teams with high DOFs; 2) they address *strong interactions*, *underactuation*, and *unilateral constraints* for cooperative locomotion; 3) they bridge the gap between reduced- and full-order models of collaborative locomotion; and 4) they stabilize *full-order models* of locomotion as opposed to the reduced-order abstractions of high-dimensional legged machines. The scalable theoretical and computational foundation for planning and distributed control of legged co-robots are technologically significant because they can be effectively solved with available software packages, making our findings easily transferable to legged robots in our laboratory to bridge the gap between theory and implementation.

1.4 Literature Review: Modeling, Planning, and Control of Legged Robots

This section provides a brief survey of the state-of-the-art approaches in modeling, trajectory optimization, and feedback control of legged locomotion. To better understand the dynamics of robotic systems, we commonly think about how to model robots. The dynamical models can be either used for trajectory optimization or control. Each purpose has different requirements on the models to improve the performance. For instance, trajectory optimization for legged robots can adopt either a full-order model or a reduced-order model based on the purpose. The trajectory from the full-order model addresses the motions of all DOFs and can be readily transferred to the legged robot. However, trajectory optimization algorithms based on full-order models are usually computationally intensive, and hence, they cannot address motion planning in real-time for complex environments. On the other hand,



Figure 1.6: Full-order modeling accounts for all links and DOFs in the model.

trajectory optimization algorithms based on reduced-order models can meet the real-time requirement while adjusting the trajectory based on the upcoming environment. The challenge is in applying these reduced-order trajectories to the full-order models of legged robots while bridging the gap between reduced- and full-order models.

1.4.1 Full-Order Lagrangian Models

A Full-order model is the most intuitive way to describe high DOF robots. The goal of this approach is to obtain a model that accurately represents the entire robot, see, e.g., [3, 11, 77, 78, 101, 124, 205, 206]. This approach results in nonlinearities in the equations of motion. Unfortunately, there is still a gap between the real robots and their full-order models due to uncertainties arising from viscous damping, friction on gears and axes, joint and frame elasticity, etc. We will consider these uncertainties negligible and proceed with an approximation of the model. To obtain the full-order model of legged machines, we make use of the Lagrangian, which is defined as follows:

$$\mathcal{L}(q, \dot{q}) := K(q, \dot{q}) - U(q), \quad (1.1)$$

where $K(q, \dot{q})$ denotes the total kinetic energy of the system and $U(q)$ represents the total potential energy. Furthermore, $q \in \mathbb{R}^{n+6}$ denotes the generalized coordinates of the robot. Here, n represents the number of internal DOFs in the robot structure (i.e., body angles) that form the robot's shape. The equations of motion can then be described by the Euler-Lagrange equations as follows:

$$D(q)\ddot{q} + C(q, \dot{q})\dot{q} + G(q) = Bu + J^\top(q)\lambda, \quad (1.2)$$

where $D(q) \in \mathbb{R}^{(n+6) \times (n+6)}$ is the symmetric and positive definite mass-inertia matrix, $C(q, \dot{q})\dot{q} + G(q) \in \mathbb{R}^{n+6}$ represents the Coriolis, centrifugal, and gravitational terms, $B \in \mathbb{R}^{(n+6) \times m}$ denotes the input distribution matrix, $u \in \mathbb{R}^m$ represents the control inputs (i.e., joint-level torques), $J(q)$ denotes the contact Jacobian matrix, λ represents the GRFs, and

$\Gamma := Bu + J^\top(q)\lambda$ denotes the sum of the generalized forces and torques acting on the rigid body. The dimension of the Jacobian matrix $J(q)$ depends on the number of contact points with the environment. Here, we assume that the robot has point feet, and hence, the interaction of the robot and environment is just through the GRFs. In this thesis, we will make use of the full-order model (1.2) to develop the low-level controllers for quadrupedal robots (see Chapters 2 and 3 for more details).

1.4.2 Full-Order Hybrid Dynamical Models

Hybrid systems exhibit characteristics of both continuous- and discrete-time systems [24, 85, 99, 212]. Models of legged locomotion are hybrid with continuous-time domains representing the Lagrangian dynamics and discrete-time transitions representing the change of contact points with the environment [4, 6, 7, 8, 9, 10, 16, 17, 19, 21, 34, 35, 36, 42, 43, 46, 47, 48, 52, 53, 89, 91, 92, 98, 104, 107, 130, 141, 152, 153, 158, 159, 168, 169, 170, 172, 177, 179, 180, 182, 183, 188, 203, 206]. Steady-state locomotion corresponds to periodic orbits of these hybrid dynamical models. The trajectory optimization (i.e., gait planning) algorithms need to address the hybrid nature of locomotion by combining both the continuous- and discrete-time dynamics. In general, gait planning algorithms are expressed as NLP. Reference [103] developed a scalable gait planning approach based on direct collocation [39, 102, 113, 153, 157] that can be effectively solved with existing NLP tools. Although the direct-collocation-based approaches generate optimal trajectories for full-order models of legged robots in a fast manner, they *cannot* address real-time trajectory optimization in complex environments. These limitations could be critical for operating robots outside the laboratory setup. For this reason, we cannot adopt the entire framework of the hybrid systems theory for collaborative locomotion of multi-agent robots. However, we can still capitalize on some of the advantages of the framework proposed in the nonlinear hybrid systems theory. The HZD approach [6, 19, 205, 206], which is one of the well-known methods used for full-order models of legged robots, can significantly help us to develop low-level controllers for collaborative locomotion. This will be clarified more in Chapters 2 and 3.

1.4.3 Reduced-Order Models

Reduced-order models represent complex dynamical models of locomotion in a simplified dynamical structure, see, e.g., [14, 56, 57, 94, 109, 147, 162, 197, 199]. In what follows, we will discuss three reduced-order models that are commonly used in the literature.

SRB Dynamics: The SRB model considers the robot as a single mass with an inertia (see Fig. 1.7). The key idea of this model is to reduce the complexity of the robot by considering its torso dynamics subject to the GRFs while ignoring the leg limbs in the abstraction [56, 57, 115, 198]. Most of the existing quadrupedal robots have concentrated mass on the body with relatively small masses on their leg limbs. The SRB model presents

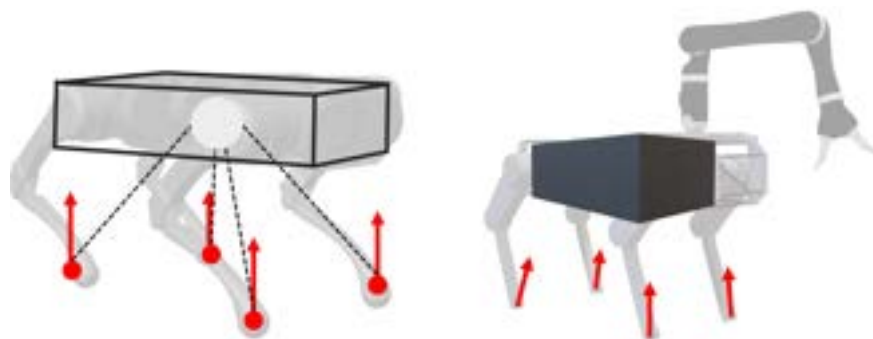


Figure 1.7: SRB model.

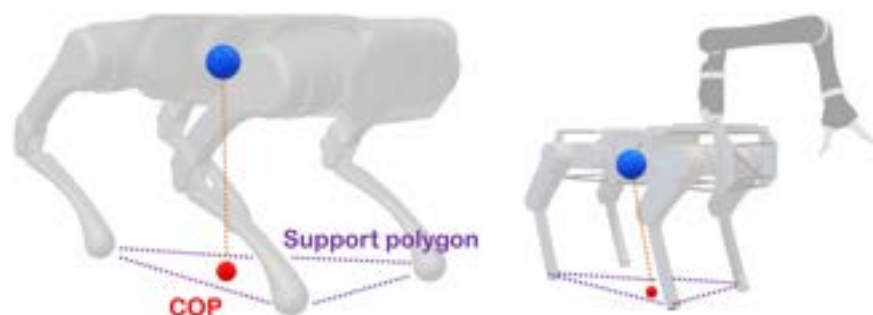


Figure 1.8: LIP model.

a good approximation for dynamical models of these robots. However, this approach has limitations when applied to quadrupedal robots or humanoids with heavy limbs.

LIP Models: The LIP model is one of the simplest models developed based on the inverted pendulum structure with a point mass on top of a massless rod whose position coincides with the robot's COM [108]. This assumption works appropriately, especially when the dynamical effects caused by the robot's mass distribution are negligible. Unlike the inverted pendulum dynamics, the dynamics for the LIP model are linear. This is due to the assumption that the height of the COM is kept constant in the development of the LIP model [109]. Based on its simplicity and linearity, the LIP model has been utilized for real-time trajectory optimization of legged robots, see, e.g., [66, 94, 95, 162]. However, the LIP model has some limitations. In particular, it assumes that the **Center of Pressure (COP)** of the robot does not leave the support polygon (i.e., the **Zero Moment Point (ZMP)** criterion [199]). Hence, the generated gaits are quasi-statically stable but not dynamically stable. Some extended LIP models have been proposed to address dynamic gaits while minimizing the model complexity. One of the extensions is the **Spring Loaded Inverted Pendulum (SLIP)** model, which includes a spring on the massless rod in the inverted pendulum structure. The SLIP model allows the consideration of dynamic motions, including nonnegligible flight phases and hopping [159], and can be used to model both walking and running [160, 175]. Another extended concept of the LIP model is the **Divergent Component of Motion (DCM)**, also referred to as the capture



Figure 1.9: Centroidal dynamics.

point in three-dimension. We remark that the DCM does not increase the complexity of the LIP model as we observe in the SLIP model. Instead, it introduces additional design variables to impose the COM to follow the DCM [67, 94, 95, 96]. These extensions show that the LIP model still has the potential to be used as a basic reduced-order model because of its unbeatable advantages.

Furthermore, we hypothesize that it is suitable for reduced-order models of collaborative locomotion, which will not have any severe dynamic motions. For this reason, the LIP model will be considered as a candidate in Chapters 3 and 4 to model the underlying dynamics to facilitate real-time motion planning for collaborative locomotion of quadrupedal robots.

Centroidal Dynamics: The significant difference between the centroidal dynamics and LIP model is the description of the mass distribution. Unlike the LIP model, which uses a point mass on the COM position, the centroidal dynamics consider linear and angular momenta together with a mass. Due to this reason, this method is currently categorized under the reduced-order models, but it can be considered as a step towards the full-order dynamical modeling [54, 111, 120, 204]. The advantage of the centroidal dynamics is that the user can decide about the complexity level of the reduced-order model for motion planning and control.

1.4.4 Trajectory Optimization

Gait planning for dynamical models of legged locomotion can be described as an optimal control problem. The objective is to minimize a cost function while steering the system's state from an initial condition to a final one and subject to a set of state and control constraints. These optimal control problems are usually formulated for discretized dynamics of the robots. This would reduce the original optimal control problem into a finite-dimensional NLP. These optimization problems are, in general, complex to solve due to nonlinearity and high dimensionality. Gait planning based on reduced-order models can generate relatively light optimal control problems that can be solved in real-time, even though they sacrifice the

dynamic richness. On the other hand, high dimensionality in full-order dynamical models makes it difficult to solve the corresponding NLPs. This section reviews NLP-based gait planning approaches [8, 9, 11, 39, 102, 103, 113, 125, 153, 157, 166, 205, 206]. Furthermore, the basic concepts of convex optimization, including [Linear Programming \(LP\)](#) and [QP](#) [56, 57, 66, 94, 95, 115, 162, 198], will be discussed.

General Optimization Problems for Gait Planning: The general gait planning problem consists of finding the open-loop control input $u(t)$ over a finite time interval $t \in [t_0, t_f]$ such that for a given initial state x_0 at t_0 , the state trajectory reaches the desired final state x_f at t_f while the state and control constraints are met. More formally, this optimization problem can be formulated with a cost function (e.g., energy or cost of mechanical transport) and a set of equality and inequality constraints. The equality constraints address the dynamics and steering problem whereas the inequality constraints consider the feasibility of the joint positions, velocities, torques, and friction cone conditions. If the cost functions or constraints are nonlinear, the optimization problem becomes an NLP. These optimization problems can be solved with commercially available solvers such as IPOPT [200], SNOPT [83], and FMINCON [135].

Convex Optimization Problems for Gait Planning: The optimization problem we are usually interested in has a specific format compared to the general optimization problem, especially in the cost function structure. In cases where the constraints are linear, and the objective function is linear or quadratic, the problem formulation results in either an LP or QP. These problems are convex and can be solved effectively in a real-time manner. The LP and QP problems often arise from the MPC problems. In these optimal control formulations, the MPC problem is usually applied to the linearized reduced-order dynamics of the robot (see Section 1.4.5 for more details). Suppose the gait planning problem becomes an NLP. In that case, a proper initial condition could potentially reduce the optimization time, but finding a feasible solution in real-time still poses a significant challenge. On the other hand, if the problem becomes an LP or QP, it can be solved fast (without violating real-time restrictions) when compared to the NLP. The LP or QP can be solved with commercially available solvers such as ECOS [59], OSQP [185], or QPSWIFT [150].

1.4.5 Existing Control Techniques for Legged Robots

This section focuses on legged robots' control problem to guarantee dynamic stability while walking from point A to point B. In the context of the optimal control problem, we consider the MPC approach to generate the optimal trajectories while asymptotically stabilizing the target points for the dynamical systems. Furthermore, nonlinear control techniques that address the full-order and hybrid dynamical models of locomotion are discussed.

MPC: MPC is a conventional method, which was initially developed for industrial and slow dynamical processes [30]. With the recent advances in computation and the development of efficient optimization algorithms, MPC-based approaches have been getting more attention

in the field of robot locomotion [14, 57, 144, 197]. One of the significant characteristics of the MPC is that it optimizes the sequence of control inputs according to the system's dynamics and state and input constraints over a finite-time control horizon. The MPC then employs the current control action and optimizes again repeatedly, thus differing from Linear-Quadratic Regulator (LQR).

MPC-based approaches integrated with reduced-order models have been used for real-time path planning of bipedal and quadrupedal locomotion, see e.g., [66, 94, 109, 162]. Most of these approaches address LIP models for bipedal locomotion while generating optimal trajectories for the COM and COP of the robot subject to the ZMP conditions [199] and feasibility of the GRF. These techniques, however, cannot be easily extended to quadrupedal locomotion as the LIP-based MPC approaches do *not* consider the feasibility of all individual GRFs. To tackle this problem, [56, 57, 197] have developed an interesting convex optimization formulation based on MPC and SRB dynamics. In particular, the MPC approach of [56, 57, 197] plans for the optimal GRFs of the contacting leg ends at every time sample (e.g., 200 Hz) for agile quadrupedal locomotion. Alternative interesting approaches for agile locomotion have utilized nonlinear MPC [145], policy-regularized MPC [27], and QP-based whole-body control [70, 118]. Although state-of-the-art techniques for MPC-based control of quadrupedal locomotion have shown a very good level of robustness, they require solving MPC at every time sample. These MPC problems are typically formulated as convex QPs for robots with light legs and may have a significant number of decision variables to be optimized. This makes the MPC-based techniques computationally intensive. In the context of distributed control of collaborative locomotion, we are interested in developing control algorithms with less computational load for which the MPC problems do not need to be solved every time sample. This will be addressed in Chapters 2, 3, and 4.

Other Nonlinear Control Approaches: State-of-the-art nonlinear control techniques that address the hybrid nature and full-order dynamical models of locomotion have been developed based on hybrid reduction [18, 20, 21, 87], controlled symmetries [179], transverse linearization [130, 176], and HZD [19, 205]. Transverse linearization and HZD approaches can systematically address underactuation. HZD controllers have been numerically and experimentally validated for the motion control of bipedal robots [19, 42, 103, 131, 166, 171, 182, 183], powered prosthetic legs [90, 213], and exoskeletons [1]. As discussed before, the full-order gait planning in the HZD approach is typically formulated as an NLP problem. We aim to develop hierarchical control algorithms based on MPC and HZD to address the real-time motion planning problem while stabilizing the full-order dynamical system. This will be discussed in Chapters 2 and 3.

1.5 Relevant Publications

As part of this dissertation, three journal articles are written, one published by the IEEE Robotics and Automation Letters (RAL) and another is published by the ASME Journal

of Dynamic Systems, Measurement, and Control. The latest journal article is planned to submit in IEEE Transactions on Robotics (T-RO).

Chapters 2, 3, and 4 comprise of the materials of these three articles as listed below:

- [J1] **J. Kim**, R. T. Fawcett, V. R. Kamidi, A. D. Ames and K. Akbari Hamed, “Layered Control for Cooperative Locomotion of Two Quadrupedal Robots: Centralized and Distributed Approaches,” *IEEE Transactions on Robotics*, In preparation.
- [J2] **J. Kim**, and K. Akbari Hamed, “Cooperative locomotion via supervisory predictive control and distributed nonlinear controllers,” *ASME Journal of Dynamic Systems, Measurement, and Control*, Vol. 144, Issue. 3, p. 031005, Dec., 2021.
- [J3] K. Akbari Hamed, **J. Kim**, and A. Pandala, “Quadrupedal locomotion via event-based predictive control and QP-based virtual constraints,” *IEEE Robotics and Automation Letters*, Vol. 5, Issue 3, pp. 4463-4470, July 2020.
- [J4] V. R. Kamidi, **J. Kim**, R. T. Fawcett, A. D. Ames and K. Akbari Hamed, “Distributed Quadratic Programming-Based Nonlinear Controllers for Periodic Gaits on Legged Robots,” *IEEE Control Systems Letters*, vol. 6, pp. 2509-2514, 2022

In addition, I have contributed to the following journal article.

- [J5] R. T. Fawcett, A. Pandala, **J. Kim**, and K. Akbari Hamed, “Real-time planning and nonlinear control for quadrupedal locomotion with articulated tails”, *ASME Journal of Dynamic Systems, Measurement, and Control*, Vol. 143, Issue. 7, p. 071004, Jul, 2021.

1.6 Outline

This dissertation is organized as follows.

Chapter 2 presents a hierarchical control scheme, based on event-based MPC, HZD, and QP, to generate and stabilize locomotion patterns in a real-time manner for dynamical models of single-agent quadrupedal robots. The higher level of the proposed control scheme is developed based on an event-based MPC that computes the optimal reduced-order trajectories. To bridge the gap between reduced- and full-order models, QP-based virtual constraint controllers are developed at the lower level of the proposed control scheme to impose the full-order dynamics to track the optimal trajectories while having all individual GRFs in the friction cone. The analytical results are numerically verified to demonstrate stable and

robust locomotion of a 22 DOF quadrupedal robot, in the presence of payloads, external disturbances, ground height variations, and uncertainty in contact models.

Chapter 3 presents a hierarchical nonlinear control algorithm for the real-time planning and control of cooperative locomotion of legged robots that collaboratively carry objects. The higher level of the proposed algorithm employs a supervisory controller, based on event-based MPC, to effectively compute the optimal reduced-order trajectories for legged co-robots. The lower level of the proposed algorithm employs distributed nonlinear controllers to reduce the gap between reduced- and full-order complex models of cooperative locomotion. The chapter numerically investigates the effectiveness of the proposed control algorithm via full-order simulations of a team of collaborative quadrupedal robots, each with a total of 22 DOFs. The chapter finally investigates the robustness of the proposed control algorithm against uncertainties in the payload mass and changes in the ground height profile.

Chapter 4 presents a layered control approach for real-time trajectory planning and control of robust cooperative locomotion by two holonomically constrained quadrupedal robots. An innovative and interconnected network of reduced-order models, based on the SRB dynamics, is developed for trajectory planning purposes. At the higher level of the control scheme, two different MPC algorithms are proposed to address the optimal control problem of the interconnected SRB dynamics: centralized and distributed MPCs. The MPCs compute the reduced-order states, GRFs, and interaction wrenches between the agents. The distributed MPC assumes two local QPs that share their optimal solutions according to a one-step communication delay and an agreement protocol. At the lower level of the control scheme, distributed nonlinear controllers, based on QP and virtual constraints, are developed to impose the full-order dynamics to track the prescribed and optimal reduced-order trajectories and GRFs. The effectiveness of the proposed layered control approach is verified with extensive numerical simulations and experiments for the blind, robust, and cooperative locomotion of two holonomically constrained A1 robots with different payloads on different terrains and in the presence of external disturbances. It is shown that the distributed MPC has a performance similar to that of the centralized MPC, while the computation time is reduced significantly.

Chapter 5 presents concluding remarks and future directions to be conducted. It briefly summarizes the work done, which consists of the materials of Chapters 2, 3, and 4.

Part I

Event-Based MPC and Nonlinear Controllers for Locomotion of Single-Agent Legged Robots

Chapter 2

Legged Locomotion via Event-Based MPC and Virtual Constraints

2.1 Introduction

The objective of this chapter is to develop a hierarchical control algorithm, based on [Model Predictive Control \(MPC\)](#), nonlinear control, and [Quadratic Programming \(QP\)](#), to generate and stabilize locomotion trajectories for complex dynamical models of single-agent quadrupedal robots in real time. The proposed approach employs a higher-level and event-based MPC at the beginning of each continuous-time domain (i.e., event) that generates optimal trajectories for a reduced-order [Linear Inverted Pendulum \(LIP\)](#) model subject to the feasibility of the net [Ground Reaction Force \(GRF\)](#). The stability of the system subject to event-based MPC is investigated to demonstrate that the MPC does not need to be solved at every time sample. This significantly reduces the computational burden associated with MPC-based path planning approaches of legged locomotion while guaranteeing stability. To reduce the difference between the reduced-order and full-order models of locomotion, a QP-based nonlinear controller is solved at the lower level of the proposed approach to impose the full-order dynamics to track the optimal trajectories while keeping all individual GRFs feasible.

2.2 Hybrid Models of Locomotion

Models of legged locomotion are hybrid and can be illustrated as directed graphs. In this representation, continuous-time dynamics are represented by vertices of the graph to describe the evolution of the system by the Lagrangian dynamics. The edges of the graph then represent the instantaneous and discrete-time transitions amongst the continuous-time dynamics to model the possible and abrupt changes in the state vector according to the rigid impacts of the leg ends with the environment [16, 97, 98, 104, 206]. In this work, we consider a general and *aperiodic* locomotion pattern for the quadrupedal robot with start and stop conditions as a directed graph $\mathcal{G} = (\mathcal{V}, \mathcal{E})$ (see Fig. 2.1), where the vertices set \mathcal{V} represents the continuous-time domains (e.g., double-, triple-, and quadruple-contact domains) and edges set $\mathcal{E} \subset \mathcal{V} \times \mathcal{V}$ denotes the discrete-time transitions (e.g., impacts and

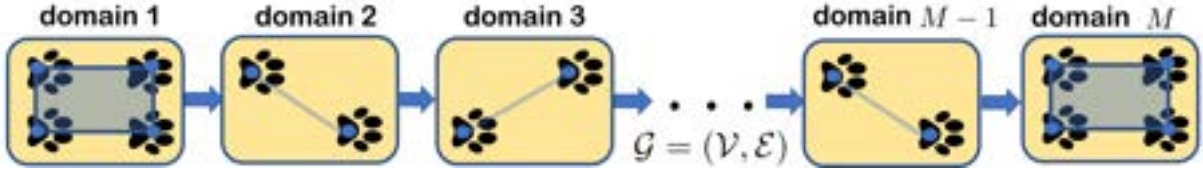


Figure 2.1: Illustration of a locomotion pattern with the corresponding graph $\mathcal{G} = (\mathcal{V}, \mathcal{E})$. Each continuous-time domain shows the support polygon as convex hull.

take-offs) (see Fig. 2.1). We further suppose that there are $M \geq 1$ continuous-time domains and each continuous-time domain consists of $N_d \geq 1$ grid points (i.e., time samples). For future purposes, the time sample is denoted by T_s .

We consider a full-order dynamical model of Vision 60 that is augmented by a Kinova robotic manipulator for locomotion and manipulation purpose. Vision 60 is a quadrupedal robot manufactured by Ghost Robotics. The floating-base model of the composite robot consists of 22 DOFs of which 12 DOFs are actuated and assigned to legs (see Fig. 2.2). In particular, each leg of the robot has an actuated 2 DOF hip joint plus an actuated 1 DOF knee joint and ends at a point foot. In addition, 4 DOFs with 4 actuators are assigned to the Kinova manipulator. The remaining 6 DOFs are unactuated and describe the absolute position and orientation of the robot with respect to an inertial world frame. The composite mechanical system weighs around 35 (kg).

The generalized coordinates of the robot can be expressed as

$$q := \text{col}(p_b, \phi_b, q_{\text{body}}) \in \mathcal{Q} \subset \mathbb{R}^{22}, \quad (2.1)$$

in which $p_b \in \mathbb{R}^3$ and $\phi_b \in \mathbb{R}^3$ describe the absolute position and orientation of the torso, respectively. Moreover, $q_{\text{body}} \in \mathbb{R}^{16}$ represents the shape (i.e., internal joints) of the robot. In our notation, \mathcal{Q} represents the configuration space, and “col” denotes the column operator. The state vector of the mechanical system is taken as

$$x := \text{col}(q, \dot{q}) \in \mathcal{X}, \quad (2.2)$$

where $\mathcal{X} := \text{T}\mathcal{Q} := \mathcal{Q} \times \mathbb{R}^{22}$ denotes the state manifold. The control inputs (i.e., joint-level torques) are finally represented by $\tau \in \mathbb{R}^{16}$. The evolution of the robot during continuous-time domains can be expressed by the following [ordinally differential equation \(ODE\)](#) arising from the Euler-Lagrange equations and the principle of virtual work

$$D(q) \ddot{q} + H(q, \dot{q}) = \Upsilon \tau + \sum_{\ell \in \mathcal{C}} J_\ell^\top(q) F_\ell, \quad (2.3)$$

where $D(q) \in \mathbb{R}^{22 \times 22}$ represents the positive definite mass-inertia matrix, $H(q, \dot{q}) \in \mathbb{R}^{22}$ denotes the Coriolis, centrifugal, and gravitational forces, and $\Upsilon \in \mathbb{R}^{22 \times 16}$ represents the input distribution matrix with the property $\text{rank} \Upsilon = 16$. In our notation, \mathcal{C} is the index

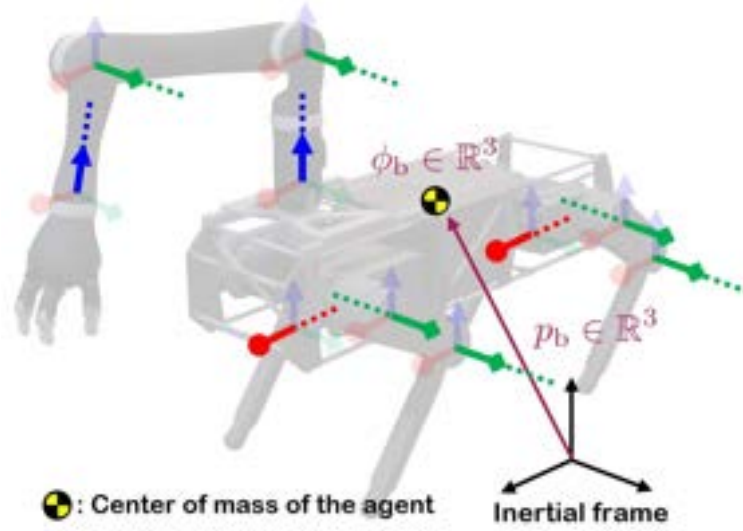


Figure 2.2: Illustration of 22 DOFs for the full-order model of the composite robot. The robot is composed of the 18-DOF Vision 60 plus the 4-DOF Kinova arm. Six unactuated DOFs are associated with the absolute position and orientation of the torso frame with respect to an inertial world frame. Each leg of the robot then consists of three actuated joints as hip roll, hip pitch, and knee joints. The arm is finally composed of four actuated joints. The axis of actuation for actuated joints are shown with dashed lines, where the axes with circle ends, axes with square ends, and axes with triangle ends represent the x, y, and z directions, respectively.

set of contact points with the ground. Furthermore, for every $\ell \in \mathcal{C}$, $J_\ell(q) \in \mathbb{R}^{3 \times 22}$ and $F_\ell \in \mathbb{R}^3$ denote the corresponding contact Jacobian matrix and GRF, respectively. The contact forces can be computed using 1) the rigid contact assumption and hybrid system approach [11, 206], 2) compliant contact models (e.g., LuGre model [55]), or 3) nonlinear and linear complementarity problems [186] as well as optimization-based techniques [105, 189].

We remark that the model (2.3) is valid if $F_\ell \in \mathcal{FC}$ for all $\ell \in \mathcal{C}$, where

$$\mathcal{FC} := \left\{ \text{col}(F_x, F_y, F_z) \mid F_z > 0, \pm F_x < \frac{\mu}{\sqrt{2}} F_z, \pm F_y < \frac{\mu}{\sqrt{2}} F_z \right\} \quad (2.4)$$

denotes the friction cone for some static friction coefficient μ . For later purposes, the equations of motion in (2.3) can be written in a state space form as

$$\begin{aligned} \dot{x} &= \begin{bmatrix} \dot{q} \\ -D^{-1}(q) H(q, \dot{q}) \end{bmatrix} + \begin{bmatrix} 0 \\ D^{-1}(q) \Upsilon \end{bmatrix} \tau + \sum_{\ell \in \mathcal{C}} \begin{bmatrix} 0 \\ D^{-1}(q) J_\ell^\top(q) \end{bmatrix} F_\ell \\ &=: f(x) + g(x) \tau + w(x) F, \end{aligned} \quad (2.5)$$

in which $F := \text{col}\{F_\ell \mid \ell \in \mathcal{C}\}$ represents the contact forces. In addition, the model assumes

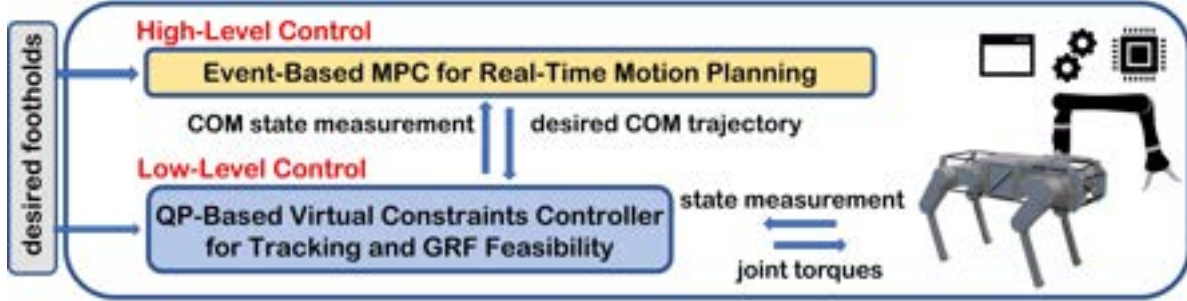


Figure 2.3: Illustration of the proposed hierarchical control algorithm based on nonlinear control, QP, and event-based MPC.

a rigid contact point between the stance leg ends of the robot and the ground. This assumption makes the leg ends acceleration zero which can be expressed as the following algebraic constraint

$$\ddot{p}_\ell^{\text{st}} = J_\ell(q) \ddot{q} + \frac{\partial}{\partial q} (J_\ell(q) \dot{q}) \dot{q} = 0, \quad \forall \ell \in \mathcal{C} \quad (2.6)$$

where $p_\ell^{\text{st}} \in \mathbb{R}^3$ denotes the Cartesian coordinates of the stance leg end $\ell \in \mathcal{C}$. For future purposes, we define $p^{\text{st}} := \text{col}\{p_\ell^{\text{st}} \mid \ell \in \mathcal{C}\}$ as the Cartesian coordinates of all contact points. In addition, $J(q) := \frac{\partial p^{\text{st}}}{\partial q}(q)$ is defined as the corresponding contact Jacobin matrix.

The evolution of the mechanical system during discrete-time transitions can be expressed via instantaneous mappings arising from rigid impact models (see e.g., [97, 104]). In this chapter, we focus on the continuous-time domains of locomotion to present the nonlinear control strategy. More details about the derivation of discrete-time transitions can be found in [11].

2.3 QP-Based Virtual Constraint Controllers

The objective of this section is to present a QP-based nonlinear controller that can asymptotically stabilize locomotion patterns for multi-domain hybrid dynamical models of locomotion while keeping the individual GRFs in the friction cone. Here, we make use of the concept of virtual constraints to design this nonlinear controller. Virtual constraints are defined as a set of kinematic constraints that can be imposed by the action of feedback control laws to coordinate the motion of links within a stride [42, 90, 93, 129, 131, 140, 159, 166, 171]. In particular, virtual constraints are defined as output functions for continuous-time dynamics of locomotion models. The output functions are then regulated via the action of a feedback controller (e.g., I-O linearization [106]). In this work, we address holonomic virtual constraints with relative degree 2 for the purpose of position tracking. Alternatively, one can use relative degree 1 nonholonomic constraints or a combination of holonomic and nonholonomic constraints as [11, 100]. The QP-based nonlinear controller will be utilized at the low

level of the proposed hierarchical control algorithm. The higher-level of the algorithm will be developed in Section 2.4 for the path planning purpose.

2.3.1 Virtual Constraints

In this work, we define a set of time-varying and holonomic virtual constraints as follows:

$$y(x, t) := h(q, t) := h_0(q) - h_d(s, \alpha), \quad (2.7)$$

in which $h_0(q)$ denotes a set of holonomic quantities to be controlled, referred to as controlled variables. In addition, $h_d(s, \alpha)$ represents the desired evolution of the controlled variables in terms of the phasing variable s . Here,

$$s := \frac{t - t^+}{N_d T_d} \quad (2.8)$$

denotes the phasing variable with t^+ being the initial time for the current domain and $N_d T_d$ representing an estimated elapsed time for the domain.

The desired trajectory $h_d(s, \alpha)$ is taken as a Bézier polynomial with a coefficient matrix α . During the quadruple-contact domains, we choose $h_0(q) \in \mathbb{R}^6$ as the roll, pitch, and yaw angles of the torso together with the COM positions. The idea is to regulate the absolute orientation of the robot while imposing the actual COM coordinates to follow the optimal and desired COM trajectory generated by the MPC in Section 2.4. Here, the coefficient matrix α can be chosen via least squares at the beginning of each domain such that $h_d(s, \alpha)$ has the best fit to the optimal and desired COM trajectory over N_d samples. For double- and triple-contact domains, $h_0(q)$ is augmented with the Cartesian coordinates of the swing leg ends for foot placement. The idea is to follow a desired foot trajectory in the workspace starting from the previous foothold and ending at the next preplanned foothold. This makes the output function 12- and 9-dimensional for the double- and triple-contact domains, respectively. To control the configuration of the manipulator, we augment $h_0(q)$ and $h_d(s, \alpha)$ by the Cartesian coordinates of the end-effector (EE) and its desired trajectory in the workspace, respectively.

2.3.2 QP-Based I-O Linearization

Differentiating the output function (2.7) along (2.5) results in the following output dynamics

$$\begin{aligned} \ddot{y} &= L_g L_f y(x, t) \tau + L_w L_f y(x, t) F + L_f^2 y(x, t) + \frac{\partial^2 y}{\partial t^2}(x, t) \\ &= -K_D \dot{y} - K_P y, \end{aligned} \quad (2.9)$$

in which K_P and K_D are positive definite matrices. In addition, $L_g L_f y$, $L_w L_f y$, and $L_f^2 y$ are Lie derivatives defined as follows:

$$\begin{aligned} L_g L_f y(x, t) &:= \frac{\partial h_0}{\partial q}(q) D^{-1}(q) \Upsilon \\ L_w L_f y(x, t) &:= \frac{\partial h_0}{\partial q}(q) D^{-1}(q) J^\top(q) \\ L_f^2 y(x, t) &:= \frac{\partial}{\partial q} \left(\frac{\partial h_0}{\partial q}(q) \dot{q} \right) \dot{q} - \frac{\partial h_0}{\partial q}(q) D^{-1}(q) H(q, \dot{q}). \end{aligned} \quad (2.10)$$

To compute the required torques that drive the outputs to zero, one would need to solve for τ from (2.9). However, since the contact force measurements are not available for the studied robot, one would need to estimate the contact forces $F = \text{col}\{F_\ell \mid \ell \in \mathcal{C}\}$. To address this problem, we assume a rigid contact model with the walking surface as given in (2.6). The rigid contact assumption together with (2.5) then yields

$$\ddot{p}^{\text{st}} = L_g L_f p^{\text{st}}(x) \tau + L_w L_f p^{\text{st}}(x) F + L_f^2 p^{\text{st}}(x) = 0, \quad (2.11)$$

where the Lie derivatives are defined as follows:

$$\begin{aligned} L_g L_f p^{\text{st}}(x) &:= J(q) D^{-1}(q) \Upsilon \\ L_w L_f p^{\text{st}}(x) &:= J(q) D^{-1}(q) J^\top(q) \\ L_f^2 p^{\text{st}}(x) &:= \frac{\partial}{\partial q} (J(q) \dot{q}) \dot{q} - J(q) D^{-1}(q) H(q, \dot{q}). \end{aligned} \quad (2.12)$$

Next, we need to look for the values of (τ, F) that satisfy (2.9) and (2.11) with contact forces being in the friction cone, that is, $F_\ell \in \mathcal{FC}$ for all $\ell \in \mathcal{C}$. For this purpose, we set up the following real-time QP

$$\begin{aligned} \min_{(\tau, F, \omega)} \quad & \frac{1}{2} \|\tau\|_2^2 + \frac{\gamma}{2} \|\omega\|_2^2 \\ \text{s.t.} \quad & L_g L_f y \tau + L_w L_f y F + L_f^2 y + \frac{\partial^2 y}{\partial t^2} + \omega = v_{\text{PD}}(y, \dot{y}) \\ & L_g L_f p^{\text{st}} \tau + L_w L_f p^{\text{st}} F + L_f^2 p^{\text{st}} = 0 \\ & F_\ell \in \mathcal{FC}, \quad \ell \in \mathcal{C}, \quad \tau_{\min} \leq \tau \leq \tau_{\max}, \end{aligned} \quad (2.13)$$

in which $v_{\text{PD}}(y, \dot{y}) := -K_P y - K_D \dot{y}$ is the PD action. The equality constraints for the QP are set up based on the output dynamics (2.9) as well as the stance foot accelerations assumption (2.11). We introduce a defect variable ω in the equality constraint of QP that corresponds to the output dynamics in case the decoupling matrix $L_g L_f y$ is singular. To minimize the effect of the defect variable, we then add a quadratic term $\frac{\gamma}{2} \|\omega\|_2^2$ to the cost function of the QP to ensure that the 2-norm of the defect variable is as small as possible. Here, $\gamma > 0$ is

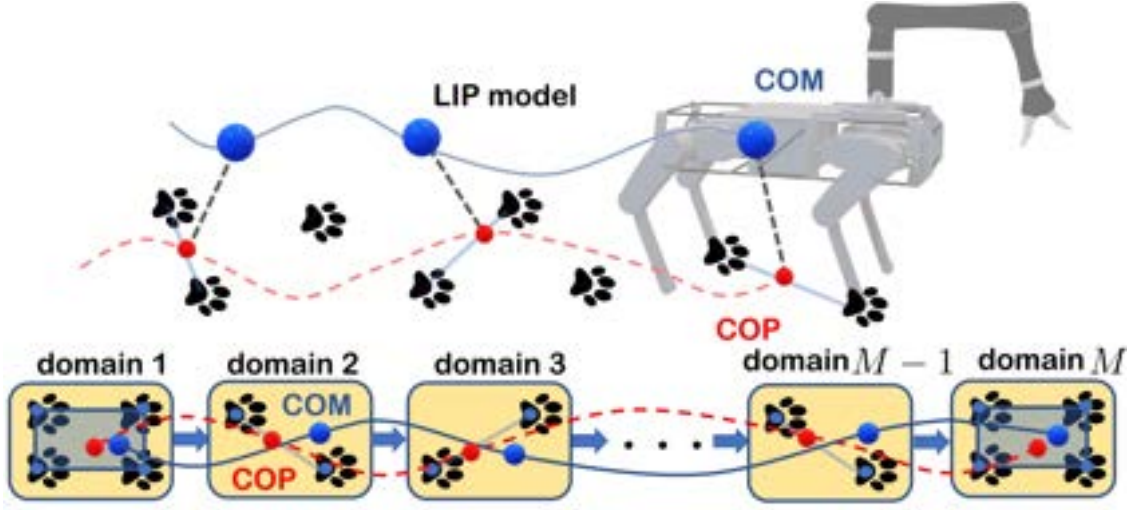


Figure 2.4: Illustration of the reduced-order model of locomotion (i.e., LIP dynamics) over different continuous-time domains. The figure also depicts the time-varying support polygon used for the ZMP condition.

a weighting factor. The other term in the cost function tries to find the minimum 2-norm (minimum power) torques that satisfy the equality and inequality constraints. Furthermore, τ_{\min} and τ_{\max} are the admissible bounds on the torques.

2.4 Event-Based Predictive Control

The objective of this section is to present the higher-level and event-based MPC that uses a reduced-order model of locomotion such as the LIP model for the real-time trajectory planning purpose. The event-based MPC addresses the steering problem of the reduced-order dynamics from an initial position to a final position while satisfying the feasibility constraints (i.e., ZMP and friction cone conditions) (see Fig. 2.4). The optimal and desired COM trajectories generated by the MPC algorithm are sent to the lower-level nonlinear controllers of Section 2.3 for the tracking purpose.

2.4.1 Reduced-Order LIP Model

The LIP model can be described by the following ODEs [109]

$$\begin{bmatrix} \ddot{r}_x^{\text{COM}} \\ \ddot{r}_y^{\text{COM}} \end{bmatrix} = \frac{g_0}{r_z^{\text{COM}}} \begin{bmatrix} r_x^{\text{COM}} - u_x^{\text{COP}} \\ r_y^{\text{COM}} - u_y^{\text{COP}} \end{bmatrix}, \quad (2.14)$$

where $r^{\text{COM}} := \text{col}(r_x^{\text{COM}}, r_y^{\text{COM}}) \in \mathbb{R}^2$ denotes the Cartesian coordinates of the COM with respect to the inertial world frame, projected onto the xy -plane, r_z^{COM} represents the constant height of the COM, g_0 is the gravitational constant, and $u^{\text{COP}} := \text{col}(u_x^{\text{COP}}, u_y^{\text{COP}}) \in \mathbb{R}^2$ denotes the Cartesian coordinates of the COP. From (2.14), the net GRF applied to the COM can be expressed as

$$F_{\text{net}} := \sum_{\ell \in \mathcal{C}} F_\ell = m_{\text{tot}} \text{col}(\ddot{r}_x^{\text{COM}}, \ddot{r}_y^{\text{COM}}, g_0), \quad (2.15)$$

in which m_{tot} represents the total mass of the robot. By defining the LIP state vector

$$x^{\text{COM}} := \text{col}(r_x^{\text{COM}}, \dot{r}_x^{\text{COM}}, r_y^{\text{COM}}, \dot{r}_y^{\text{COM}}) \in \mathbb{R}^4 \quad (2.16)$$

and employing the zero-order hold (ZOH) discretization approach for the sampling time T_d , the ODEs in (2.14) can be discretized as follows

$$x^{\text{COM}}[k+1] = A_d x^{\text{COM}}[k] + B_d u^{\text{COP}}[k], \quad (2.17)$$

where $k \in \mathbb{Z}_{\geq 0}$ represents a non-negative integer with $A_d \in \mathbb{R}^{4 \times 4}$ and $B_d \in \mathbb{R}^{4 \times 2}$ being the state and input matrices, respectively.

2.4.2 Steering Problem

We are interested in steering the discrete-time dynamics (2.17) from an initial state to a final state over M continuous-time domains. We define the *domain indicator function* as $\zeta : \mathbb{Z}_{\geq 0} \rightarrow \{1, 2, \dots, M\}$ by $\zeta[k] := \lfloor \frac{k}{N_d} \rfloor + 1$ for $0 \leq k < MN_d$ and $\zeta[k] := M$ for $k \geq MN_d$ to assign the domain index for every time sample $k \in \mathbb{Z}_{\geq 0}$. Here, $\lfloor \cdot \rfloor$ represents the floor function. For the feasibility of the model, we assume that the input $u^{\text{COP}}[k]$ lies in the support polygon which is defined as the convex hull of the contacting points with the ground. That is,

$$u^{\text{COP}}[k] \in \mathcal{U}_{\zeta[k]} \quad (2.18)$$

for all $k \in \mathbb{Z}_{\geq 0}$, where $\mathcal{U}_{\zeta[k]} \subset \mathbb{R}^2$ is the corresponding convex hull for the domain $\zeta[k]$ (see Fig. 2.5). If we define the *contact coordinates matrix* for the domain $\zeta[k]$ as $C_{\zeta[k]}$ whose columns represent the Cartesian coordinates of the contacting feet with the ground, $u^{\text{COP}}[k] \in \mathcal{U}_{\zeta[k]}$ is equivalent to the existence of a time-varying vector $\lambda[k]$ such that

$$\mathbf{0} \leq \lambda[k] \leq \mathbf{1}, \quad \mathbf{1}^\top \lambda[k] = 1, \quad u^{\text{COP}}[k] = C_{\zeta[k]} \lambda[k]. \quad (2.19)$$

We remark that in our notation, $\mathbf{0}$ and $\mathbf{1}$ denote vectors whose elements are zero and one, respectively. In addition, for the feasibility of the LIP model, the net force must lie in the

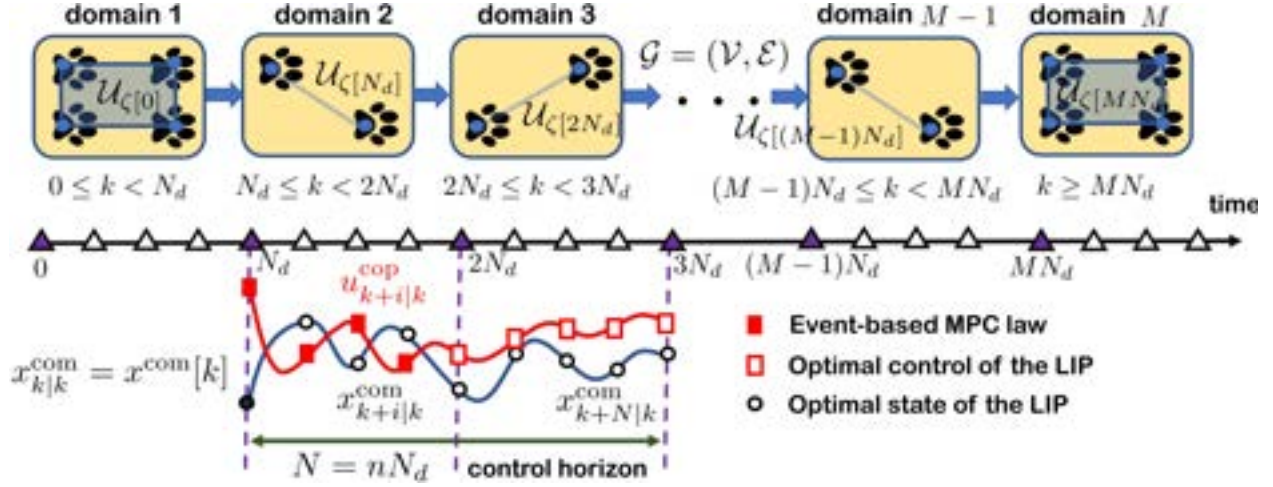


Figure 2.5: Illustration of a locomotion pattern with the corresponding graph $\mathcal{G} = (\mathcal{V}, \mathcal{E})$ and event-based MPC law.

friction cone, i.e., $F_{\text{net}} \in \mathcal{FC}$. This latter condition together with (2.14) can be expressed as

$$\Phi x^{\text{COM}}[k] + \Psi u^{\text{COP}}[k] \leq \eta, \quad \forall k \in \mathbb{Z}_{\geq 0} \quad (2.20)$$

for some proper Φ and Ψ matrices and some proper η vector.

Problem 1 (Optimal Steering Problem). *For a given locomotion graph \mathcal{G} , a phase index function ζ , a set of known contact coordinates matrices $\{C_{\zeta[k]}\}_{k \in \mathbb{Z}_{\geq 0}}$, an initial state x_0^{COM} , a final state x_f^{COM} , and a steering time $T_f \in \mathbb{Z}_{\geq 0}$, the optimal steering problem consists of finding an optimal sequence of control (i.e., COP) inputs $u^{\text{COP}}[k]$ for $0 \leq k \leq T_f - 1$ that steer (2.17) from x_0^{COM} to x_f^{COM} subject to (2.19) and (2.20).*

2.4.3 Event-Based MPC

To address Problem 1, we set up an event-based MPC that is solved at the beginning of each domain (i.e., event) with some control horizon $N = nN_d$ and $n \geq 1$. In particular, for every time sample $k = mN_d$ with $m \in \mathbb{Z}_{\geq 0}$, we consider the following finite-time optimal control problem

$$\begin{aligned} \min_{U_{k \rightarrow k+N-1|k}^{\text{COP}}} \mathcal{J}_k \left(x^{\text{COM}}[k], U_{k \rightarrow k+N-1|k}^{\text{COP}} \right) &= p \left(x_{k+N|k}^{\text{COM}} \right) + \sum_{i=0}^{N-1} \mathcal{L} \left(x_{k+i|k}^{\text{COM}}, u_{k+i|k}^{\text{COP}} \right) \\ \text{s.t.} \quad x_{k+i+1|k}^{\text{COM}} &= A_d x_{k+i|k}^{\text{COM}} + B_d u_{k+i|k}^{\text{COP}} \\ \Phi x_{k+i|k}^{\text{COM}} + \Psi u_{k+i|k}^{\text{COP}} &\leq \eta \\ u_{k+i|k}^{\text{COP}} &\in \mathcal{U}_{\zeta[k+i]}, \quad i = 0, 1, \dots, N-1, \end{aligned} \quad (2.21)$$

where $U_{k \rightarrow k+N-1|k}^{\text{COP}} := \text{col}(u_{k|k}^{\text{COP}}, \dots, u_{k+N-1|k}^{\text{COP}})$ and $x_{k+i|k}^{\text{COM}}$ represents the estimated state vector at time $k+i$ predicted at time k according to the recursive law $x_{k+i+1|k}^{\text{COM}} = A_d x_{k+i|k}^{\text{COM}} + B_d u_{k+i|k}^{\text{COP}}$ starting from the current state $x_{k|k}^{\text{COM}} := x^{\text{COM}}[k]$. In an analogous manner, $u_{k+i|k}^{\text{COP}}$ denotes the COP input at time $k+i$ computed at time k . Furthermore, $p(x_{k+N|k}^{\text{COM}})$ and $\mathcal{L}(x_{k+i|k}^{\text{COM}}, u_{k+i|k}^{\text{COP}})$ are the terminal and stage costs, respectively, defined as $p(x_{k+N|k}^{\text{COM}}) := \|x_{k+N|k}^{\text{COM}} - d_{k+N|k}^{\text{COM}}\|_P^2$ and $\mathcal{L}(x_{k+i|k}^{\text{COM}}, u_{k+i|k}^{\text{COP}}) := \|x_{k+i|k}^{\text{COM}} - d_{k+i|k}^{\text{COM}}\|_Q^2 + \|u_{k+i|k}^{\text{COP}}\|_R^2$ for some positive definite matrices $P \in \mathbb{R}^{4 \times 4}$, $Q \in \mathbb{R}^{4 \times 4}$, and $R \in \mathbb{R}^{2 \times 2}$, in which $\|z\|_P^2 := z^\top P z$. In our notation, $d_{k+i|k}^{\text{COM}}$ represents a desired state trajectory for $x_{k+i|k}^{\text{COM}}$ that is smooth in i (e.g., linear) while starting at the current state $x^{\text{COM}}[k]$ and ending at the final state x_f^{COM} . Let $U_{k \rightarrow k+N-1|k}^* := \text{col}(u_{k|k}^{*\text{COP}}, \dots, u_{k+N-1|k}^{*\text{COP}})$ be the optimal solution of the problem (2.21). Then in our proposed approach, the first N_d components of $U_{k \rightarrow k+N-1|k}^*$, that correspond to the time samples of the current continuous-time domain, are employed to the system (2.17) (see Fig. 2.5), that is,

$$u^{\text{COP}}[k+j] = u_{k+j|k}^{*\text{COP}}, \quad j = 0, 1, \dots, N_d - 1. \quad (2.22)$$

Remark 2.1. We remark that the MPC formulation (2.21) together with (2.19) can be expressed as QP in terms of the decisions variables $\{x_{k+i|k}^{\text{COM}}\}_{i=1}^N$, $\{u_{k+i|k}^{\text{COP}}\}_{i=0}^{N-1}$, and $\{\lambda_{k+i|k}\}_{i=0}^{N-1}$ to retain the sparsity structure of [201]. To make the cost function of this QP positive definite in terms of all decision variables, one can add a term corresponding to $\lambda_{k+i|k}$, i.e., $\mathcal{J}_k = p(x_{k+N|k}^{\text{COM}}) + \sum_{i=0}^{N-1} \mathcal{L}(x_{k+i|k}^{\text{COM}}, u_{k+i|k}^{\text{COP}}) + \mathcal{H}(\lambda_{k+i|k})$, where $\mathcal{H}(\lambda_{k+i|k}) := \|\lambda_{k+i|k} - \lambda_{k+i|k}^{\text{des}}\|_{\hat{R}}^2$ for some desired trajectory $\lambda_{k+i|k}^{\text{des}}$ and some positive definite matrix \hat{R} .

2.5 Numerical Simulations

The objective of this section is to numerically verify the effectiveness of the theoretical results. We consider five different directions (i.e., forward, backward, sideways, diagonal, and in-place) of trot gaits with start and stop conditions whose graphs \mathcal{G} consist of $M = 20$ continuous-time domains (see Fig. 2.5). We choose the sampling time to discretize the LIP dynamics as $T_d = 80$ (ms) with $N_d = 4$ grids per each domain. The control horizon for the event-based MPC is chosen as $N = nN_d = 8$ which considers two domains ahead. We have observed that for every T_d in $[60, 80]$ (ms) with $N_d = 4$, the proposed control scheme can stabilize the locomotion patterns. Since we prefer to have longer duration for domains of locomotion such that the lower-level controller has enough time to track the prescribed optimal motion by the MPC, we choose $T_d = 80$ (ms). The control horizon N can also be chosen to include more than two domains, but this will increase the number of decision variables and the computation time. In addition, for $N = N_d = 4$ –which only considers the current domain– the event-based MPC cannot stabilize the motion. Hence, we choose $N = 2N_d = 8$. The other parameters are taken as $P = 10^3 I_{4 \times 4}$, $Q = I_4$, $R = I_{2 \times 2}$, and $\hat{R} = 0.01I$. With the height of the COM being 0.5 (m) and the friction coefficient $\mu = 0.4$, the higher-level MPC is solved in an event-based manner, that is approximately

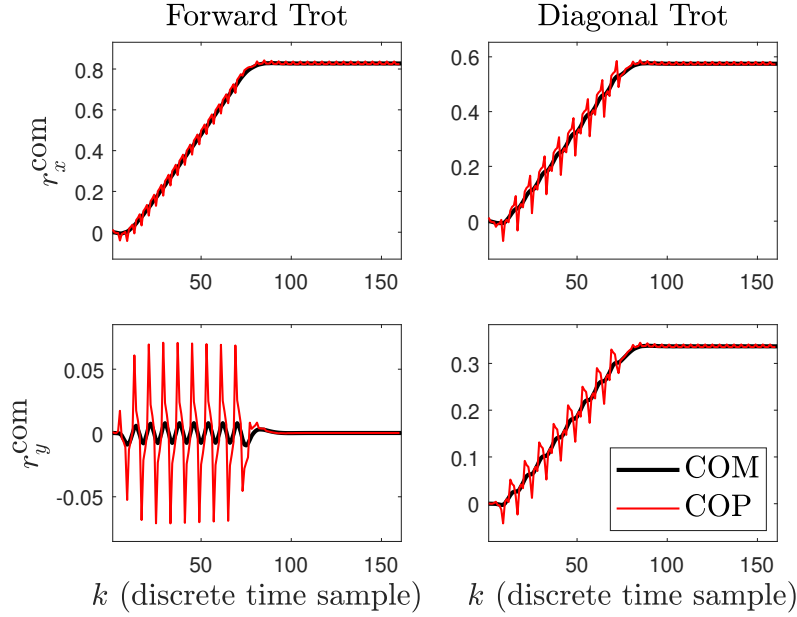


Figure 2.6: Plot of the COM and COP trajectories for the forward and diagonal trot gaits of the reduced-order system. Convergence to the target points $(0.82, 0)$ and $(0.58, 0.34)$ is clear.

every $N_d T_d = 0.32$ seconds. For the first, middle, and last domains, the MPC has 64, 72, and 80 decision variables, respectively, as the dimension of $\lambda_{k+i|k}$ changes per domain.

Figure 2.6 depicts the evolution of the COM and COP for the forward and diagonal trot gaits of the discrete-time dynamics with the step lengths of $(10, 0)$ (cm) and $(7, 4)$ (cm) in \mathbb{R}^2 , respectively. Here, we make use of ECOS QP [59] to solve the MPC in MATLAB. Convergence to the target (final) points $(0.82, 0)$ and $(0.58, 0.34)$ is clear. Target points are chosen as the geometric center of the contact points in the last domain. We remark that the proposed MPC problem of this work has less computational load compared to [57] with $\frac{1}{3}$ of the number of decision variables that are optimized at a slower rate. Next, we study the full-order model of the robot in RaiSim [105] with rigid contact models. The lower-level QP for I-O linearization has 37 decision variables for both double- and quadruple-contact domains, which is approximately 50% of the number of decisions variables used for the higher-level QP. The lower-level QP is solved with qpSWIFT [150] in RaiSim and $\gamma = 10^7$ at every 1 (ms). The computation time of the MPC on a laptop computer with an Intel(R) Core(TM) i7-5600U CPU 2.60GHz (2 cores) and 8GB of RAM is 0.2528 (ms). The low-level QP problem for the double- and quadruple-contact domains also takes 0.2334 (ms) and 0.4735 (ms), respectively. All state components of the robot, except the absolute Cartesian coordinates of the torso (i.e., p_b), are measurable by an inertial measurement unit as well as encoders. Analogous to the approach of [28], we utilize a Kalman filter to estimate p_b . Figures 2.7(a) and 2.7(b) illustrate the evolution of the virtual constraints and torque inputs (i.e., before the gear ratio) for the full-order model of the forward and diagonal trot gaits with the maximum speed of

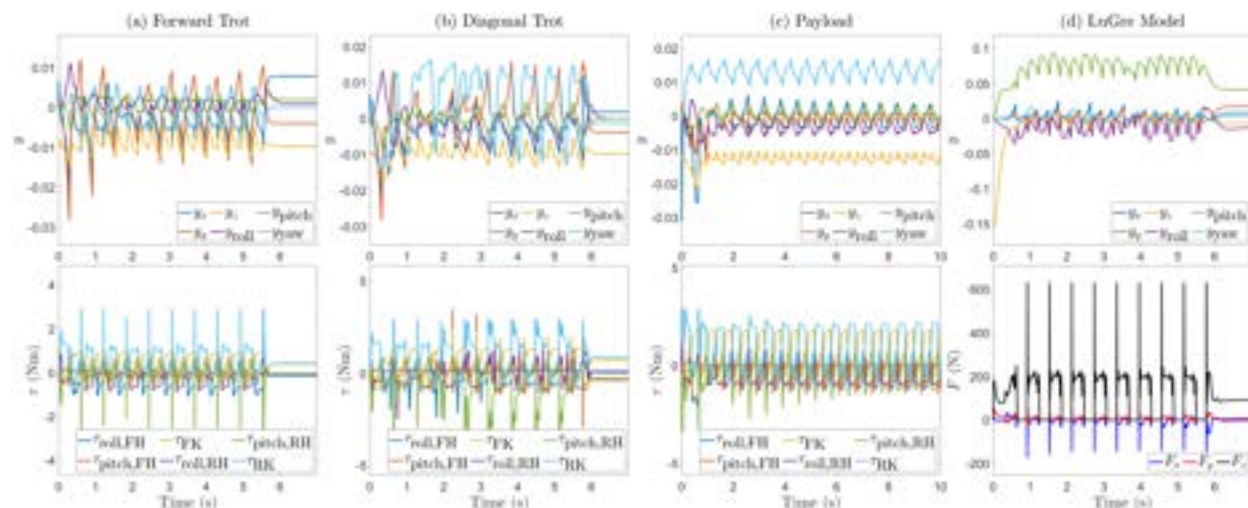


Figure 2.7: Plot of the virtual constraints and torque inputs in RaiSim for (a) forward trot, (b) diagonal trot, and (c) forward trot with payloads. Here, y_x , y_y , y_z , y_{roll} , y_{pitch} , y_{yaw} denote the first six components of the virtual constraints that relate to the absolute position and orientation of the body. In addition, FH, FK, RH, and RK stand for the front hip, front knee, rear hip, and rear knee of the left-hand-side of the robot, respectively. The subscripts “roll” and “pitch” for the torque plots also denote the roll and pitch motions of the hip joints. (d) Plot of the virtual constraints and torques for trot gait subject to the LuGre contact model in MATLAB/Simulink when the control frequency is reduced to 500 Hz with a delay of 2 (ms) in solving QPs.

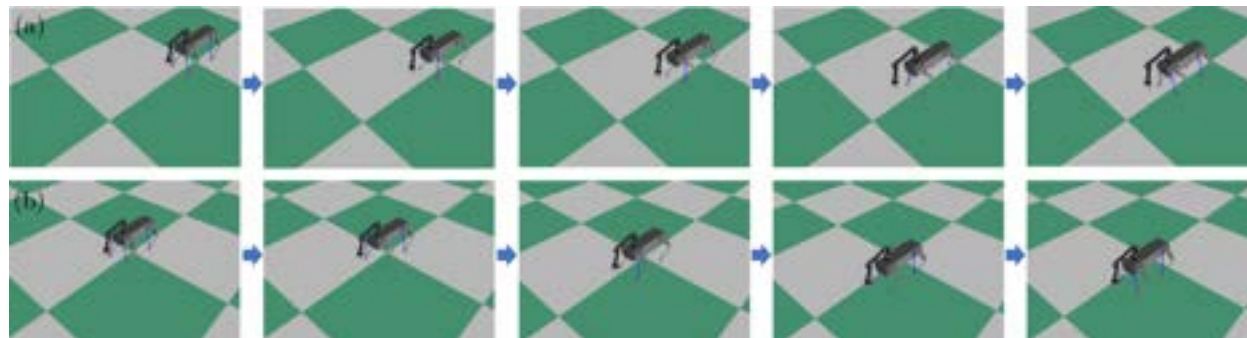


Figure 2.8: Snapshots of (a) the forward trot gait and (b) the diagonal trot gait with the proposed event-based MPC and QP-based virtual constraint controller.

0.3 (m/s). Snapshots of the forward and diagonal trot gaits can be found in Figs. 2.8(a) and 2.8(b), respectively. To show the robustness of the control system against different contact models, the full-order model is also simulated in MATLAB/Simulink with LuGre contact models [55]. The robot still travels in a stable and robust manner towards the target. To



Figure 2.9: Snapshots of the forward trot gait with an unknown payload of 12 (kg) on the robot’s torso and an unknown payload of 1.4 (kg) at the robot’s EE.

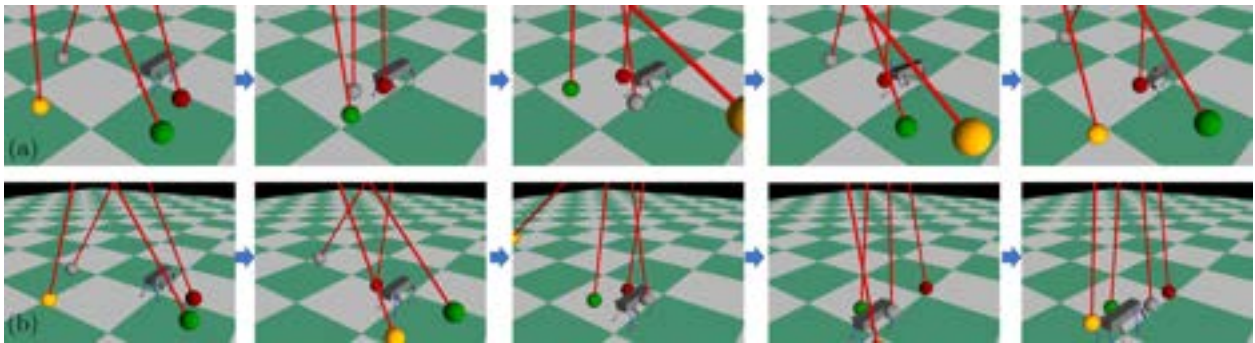


Figure 2.10: (a) Snapshots of the unstable locomotion with an MPC that is only solved once at the beginning of the gait. (b) Snapshots of the robustly stable locomotion with the proposed event-based MPC in the presence of unknown disturbances.

demonstrate the robustness of the proposed control algorithm against the control frequency as well as time delays, we next assume that the control frequency is reduced from 1 kHz to 500 Hz while there is a latency of 2 (ms) in solving QPs. Figure 2.7(d) illustrates the virtual constraints profile and the GRFs in one of the stance legs for this case.

Robustness Analysis: To demonstrate the robustness of the closed-loop system against payloads, we assume that there are two payloads on the robot whose masses are *not* known for the controller: a payload of 1.4 (kg) in the robot’s EE together with a payload of 12 (kg) on the torso (40% uncertainty in the total mass). Figure 2.7(c) illustrates the evolution of the virtual constraints and torques inputs versus time. It is observed that the robot is capable of rejecting the effect of uncertainties in the total mass during locomotion. The snapshots of the numerical simulation can be found in Fig. 2.9.

To show the robustness of the proposed controller against external forces acting on the robot, we study three different scenarios in RaiSim. In the first and second simulations, we consider persistent external forces along the x - (i.e., direction walking) and y -axes (i.e., lateral direction), respectively. The forces are taken as sinusoidal disturbance inputs with the period of $0.5\pi = 1.57$ (s), where the magnitudes along the x - and y -axes are chosen as 30 (N) and 8 (N), respectively. In the third simulation, we investigate the balance control of the robot while being pushed from the sides. More specifically, we make use of 4 pendulums with the

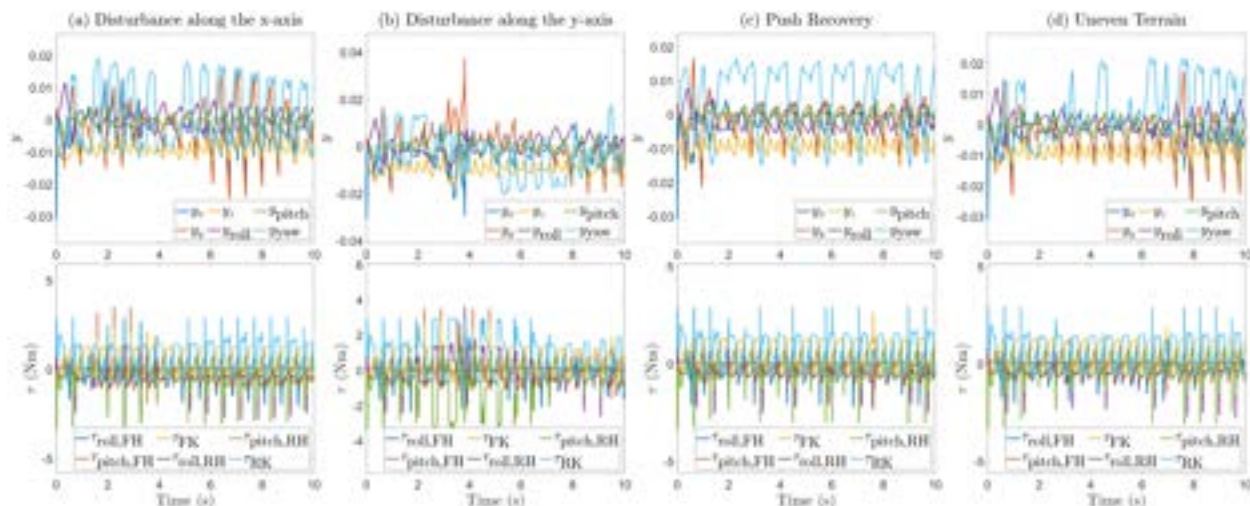


Figure 2.11: Plot of the virtual constraints and torque inputs of the full-order closed-loop system in RaiSim for forward trot with (a) and (b) external disturbances, (c) external push, and (d) ground height variations.

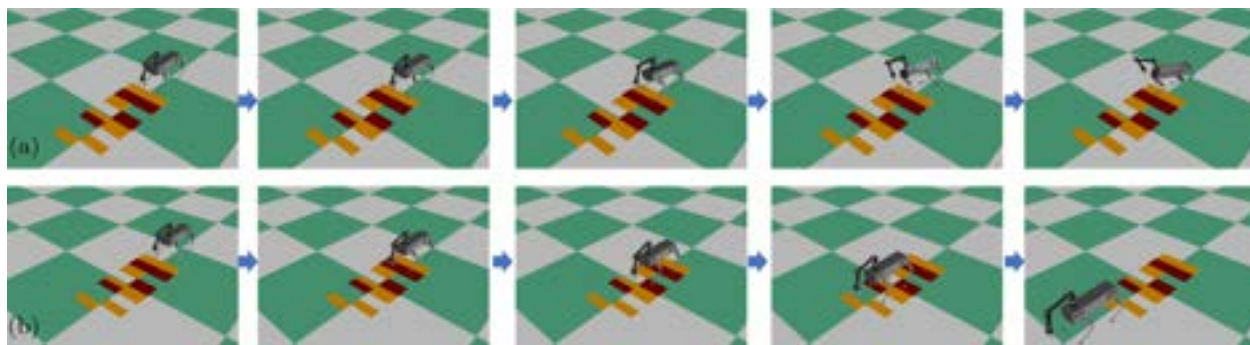


Figure 2.12: (a) Snapshots of the unstable locomotion with an MPC that is only solved once at the beginning of the gait. (b) Snapshots of the robustly stable locomotion with the proposed event-based MPC in the presence of ground height variations.

mass of 3 (kg) and length of 2.5 (m) that hit the robot during locomotion. The snapshots of these simulations can be found in 2.10(b). It is observed that the robot is capable of stable locomotion subject to the above-mentioned external forces. Figures 2.11(a)-(c) depict the evolution of the virtual constraints and torque inputs versus time. To compare the performance of the event-based MPC with an MPC algorithm that is only solved once at the beginning of the gait, Fig. 2.10(a) presents additional simulations. We observe that the closed-loop system becomes unstable if the MPC is only solved once.

To illustrate the robustness of the controller against ground height variations, we finally consider a random sequence of ground heights in the discrete set $\{\pm 1, \pm 2\}$ (cm) over 150

domains of blind locomotion. The time evolution of the outputs and inputs is depicted in Fig. 2.11(d). The snapshots of these simulations are depicted in Fig. 2.12(b). Figure 2.10(a) also represents additional simulations to compare the performance of the closed-loop system with the event-based MPC and an MPC that is only solved once. It is clear that the event-based MPC can stabilise the system in the presence of disturbances. Animations of these simulations can be found online¹.

2.6 Summary

This chapter introduced a hierarchical control scheme for quadrupedal locomotion based on convex optimization, event-based MPC, and virtual constraints. At the higher level of the control scheme, the event-based MPC computes the optimal trajectory for the COM of the LIP model to steer the robot from an initial state to a final state while the net GRF is feasible. It was shown that one would *not* need to employ the MPC at every time sample to stabilize the locomotion. The MPC can instead be employed in an event-based manner at the beginning of each domain to stabilize the target point. This significantly reduces the complexity for real-time implementation of MPC techniques. The lower-level controller then fills the gap between the reduced- and full-order dynamics. In particular, we formulated a QP-based I-O linearization approach to impose the full-order dynamics to follow the optimal COM trajectory of the reduced-order model while tracking the desired footholds with feasible individual GRFs. The effectiveness and robustness of the proposed control scheme were demonstrated via numerical simulations of a full-order model for a 22 DOF quadrupedal robot in the presence of payloads, external disturbances, ground height variations, and different contact models. The framework can systematically address a range of locomotion patterns such as forward, backward, lateral, diagonal, and in-place gaits.

In the next chapter, we will extend the concept of event-based MPC for cooperative locomotion of multi-agent legged robots.

¹<https://youtu.be/RJT7kJaONCc>

Part II

Cooperative Locomotion via Supervisory MPC and Distributed Nonlinear Controllers

Chapter 3

Collaborative Locomotion with Supervisory MPC

3.1 Introduction

Legged robots can form collaborative robot (co-robot) teams that assist humans in labor-intensive tasks such as construction, manufacturing, and assembly. The evolution of legged robots that cooperatively manipulate/transport objects can be described by high-dimensional and inherently unstable complex systems. Although powerful computational approaches have allowed the deployment of distributed control algorithms for complex robot systems, state-of-the-art techniques are tailored to the control of [multi-robot systems \(MRSs\)](#) (see e.g., [191, 209]) composed of collaborative robotic arms and multi-fingered hands [143], aerial vehicles [184, 193], and ground vehicles [33, 50, 138], but *not* sophisticated legged machines that cooperatively transport objects.

The objective of this chapter is to develop a hierarchical computational algorithm to enable the real-time planning and control of collaborative locomotion for multiagent legged robotic systems that carry objects. The higher-level of the proposed algorithm employs a supervisory control, based on event-based [Model Predictive Control \(MPC\)](#), to generate optimal trajectories for individual agents. In particular, the MPC is formulated for the optimal control of an interconnected network of holonomically constrained reduced-order systems, developed based on [Linear Inverted Pendulum \(LIP\)](#) models, subject to having feasible individual [Ground Reaction Force \(GRF\)](#)s. To reduce the gap between the network of reduced- and full-order complex models of collaborative locomotion, distributed nonlinear controllers, based on [Quadratic Programming \(QP\)](#) and virtual constraints, are implemented at the lower level of the proposed algorithm to impose the full-order dynamics of each agent to asymptotically track the optimal trajectories while keeping the GRFs at all contacting leg ends in the friction cone. The lower-level controller was developed in Section 2.3, and here, it is integrated with the supervisory MPC. It is shown that the proposed control approach can generate and robustly stabilize collaborative locomotion patterns for multiagent quadrupedal robotic systems in the presence of model uncertainties arising from unknown payloads and ground height variations.

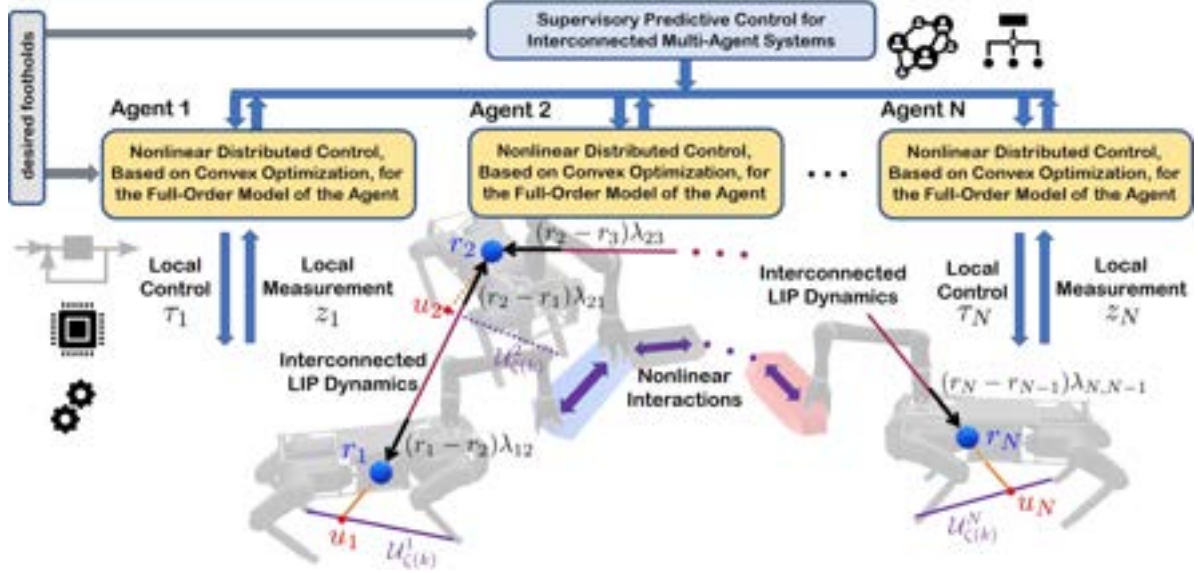


Figure 3.1: Overview of the proposed hierarchical nonlinear control algorithm for collaborative locomotion of legged robots subject to holonomic constraints. The figure also illustrates the concept of the interconnected LIP dynamics.

3.2 Interconnected LIP Dynamics

The objective of this section is to derive an interconnected network of reduced-order models for the cooperative locomotion of $N \geq 2$ legged co-robots that carry an object. The reduced-order network, referred to as the *interconnected LIP dynamics*, will be utilized for the real-time trajectory planning in Section 3.3. Here, we consider an open path graph for the network of LIP dynamics with N vertices and $N - 1$ edges. In particular, all inner vertices have degree 2 except the end vertices 1 and N that have degree 1 (see Fig. 3.1). The vertices of the graph represent the agents, and the edges represent interconnection between agents. In our notation, $\mathcal{N}(i)$ denotes the set of all agents that are adjacent to the agent $i \in \mathcal{V} := \{1, \dots, N\}$.

Remark 3.1 (Path Graphs). The reason for the assumption of open path graph is to simplify the presentation of the interaction forces and the interconnected LIP dynamics in Theorem 3.4. This also allows us to easily present the proposed control scheme.

We consider the following LIP dynamics [109] for the locomotion of the agent $i \in \mathcal{V}$

$$\ddot{r}_i = \frac{g}{\ell}(r_i - u_i) + \frac{1}{m}f_i, \quad (3.1)$$

where $r_i := \text{col}(r_i^x, r_i^y) \in \mathbb{R}^2$ represents the Cartesian coordinates of the COM of the agent i in the horizontal plane with respect to the inertial world frame, ℓ denotes the height of

the COM, g is the gravitational constant, $u_i := \text{col}(u_i^x, u_i^y) \in \mathbb{R}^2$ represents the Cartesian coordinates of the center of pressure (COP), $f_i \in \mathbb{R}^2$ denotes the external force on the COM of the agent i , and m is the total mass of the agent.

Assumption 3.2 (Rigidity). *We suppose that there are holonomic constraints amongst the adjacent agents as follows:*

$$\|r_i - r_j\|^2 := (r_i - r_j)^\top (r_i - r_j) = c_{ij}, \quad (3.2)$$

for all $i = 1, \dots, N-1$, $j = i+1$ and some constants $c_{ij} > 0$. The forces between agents i and $j \in \mathcal{N}(i)$ are further assumed to be $f_{ij} = -f_{ji} = (r_i - r_j) \lambda_{ij}$, where λ_{ij} denotes the Lagrange multipliers with the symmetry property $\lambda_{ij} = \lambda_{ji}$ (see Fig. 3.1).

We remark that from Assumption 3.2 as well as the symmetry condition, there are $N-1$ independent Lagrange multipliers λ_{ij} to be determined. For future purposes, we show these independent Lagrange multipliers as a vector $\boldsymbol{\lambda} := \text{col}(\lambda_{ij} \mid i = 1, \dots, N-1, j = i+1) \in \mathbb{R}^{N-1}$, where “col” represents the column operator. Throughout this chapter, the boldface variables will correspond to the global variables of the interconnected LIP network.

Remark 3.3. Assumption 3.2 considers the holonomic constraints amongst the COMs of the adjacent agents as the LIP dynamics cannot address the moments about the COM. In particular, the addition of robotic manipulators to the reduced-order model can result in moments around the COM generated by the arms. Hence, the interconnected LIP dynamics do not include the manipulator models. However, we remark that the full-order dynamical model of cooperative locomotion in Section 3.5 will consider the holonomic constraints amongst the manipulators’ end effectors (EEs). We further assume that the EE’s motion with respect to the body is almost static. The numerical results of Section 3.5 will show the adequacy and validity of this assumption for the development of the supervisory MPC. The numerical results will also show that the proposed control algorithms can bridge the gap between the developed interconnected LIP model and the detailed full-order model. Section 3.6.2 will discuss this assumption and the results with more details.

Using these assumptions, the interconnected network of LIP dynamics can be expressed as

$$\ddot{r}_i = \frac{g}{\ell}(r_i - u_i) + \frac{1}{m} \sum_{j \in \mathcal{N}(i)} (r_i - r_j) \lambda_{ij}, \quad i \in \mathcal{V} \quad (3.3)$$

subject to the holonomic constraints (3.2). For future purposes, we define the augmented position, velocity, and control input vectors as $\boldsymbol{r} := \text{col}(r_i \mid i \in \mathcal{V}) \in \mathbb{R}^{2N}$, $\dot{\boldsymbol{r}} := \text{col}(\dot{r}_i \mid i \in \mathcal{V}) \in \mathbb{R}^{2N}$, and $\boldsymbol{u} := \text{col}(u_i \mid i \in \mathcal{V}) \in \mathbb{R}^{2N}$. By differentiating the holonomic constraint (3.2) twice along the trajectories of (3.3), we get

$$(r_i - r_j)^\top (\ddot{r}_i - \ddot{r}_j) + \|\dot{r}_i - \dot{r}_j\|^2 = 0. \quad (3.4)$$

Combining (3.3) and (3.4) then results in

$$\begin{aligned} & \frac{g}{\ell} \|r_i - r_j\|^2 - \frac{g}{\ell} (r_i - r_j)^\top (u_i - u_j) + \|\dot{r}_i - \dot{r}_j\|^2 \\ & + \frac{(r_i - r_j)^\top}{m} \left\{ \sum_{l \in \mathcal{N}(i)} (r_i - r_l) \lambda_{il} - \sum_{k \in \mathcal{N}(j)} (r_j - r_k) \lambda_{jk} \right\} = 0, \end{aligned}$$

for all $i = 1, \dots, N-1$ and $j = i+1$ which can be written in a compact form to solve for the Lagrange multipliers $\boldsymbol{\lambda}$, i.e.,

$$\boldsymbol{\Lambda}_N(\mathbf{r}) \boldsymbol{\lambda} = \mathbf{b}(\mathbf{r}, \dot{\mathbf{r}}, \mathbf{u}). \quad (3.5)$$

Here, $\boldsymbol{\Lambda}_N \in \mathbb{R}^{(N-1) \times (N-1)}$ is a symmetric matrix as follows:

$$\begin{bmatrix} 2\|e_{12}\|^2 & -e_{12}^\top e_{23} & 0 & 0 & \cdots & 0 \\ -e_{23}^\top e_{12} & 2\|e_{23}\|^2 & -e_{23}^\top e_{34} & 0 & \cdots & 0 \\ 0 & -e_{34}^\top e_{23} & 2\|e_{34}\|^2 & -e_{34}^\top e_{45} & \cdots & 0 \\ \vdots & \vdots & \vdots & \vdots & \ddots & \vdots \\ 0 & 0 & 0 & 0 & \cdots & 2\|e_{N-1,N}\|^2 \end{bmatrix},$$

in which $e_{ij} := r_i - r_j \in \mathbb{R}^2$. In addition, $\mathbf{b} := \text{col}(b_i \mid i = 1, \dots, N-1) \in \mathbb{R}^{N-1}$, where $b_i := \frac{mg}{\ell} (r_i - r_j)^\top (u_i - u_j) - \frac{mg}{\ell} \|r_i - r_j\|^2 - m \|\dot{r}_i - \dot{r}_j\|^2$ with $j = i+1$. In what follows, we study the conditions under which there is a unique solution $\boldsymbol{\lambda}$ for the algebraic equation (3.5).

Theorem 3.4 (Uniqueness of $\boldsymbol{\lambda}$). *Suppose that $N \geq 2$ and Assumption 3.2 is met. Then, the matrix $\boldsymbol{\Lambda}_N(\mathbf{r})$ is positive definite if $r_i \neq r_j$ (or, equivalently, $e_{ij} \neq 0$) for all $i \in \mathcal{V}$ and $j \in \mathcal{N}(i)$.*

Proof. Let us take an arbitrary nonzero vector $\alpha := \text{col}(\alpha_1, \dots, \alpha_{N-1})$. Then, $\alpha^\top \boldsymbol{\Lambda}_N \alpha$ can be expanded as

$$\begin{aligned} \alpha^\top \boldsymbol{\Lambda}_N \alpha &= \|e_{12}\|^2 \alpha_1^2 + \|e_{N-1,N}\|^2 \alpha_{N-1}^2 \\ &+ \sum_{k=1}^{N-2} \{ \|e_{k,k+1}\|^2 \alpha_k^2 - 2e_{k,k+1}^\top e_{k+1,k+2} \alpha_k \alpha_{k+1} + \|e_{k+1,k+2}\|^2 \alpha_{k+1}^2 \} \\ &\geq \|e_{12}\|^2 \alpha_1^2 + \|e_{N-1,N}\|^2 \alpha_{N-1}^2 \\ &+ \sum_{k=1}^{N-2} \{ \|e_{k,k+1}\|^2 \alpha_k^2 - 2\|e_{k,k+1}\| \|e_{k+1,k+2}\| |\alpha_k| |\alpha_{k+1}| + \|e_{k+1,k+2}\|^2 \alpha_{k+1}^2 \} \\ &= \|e_{12}\|^2 \alpha_1^2 + \|e_{N-1,N}\|^2 \alpha_{N-1}^2 + \sum_{k=1}^{N-2} (\|e_{k,k+1}\| |\alpha_k| - \|e_{k+1,k+2}\| |\alpha_{k+1}|)^2 > 0, \quad (3.6) \end{aligned}$$

where in the fourth line, we have made use of the norm property, that is, $e_{k,k+1}^\top e_{k+1,k+2} \alpha_k \alpha_{k+1} \leq \|e_{k,k+1}\| \|e_{k+1,k+2}\| |\alpha_k| |\alpha_{k+1}|$. We remark that the last result in (3.6) is indeed positive. To clarify this point, let us assume that the $|\alpha_k| = \frac{\|e_{k+1,k+2}\|}{\|e_{k,k+1}\|} |\alpha_{k+1}|$ for all $k = 1, \dots, N-2$. Then $\sum_{k=1}^{N-2} (\|e_{k,k+1}\| |\alpha_k| - \|e_{k+1,k+2}\| |\alpha_{k+1}|)^2 = 0$. However, because of the term $\|e_{12}\|^2 \alpha_1^2 + \|e_{N-1,N}\|^2 \alpha_{N-1}^2$, the quadratic function $\alpha^\top \mathbf{\Lambda}_N \alpha$ is strictly positive which completes the proof. \square

Using Theorem 3.4, the Lagrange multipliers can be solved as $\boldsymbol{\lambda} = \mathbf{\Lambda}_N^{-1}(\mathbf{r}) \mathbf{b}(\mathbf{r}, \dot{\mathbf{r}}, \mathbf{u})$ which in combination with (3.3) results in the following compact and nonlinear equations of motion

$$\ddot{\mathbf{r}} = \frac{g}{\ell}(\mathbf{r} - \mathbf{u}) + \frac{1}{m} \mathbf{L}(\boldsymbol{\lambda}) \mathbf{r}, \quad (3.7)$$

where $\mathbf{L}(\boldsymbol{\lambda}) := [L_{ij}] \in \mathbb{R}^{2N \times 2N}$ is a weighted Laplacian matrix with the blocks $L_{ij} \in \mathbb{R}^{2 \times 2}$ for $1 \leq i, j \leq N$ such that $L_{ii} := (\sum_{k \in \mathcal{N}(i)} \lambda_{ik}) I_2$, $L_{ij} := -\lambda_{ij} I_2$ for $j \in \mathcal{N}(i)$, and $L_{ij} := 0_2$ for $j \notin \mathcal{N}(i)$. Here, I_2 and 0_2 denote the identity and zero matrices of order 2, respectively. We remark that according to the construction procedure, the state manifold for the interconnected LIP dynamics can be expressed as

$$\mathcal{M} := \{(\mathbf{r}, \dot{\mathbf{r}}) \mid \|e_{ij}\|^2 = c_{ij}, e_{ij}^\top \dot{e}_{ij} = 0, i \in \mathcal{V}, j \in \mathcal{N}(i)\},$$

for some $c_{ij} > 0$ which is invariant under the flow of (3.7). In addition, we can show that \mathcal{M} is a $2N + 2$ -dimensional embedded submanifold of \mathbb{R}^{4N} .

Example 3.5. For the case of two agents, the interconnected LIP dynamics can be expressed as the following nonlinear system

$$\begin{aligned} \ddot{r}_1 &= \frac{g}{\ell}(r_1 - u_1) - \frac{g}{2\ell}(r_1 - r_2) + \frac{g(r_1 - r_2)(r_1 - r_2)^\top (u_1 - u_2)}{2\ell \|r_1 - r_2\|^2} - \frac{(r_1 - r_2) \|\dot{r}_1 - \dot{r}_2\|^2}{2 \|r_1 - r_2\|^2} \\ \ddot{r}_2 &= \frac{g}{\ell}(r_2 - u_2) + \frac{g}{2\ell}(r_1 - r_2) - \frac{g(r_1 - r_2)(r_1 - r_2)^\top (u_1 - u_2)}{2\ell \|r_1 - r_2\|^2} + \frac{(r_1 - r_2) \|\dot{r}_1 - \dot{r}_2\|^2}{2 \|r_1 - r_2\|^2}. \end{aligned} \quad (3.8)$$

By defining the augmented state vector $\mathbf{x} := \text{col}(\mathbf{r}, \dot{\mathbf{r}}) \in \mathbb{R}^{4N}$, the nonlinear state equation for the coupled LIP dynamics can be expressed as $\dot{\mathbf{x}} = \mathbf{f}(\mathbf{x}, \mathbf{u})$, where $\mathbf{f} : \mathcal{M} \times \mathbb{R}^{2N} \rightarrow \text{T}\mathcal{M}$ is differentiable and $\text{T}\mathcal{M}$ denotes the tangent bundle of the manifold \mathcal{M} . In addition, the continuous-time dynamics can be discretized using the Euler approach as follows:

$$\begin{aligned} \mathbf{x}[k+1] &= \mathbf{x}[k] + T_s \mathbf{f}(\mathbf{x}[k], \mathbf{u}[k]) \\ &=: \mathcal{F}(\mathbf{x}[k], \mathbf{u}[k]), \end{aligned} \quad (3.9)$$

in which T_s denotes the sampling time and $\mathbf{x}[k]$ and $\mathbf{u}[k]$ represent the state vector and control inputs at the time sample $k \in \mathbb{Z}_{\geq 0} := \{0, 1, \dots\}$, respectively.

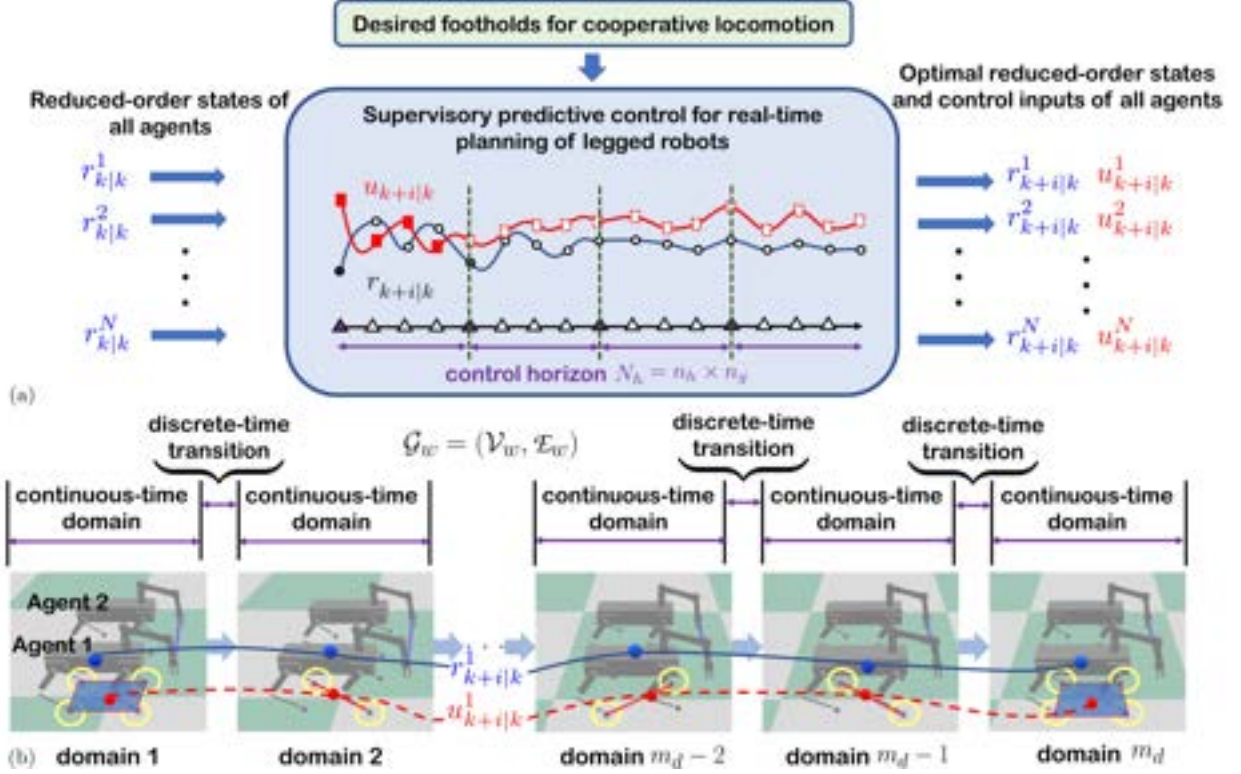


Figure 3.2: (a) Illustration of the proposed supervisory predictive control. Here, agents share their actual and reduced-order states with the higher-level supervisory control. The supervisory control then optimizes for the COM motions subject to the interconnected LIP dynamics and feasibility conditions. (b) Illustration of the directed cycle to represent the locomotion pattern of each agent with different continuous-time domains. Snapshot of the cooperative locomotion highlights different domains for each agent.

3.3 Supervisory Predictive Control

The objective of this section is to develop a supervisory control algorithm, based on the interconnected LIP dynamics, MPC, and convex optimization, to effectively plan and coordinate multi-agent legged robots in real-time.

Models of legged locomotion are hybrid and can be illustrated as directed graphs. In this representation, continuous-time dynamics are represented by vertices of the graph to describe the evolution of the system by the Lagrangian dynamics. The edges of the graph then represent the instantaneous and discrete-time transitions amongst the continuous-time dynamics to model the possible and abrupt changes in the state vector according to the rigid impacts of the leg ends with the environment. In this chapter, we consider a general locomotion (walking) pattern for the quadrupedal agents with start and stop conditions as a directed graph $\mathcal{G}_w = (\mathcal{V}_w, \mathcal{E}_w)$ (see Fig. 3.2), where the vertices set \mathcal{V}_w represents the

continuous-time domains (e.g., double-, triple-, and quadruple-contact domains) and edges set $\mathcal{E}_w \subset \mathcal{V}_w \times \mathcal{V}_w$ denotes the discrete-time transitions (e.g., impacts and take-offs) (see Fig. 3.2b). We further suppose that there are $m_d \geq 1$ continuous-time domains and each continuous-time domain consists of $n_g \geq 1$ grid points (i.e., time samples) (see Fig. 3.2a). In this chapter, we consider a general *aperiodic* locomotion pattern. Hence, domains are enumerated to show the successive continuous-time domains from start to stop. Consequently, there can be two distinct domains with the same stance legs (e.g., domains 2 and $m_d - 1$ in Fig. 3.2b). The domain indicator function is then defined as $\zeta : \mathbb{Z}_{\geq 0} \rightarrow \{1, 2, \dots, m_d\}$ by $\zeta(k) := \lfloor \frac{k}{n_g} \rfloor + 1$ for $0 \leq k < m_d n_g$ and $\zeta(k) := m_d$ for $k \geq m_d n_g$ to assign the domain index for every time sample. Here, $\lfloor \cdot \rfloor$ represents the floor function.

For the feasibility of the interconnected LIP model, we assume that all local control inputs (i.e., COPs) $u_i[k]$ for $i \in \mathcal{V}$ lie in a time-varying support polygon which is defined as the convex hull of the contacting points with the ground. That is,

$$u_i[k] \in \mathcal{U}_{\zeta(k)}^i, \quad \forall k \in \mathbb{Z}_{\geq 0}, \quad \forall i \in \mathcal{V}, \quad (3.10)$$

in which $\mathcal{U}_{\zeta(k)}^i \subset \mathbb{R}^2$ is the corresponding support polygon for the agent i in the domain $\zeta(k)$ (see Fig. 3.1). In addition, the net GRF acting on the COM of the agent i must be in the friction cone. This latter condition together with (3.1) and (3.7) can be expressed as the following nonlinear inequality constraints

$$\mathbf{c}_{\text{ineq}}(\mathbf{x}[k], \mathbf{u}[k]) \leq 0, \quad \forall k \in \mathbb{Z}_{\geq 0}. \quad (3.11)$$

Problem 2 (Real-Time Planning of Agents). *Let us consider the locomotion pattern \mathcal{G}_w with a given set of desired footholds encoded in the convex hulls (i.e., support polygons) $\mathcal{U}_{\zeta(k)}^i$ for all agents $i \in \mathcal{V}$. For a given initial state $\mathbf{x}_0 \in \mathcal{M}$ and final state $\mathbf{x}_f \in \mathcal{M}$, the planning problem consists of finding an optimal augmented control input $\mathbf{u}[k]$ in real time that steers the interconnected LIP dynamics (3.9) from \mathbf{x}_0 to \mathbf{x}_f subject to the constraints (3.10) and (3.11).*

Remark 3.6 (Computation of Footholds). We remark that the desired footholds are computed at the beginning of the locomotion and are used during the locomotion to form the support polygons in Problem 2. One way to compute the desired footholds is as follows. We can first consider a straight line connecting the initial position of each agent to its final position in the horizontal plane. We then generate a sequence of footholds along this line via a proper step length.

To address Problem 2, we consider a supervisory predictive control that has access to the global positions (i.e., reduced-order states) of all agents (i.e., r_i for $i \in \mathcal{V}$) via a direct communication network [191]. We then extend the event-based MPC approach of Chapter 2—that generates optimal trajectories for locomotion of a single agent—to address the motion planning problem for cooperative locomotion of multi-agent robots. In the proposed approach,

the supervisory predictive control is solved at the event samples, taken at the beginning of continuous-time domains, to reduce the computational burden of the networked system.

Remark 3.7 (Supervisory MPC). The supervisory predictive control can be either solved on one of the agents' onboard computers or all agents' computers. The first approach would result in a heterogeneous team with a leader, and the latter one would result in a homogeneous team. In the first approach, the supervisory MPC is solved at the beginning of each continuous-time domain for the leader. In contrast, in the second approach, the MPC is solved at the beginning of continuous-time domains for each agent. Although the first approach generally requires less computation burden than the second one, our numerical results show that both of these techniques are computationally tractable for cooperative locomotion of a team of legged robots with up to four agents. In particular, the computation time for the supervisory MPC in these techniques takes less than 1 (ms) (see Section 3.5 for details).

The nonlinear interconnected LIP dynamics in (3.9) are linearized at the event samples to formulate a convex optimization problem. More specifically, we consider an affine approximation of (3.9) at the event sample $k = l n_g$ for some integer $l \geq 0$ to estimate the future states as follows:

$$\begin{aligned} \mathbf{x}_{k+j+1|k} &= \mathbf{A} \mathbf{x}_{k+j|k} + \mathbf{B} \mathbf{u}_{k+j|k} + \mathbf{d}, \quad j = 0, 1, \dots, N_h - 1 \\ \mathbf{x}_{k|k} &= \mathbf{x}[k], \end{aligned} \quad (3.12)$$

where $N_h = n_h n_g$ denotes the control horizon for some positive integer $n_h \geq 1$, $\mathbf{x}_{k+j|k}$ represents the estimated state of the interconnected LIP network model at time $k+j$ predicted at time k , and $\mathbf{u}_{k+j|k}$ denotes the input of the LIP network (i.e., COPs) at time $k+j$ computed at time k . In addition, the Jacobian matrices and affine term are computed from (3.9) and updated at every event sample according to

$$\begin{aligned} \mathbf{A} &:= \frac{\partial \mathcal{F}}{\partial \mathbf{x}}(\mathbf{x}[k], \mathbf{u}[k-1]) \in \mathbb{R}^{4N \times 4N} \\ \mathbf{B} &:= \frac{\partial \mathcal{F}}{\partial \mathbf{u}}(\mathbf{x}[k], \mathbf{u}[k-1]) \in \mathbb{R}^{4N \times 2N} \\ \mathbf{d} &:= \mathcal{F}(\mathbf{x}[k], \mathbf{u}[k-1]) - \mathbf{A} \mathbf{x}[k] - \mathbf{B} \mathbf{u}[k-1] \in \mathbb{R}^{4N}. \end{aligned} \quad (3.13)$$

An analogous technique can be used to estimate (3.11) as the following affine inequality

$$\Phi \mathbf{x}_{k+j|k} + \Psi \mathbf{u}_{k+j|k} + \boldsymbol{\eta} \leq 0, \quad j = 0, 1, \dots, N_h - 1. \quad (3.14)$$

We then formulate a convex MPC problem over the control horizon N_h to steer (3.12) from

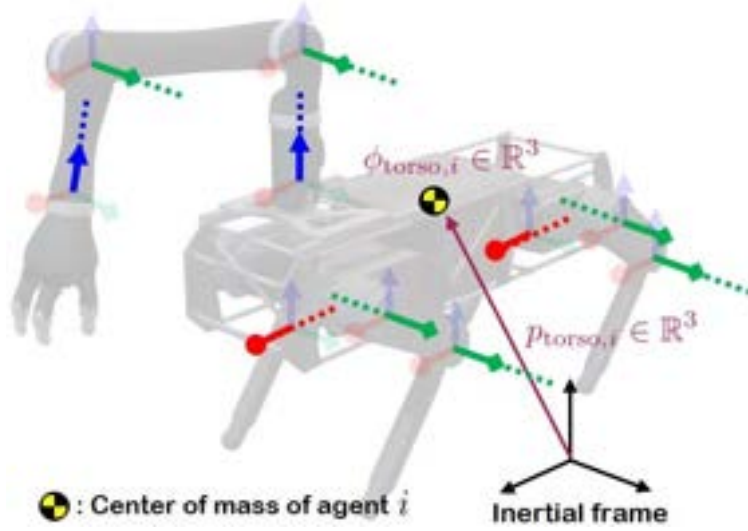


Figure 3.3: Illustration of 22 DOFs for the full-order model of each robotic agent. The agents are composed of the 18-DOF quadrupedal robot Vision 60 plus the 4-DOF Kinova arm.

$\mathbf{x}_0 \in \mathcal{M}$ to $\mathbf{x}_f \in \mathcal{M}$ subject to (3.10) and (3.14), that is,

$$\begin{aligned} \min_{\mathbf{U}_{k+N_h-1|k}} \quad & p(\mathbf{x}_{k+N_h|k}) + \sum_{j=0}^{N_h-1} \mathcal{L}(\mathbf{x}_{k+j|k}, \mathbf{u}_{k+j|k}) \\ \text{s.t.} \quad & \text{Dynamics (3.12) and inequalities (3.10) and (3.14),} \end{aligned} \quad (3.15)$$

where $\mathbf{U}_{k+N_h-1|k} := \text{col}(\mathbf{u}_{k|k}, \dots, \mathbf{u}_{k+N_h-1|k}) \in \mathbb{R}^{2N_h}$. Here, the terminal and stage cost functions are given by $p(\mathbf{x}_{k+N_h|k}) := \|\mathbf{x}_{k+N_h|k} - \mathbf{x}_{k+N_h|k}^{\text{des}}\|_{\mathbf{P}}^2$ and $\mathcal{L}(\mathbf{x}_{k+j|k}, \mathbf{u}_{k+j|k}) := \|\mathbf{x}_{k+j|k} - \mathbf{x}_{k+j|k}^{\text{des}}\|_{\mathbf{Q}}^2 + \|\mathbf{u}_{k+j|k}\|_{\mathbf{R}}^2$, respectively, for some positive definite matrices $\mathbf{P} \in \mathbb{R}^{4N \times 4N}$, $\mathbf{Q} \in \mathbb{R}^{4N \times 4N}$, and $\mathbf{R} \in \mathbb{R}^{2N \times 2N}$. In addition, $\mathbf{x}_{k+j|k}^{\text{des}}$ denotes a desired state trajectory and $\|z\|_{\mathbf{P}}^2 := z^\top \mathbf{P} z$. We remark that the supervisory event-based MPC can be translated into QP. Let $(\mathbf{x}_{k+j|k}^*, \mathbf{u}_{k+j|k}^*)$ denote the optimal solution over the control horizon. Then the optimal COM trajectory of the agents over one continuous-time domain (i.e., $\mathbf{x}_{k+j|k}^*$ for $j = 0, \dots, n_g - 1$) will be utilized as the reference trajectory to be tracked by the low-level distributed controllers in Section 3.4. The MPC problem will be solved again at the beginning of the next continuous-time domain.

3.4 Distributed Virtual Constraint Controllers

The objective of this section is to present the low-level distributed controllers to impose the full-order dynamical models of individual agents to asymptotically track the optimal reduced-order trajectories prescribed by the supervisory predictive control while having fea-

sible contact forces. Here, we extend the virtual constraints controller of Chapter 2 for the development of distributed controllers for multi-agent systems. More specifically, the distributed low-level controller formulates the I-O linearization problem as a QP that addresses the feasibility of each agent’s individual GRFs at the contacting leg ends while tracking the optimal COM trajectories for collaborative locomotion and desired swing leg path of each agent. We remark that, unlike the supervisory MPC, the distributed low-level controller only considers the full-order dynamical model of each agent. Hence, it does not require the full state measurements of the other agents.

Each legged agent is assumed to consist of the 18-DOF quadrupedal robot Vision 60, manufactured by Ghost Robotics¹, plus a 4-DOF Kinova arm for the locomotion and manipulation purposes. The total mass of this augmented agent is 35 (kg). The DOFs on Vision 60 are composed of 6 underactuated DOFs for the absolute position and orientation of the robot plus 12 actuated DOFs associated with the legs. More specifically, each leg of the robot consists of 3 actuated DOFs for the hip roll, hip pitch, and knee joints. All DOFs of the Kinova arm are further assumed to be actuated. The detailed view of the joint arrangement and DOFs of the robot are represented in Fig. 3.3. In our notation for distributed controllers, the local configuration vector and local control inputs (i.e., joint-level torques) for the agent $i \in \mathcal{V}$ are denoted by

$$q_i := \text{col}(p_{\text{torso},i}, \phi_{\text{torso},i}, q_{\text{body},i}) \in \mathbb{R}^{22} \quad (3.16)$$

and $\tau_i \in \mathbb{R}^{16}$, respectively, where $p_{\text{torso},i} \in \mathbb{R}^3$ and $\phi_{\text{torso},i} \in \mathbb{R}^3$ describe the absolute position and orientation of the torso for the agent i with respect to the inertial frame (see Fig. 3.3). The remaining portion, $q_{\text{body},i} \in \mathbb{R}^{16}$ then represents the body joint variables of the robot that form the shape of the robot. Finally, let

$$z_i = \text{col}(q_i, \dot{q}_i) \in \mathbb{R}^{44} \quad (3.17)$$

and $F_i \in \mathbb{R}^{3\ell_{c,i}}$ denote the local full states and contact forces at the leg ends of the agent. Here, $\ell_{c,i}$ represents the number of contacting legs with the ground.

We now define the following local holonomic outputs to be regulated for the motion control of the agent i

$$y_i(z_i, t) := h_0(q_i) - h_{d,i}(t), \quad (3.18)$$

where $h_0(q_i)$ represents the set of holonomic quantities to be controlled, referred to as the controlled variables, and $h_{d,i}(t)$ denotes the desired evolution of the controlled variables. The controlled variables, $h_0(q_i)$, are chosen as the orientation of the agent (i.e., roll, pitch, and yaw) together with its COM position, the Cartesian coordinates of the swing leg ends, and the Cartesian coordinates of the manipulator’s EE in the inertial world frame. The desired evolution of the COM position in $h_{d,i}(t)$ is defined as a Bézier polynomial [164] that passes through the discrete and optimal reduced-order trajectory generated by the supervisory predictive control. In particular, we consider a Bézier polynomial whose coefficients are

¹<https://www.ghostrobotics.io/>

solved via least-squares at the beginning of each domain such that the polynomial has the best fit to the optimal COM trajectory of the agent i for the current domain. For the swing leg ends, $h_{d,i}(t)$ is taken as a Bézier foot trajectory in the task space starting from the previous foothold with zero velocity and ending at the next preplanned foothold with zero velocity. Finally, the desired evolution for the EE's Cartesian coordinates is chosen as the desired COM trajectory plus a constant vector representing the EE's position with respect to the torso.

To compute the local control torques τ_i , we consider the full-order and *floating-base* dynamics of the agent i *without* considering the interaction forces arising from manipulation. Although the low-level distributed controllers do not consider the interaction forces amongst the EE and objects for simplifying the controller synthesis, the full-order simulation models of the cooperative locomotion in Section 3.5 will consider these interacting forces to illustrate the validity of this assumption and robustness of the proposed control algorithms. We now consider the following local dynamics for the controller synthesis

$$D_i(q_i) \ddot{q}_i + H_i(q_i, \dot{q}_i) = \Upsilon_i \tau_i + J_{c,i}^\top(q_i) F_i, \quad (3.19)$$

where $D_i(q_i) \in \mathbb{R}^{22 \times 22}$ denotes the positive definite mass-inertia matrix of the agent i , $H_i(q_i, \dot{q}_i) \in \mathbb{R}^{22}$ represents the Coriolis, centrifugal, and gravitational forces of the agent i , and $\Upsilon_i \in \mathbb{R}^{22 \times 16}$ is the input distribution matrix. Furthermore, $J_{c,i}(q_i) \in \mathbb{R}^{3\ell_{c,i} \times 22}$ represents the contact Jacobian matrix. For future purposes, the local dynamics (3.19) can be written in the state-space form as follows:

$$\begin{aligned} \dot{z}_i &= \begin{bmatrix} \dot{q}_i \\ -D_i^{-1} H_i \end{bmatrix} + \begin{bmatrix} 0 \\ D_i^{-1} \Upsilon_i \end{bmatrix} \tau_i + \begin{bmatrix} 0 \\ D_i^{-1} J_{c,i}^\top \end{bmatrix} F_i \\ &=: f_i(z_i) + g_i(z_i) \tau_i + w_i(z_i) F_i. \end{aligned} \quad (3.20)$$

Differentiating the local output y_i in (3.18) along the full-order dynamics of the agent i described in (3.20) results in the following output dynamics

$$\begin{aligned} \ddot{y}_i &= L_{g_i} L_{f_i} y_i(z_i, t) \tau_i + L_{w_i} L_{f_i} y_i(z_i, t) F_i + L_{f_i}^2 y_i(z_i, t) + \frac{\partial^2 y_i}{\partial t^2}(z_i, t) \\ &= -K_P y_i - K_D \dot{y}_i, \end{aligned} \quad (3.21)$$

where $L_{g_i} L_{f_i} y_i$, $L_{w_i} L_{f_i} y_i$, and $L_{f_i}^2 y_i$ are Lie derivatives that are used for I-O linearization [106], and K_P and K_D are positive definite matrices. Closed-form expressions for the Lie

derivatives can be expressed as follows:

$$\begin{aligned}
L_{g,i}L_{f,i}y_i(z_i) &= \frac{\partial h_0(q_i)}{\partial q_i} D_i^{-1}(q_i) \Upsilon_i \\
L_{w,i}L_{f,i}y_i(z_i) &= \frac{\partial h_0(q_i)}{\partial q_i} D_i^{-1}(q_i) J_{c,i}^\top(q_i) \\
L_{f,i}^2 y_i(z_i) &= \frac{\partial}{\partial q_i} \left(\frac{\partial h_0(q_i)}{\partial q_i} \dot{q}_i \right) \dot{q}_i - \frac{\partial h_0(q_i)}{\partial q_i} D_i^{-1} H(q_i, \dot{q}_i).
\end{aligned} \tag{3.22}$$

In addition, the local controller assumes a rigid contact model between the stance leg ends of the agent and the ground. In particular, the acceleration of the stance leg ends is assumed to be zero which can be expressed as

$$\ddot{p}_i = J_{c,i}(q_i) \ddot{q}_i + \frac{\partial}{\partial q} (J_{c,i}(q_i) \dot{q}_i) \dot{q}_i = 0, \tag{3.23}$$

where p_i denotes the Cartesian coordinates of the stance leg ends. The condition in (3.23) along with the local dynamics (3.19) yields the following affine condition in (τ_i, F_i)

$$\ddot{p}_i = L_{g_i}L_{f_i}p_i(z_i) \tau_i + L_{w_i}L_{f_i}p_i(z_i) F_i + L_{f_i}^2 p_i(z_i) = 0, \tag{3.24}$$

where the Lie derivatives can be written as follows:

$$\begin{aligned}
L_{g_i}L_{f_i}p_i(z_i) &= J_{c,i}(q_i) D_i^{-1}(q_i) \Upsilon_i \\
L_{w_i}L_{f_i}p_i(z_i) &= J_{c,i}(q_i) D_i^{-1}(q_i) J_{c,i}^\top(q_i) \\
L_{f_i}^2 p_i(z_i) &= \frac{\partial}{\partial q_i} (J_{c,i}(q_i) \dot{q}_i) \dot{q}_i - J_{c,i}(q_i) D_i^{-1}(q_i) H(q_i, \dot{q}_i).
\end{aligned}$$

In order to solve for the local torques τ_i , we are interested in solving for (τ_i, F_i) subject to (3.21) and (3.24) such that 1) the contact forces belong to the friction cone (i.e., $F_i \in \mathcal{FC}$) while having feasible torques (i.e., $\tau_{\min} \leq \tau \leq \tau_{\max}$), and 2) the local torques are minimum 2-norm. Hence, we set up the following set of distributed real-time QPs that can be solved at 1kHz

$$\begin{aligned}
\min_{(\tau_i, F_i, \delta)} & \frac{1}{2} \|\tau_i\|^2 + \frac{\omega}{2} \|\delta\|^2 \\
\text{s.t.} & L_{g_i}L_{f_i}y_i \tau_i + L_{w_i}L_{f_i}y_i F_i + L_{f_i}^2 y_i + \frac{\partial^2 y_i}{\partial t^2} + \delta = -K_P y_i - K_D \dot{y}_i \\
& L_{g_i}L_{f_i}p_i \tau_i + L_{w_i}L_{f_i}p_i F_i + L_{f_i}^2 p_i = 0 \\
& F_i \in \mathcal{FC}, \quad \tau_{\min} \leq \tau \leq \tau_{\max}.
\end{aligned} \tag{3.25}$$

Here, δ is a defect variable added to the output dynamics (3.21) to guarantee the existence

of a feasible solution in two different scenarios. 1) If the coefficient matrix loses rank at particular configurations, there may not be a pair of control torques and GRFs, i.e., (τ_i, F_i) , that satisfies (3.21) and (3.24). To tackle this issue, we introduce the defect variable δ to make the equality constraints feasible. 2) If the torques and GRFs, i.e., (τ_i, F_i) , do not belong to the admissible sets (i.e., the inequality constraints are violated), the defect variable δ can again help us to find a feasible solution. To reduce the effect of the defect variable δ on the output dynamics, we minimize its 2-norm via a large weighting factor in the cost function. More specifically, the cost function (3.25) tries to minimize a weighted sum of the 2-norms of the local torques and the defect variable, where $\omega > 0$ is the weighting factor. We remark that using the defect variable δ , the output dynamics become $\ddot{y}_i + K_D \dot{y}_i + K_P y_i = -\delta(t)$, which is input-to-state stable (ISS) [114]. Hence, if $\delta(t)$ remains bounded, the output profile $y(t)$ will be also bounded. This will be analyzed more in the numerical simulations of Section 3.5. The optimal solutions of these QPs are finally denoted by $\tau_i = \Gamma_i(t, z_i)$ for $i \in \mathcal{V}$ and are employed as local whole-body motion controllers.

3.5 Numerical Simulations

The objective of this section is to numerically verify the effectiveness of the proposed hierarchical control algorithm for cooperative transportation of objects by a team of composite robotic agents. We study both reduced- and full-order coupled models of legged agents to show the stability of locomotion patterns for the closed-loop system. We further investigate the robustness of the closed-loop system in the presence of unknown payloads and uncertainty in the ground height profile.

Control Parameters: We consider the cooperative locomotion of two and three agents with trot gaits including start and stop domains. We have observed that for every sampling time T_s in [60, 80] (ms) with $n_g = 4$ grids per domain, the proposed control scheme can stabilize the locomotion patterns. Here, we choose $T_s = 80$ (ms). The control horizon for the supervisory predictive control is taken as $N_h = n_h n_g = 4$ which considers one domain ahead. The other parameters for the supervisory predictive control are tuned as $\mathbf{P} = 10^3 I_{4N \times 4N}$, $\mathbf{Q} = I_{4N \times 4N}$, $\mathbf{R} = 10^{-10} I_{2N \times 2N}$ which stabilize the cooperative motion. We have numerically observed that for $l \in [0.35, 0.55]$ (m), the robots behave safely, and the joint-level torques remain in an acceptable range. For the purpose of this chapter, we choose $l = 0.5$ (m). The friction coefficient is assumed to be $\mu = 0.6$. The supervisory predictive control is solved in an event-based manner (i.e., at the beginning of each domain), that is approximately every $n_g T_s = 0.32$ seconds. Analogous to Remark 2.1 in Chapter 2, we make use of a sparse QP structure to effectively solve the MPC (3.15). We can show that the number of decision variables for the sparse QP are $8NN_h$ and $10NN_h$ during the middle and start/stop domains, respectively.

Reduced-Order Coupled Models: The evolution of the COM and COP for forward trot gaits of the individual agents in the interconnected LIP dynamics with $N = 2$ and

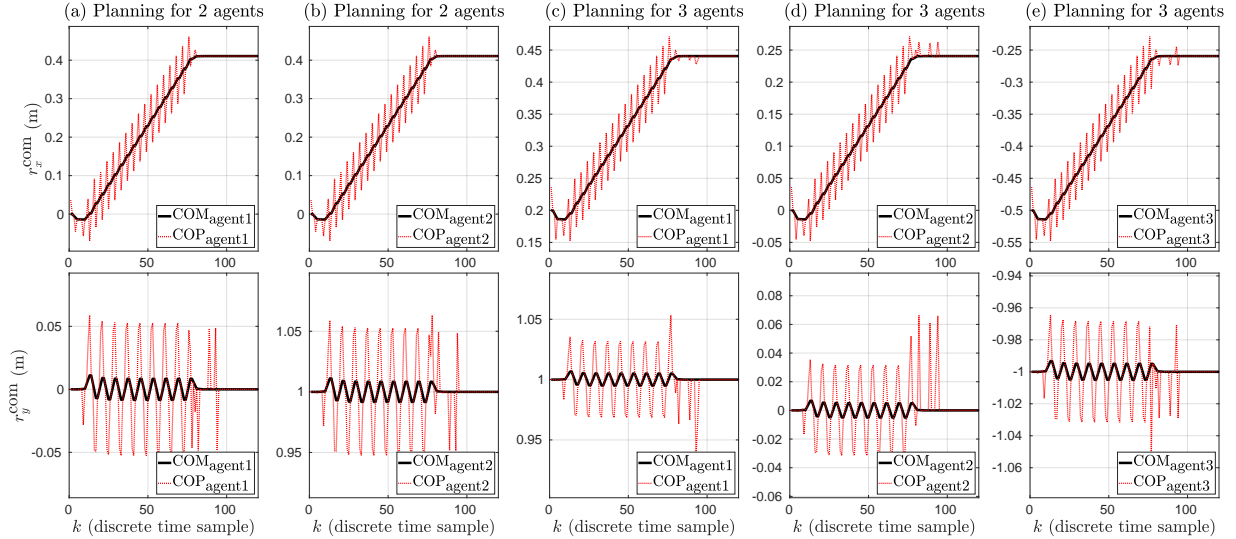


Figure 3.4: COM and COP trajectories of the individual agents in the interconnected LIP dynamics (3.9) during forward trot gaits with $N = 2$ agents ((a) and (b)) and $N = 3$ agents ((c)-(e)). Here, the optimal control inputs (i.e., COPs) are computed via the supervisory predictive control (3.15). The sampling time for the supervisory predictive control in (a)-(e) are assumed to be $T_s = 80$ (ms).

$N = 3$ agents is depicted in Fig. 3.4(a)-(b) and Fig. 3.4(c)-(e), respectively. Here we make use of MATLAB for simulating the interconnected LIP dynamics (3.9) subject to the holonomic constraints and the supervisory predictive control (3.15). The initial configurations of the LIP models are chosen as $r_1[0] = (0, 0)^\top$ (m) and $r_2[0] = (0, 1)^\top$ (m) for $N = 2$ agents. Moreover, the initial positions of the LIP models are taken as $r_1[0] = (0.2, 1)^\top$ (m), $r_2[0] = (0, 0)^\top$ (m), and $r_3[0] = (-0.5, -1)^\top$ (m) for $N = 3$ agents. The step length for $N = 2$ and $N = 3$ is chosen as $(0.05, 0)$ (m) and $(0.03, 0)$ (m) in \mathbb{R}^2 , respectively. The target points are taken as the geometric center of the contact points in the last (i.e., stop) domain. Convergence to the target points with different number of agents and after $m_d = 20$ continuous-time domains is clear.

Full-Order Coupled Models: Next, we study the full-order complex model of cooperative locomotion with the proposed hierarchical control algorithm over $m_d = 50$ domains in RaiSim [105]. Here, we assume massless bars to be carried by the EEs of Vision 60 agents augmented with Kinova arms. The contact between the bar and the EE of kinova arm is considered as a point contact. Based on this contact condition, the wrench between the object and EE of the arm only consists of the interaction forces. The QP arising from the supervisory predictive control is solved with qpSWIFT [150]. The average computation time of the higher-level QP on a laptop computer with an Intel(R) Core(TM) i7-10750H CPU 2.60GHz and 16GB RAM is 0.35 (ms) and 0.59 (ms) for $N = 2$ and $N = 3$ agents, respectively. The distributed and low-level controllers of (3.25) are also solved with qpSWIFT in 1kHz and the weighting factor ω is chosen as 10^7 .

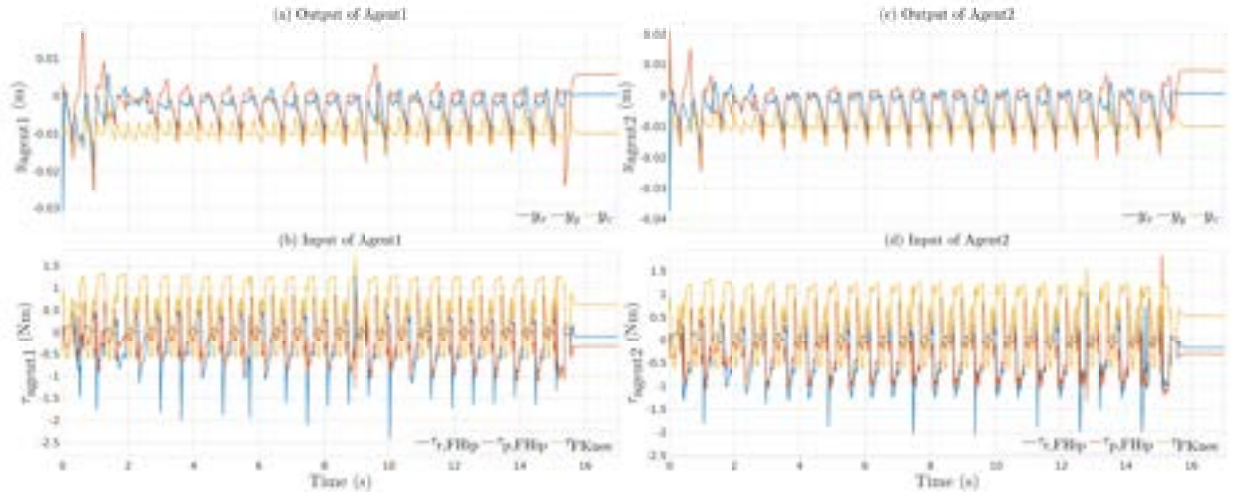


Figure 3.5: Evolution of the virtual constraints and torque inputs in RaiSim for stable forward trot gait with $N = 2$ agents. Subplots (a) and (c) illustrate the evolution of outputs whereas subplots (b) and (d) depict the evolution of torque inputs. Here, y_x , y_y , y_z denote the virtual constraints corresponding to the absolute position (i.e., x , y , and z) of the agent. In addition, the subscript “rFHip”, “pFHip”, and “FKnee” in the torque plots represent the roll torque of the front hip, pitch torque of the front hip, and pitch torque of the front knee for the left side of the robot, respectively.

The numerical simulation results for the stable cooperative locomotion of robots are provided in Figs. 3.5 and 3.6. Figures 3.5(a)-(d) and Figs. 3.6(a)-(c) illustrate the evolution of the virtual constraints and torque inputs for the individual agents during collaborative and forward trot gaits with $N = 2$ and $N = 3$ agents, respectively. Here, the speed of cooperative locomotion for two and three agents is 0.15 (m/s) and 0.1 (m/s). From these figures, we observe that the control inputs (joint-level torques) for all agents are bounded. In addition, the outputs (i.e., virtual constraints) remain bounded during the cooperative locomotion. We remark that Figs. 3.5 and 3.6 depict the first three components of the virtual constraints (i.e., y_x , y_y , and y_z) that represents the COM tracking error. In particular, these figures show that the COM of the full-order dynamical model of each agent tracks the optimal and reduced-order COM trajectory generated by the supervisory MPC. We also remark that the range of the control inputs (torques) is bounded between -5 (Nm) and 5 (Nm) by the low-level nonlinear controller. Finally, the control inputs in Figs. 3.5 and 3.6 depict the motor torques *before* the gearbox system. Figure 3.7 depicts the evolution of the 2-norm of the defect variable δ for the cooperative locomotion of two agents. From this figure, we observe that δ remains very small.

Robustness Analysis: To demonstrate the robustness of the proposed control algorithm against uncertainties, we assume that the mass of the bars between the adjacent agents’ EEs is increased to 0.5 (kg) which is *unknown* for the controller. We further assume that

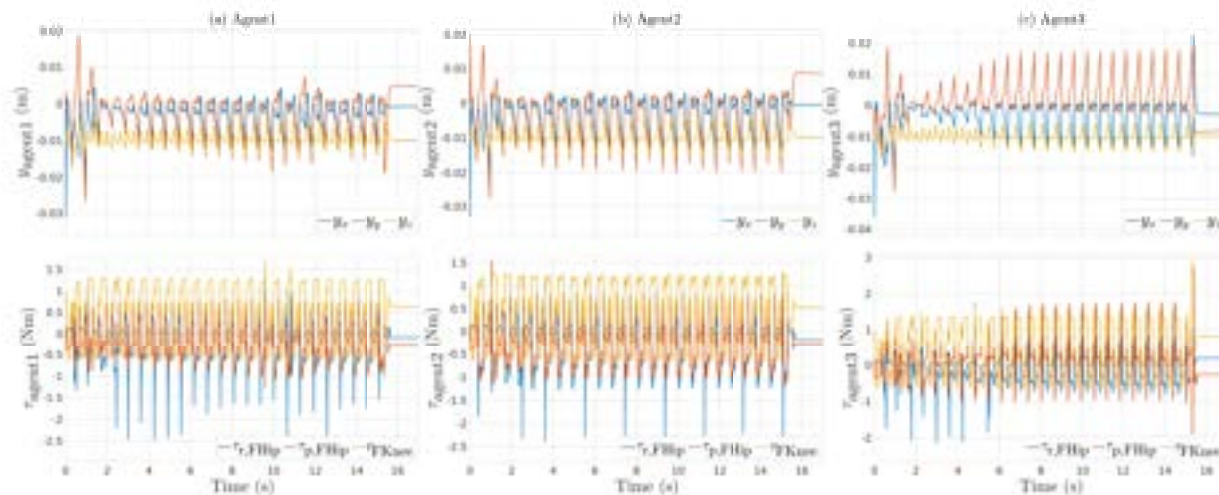


Figure 3.6: Plot of the virtual constraints and torque inputs in RaiSim for stable forward trot gait with $N = 3$ agents. Subplots (a), (b), and (c) correspond to the agents 1, 2, and 3, respectively. Subplots in the first and second rows correspond to the virtual constraints and torque inputs of each agent, respectively.

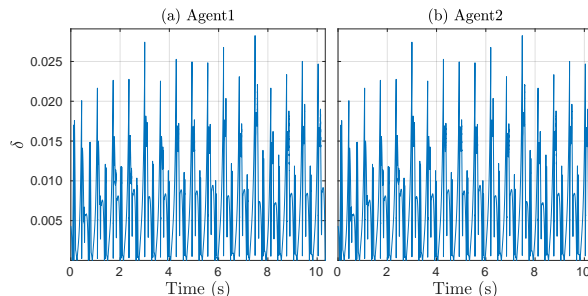


Figure 3.7: Evolution of the 2-norm of the defect variable δ in RaiSim for $N = 2$ agents. Subplots illustrate the evolution for each agent.

additional unknown payloads of 20 (kg), 34(kg), and 48(kg) are cooperatively transported by two, three, and four agents on their torsos, respectively. Figure 3.8(a)-(d) and Fig. 3.9(a)-(c) depict the evolution of the virtual constraints and torque inputs for $N = 2$ and $N = 3$ agents, respectively. Furthermore, Fig. 3.10(a)-(d) shows the evolution of the virtual constraints and torque inputs for $N = 4$ agents. From these figures, it is observed that the control inputs (i.e., torques) and outputs (i.e., virtual constraints) remain bounded during the cooperative locomotion with uncertainties. Hence, the proposed control algorithm is capable of addressing the uncertainty arising from the payload mass. To demonstrate the effectiveness of the proposed control algorithms based on the interconnected LIP dynamics, we study the same numerical simulations with the MPC control algorithm of Chapter 2, in which the MPC is designed for individual robots without considering the interconnected LIP

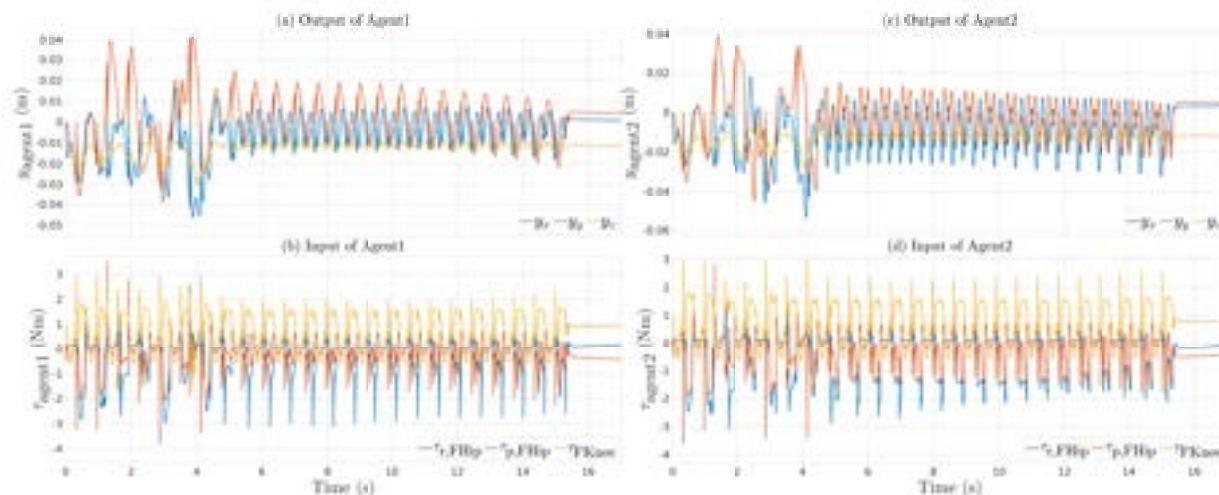


Figure 3.8: Evolution of the virtual constraints and torque inputs in RaiSim for robust trot gait subject to a payload with $N = 2$ agents. Subplots (a) and (c) illustrate the evolution of outputs whereas subplots (b) and (d) depict the evolution of torque inputs.

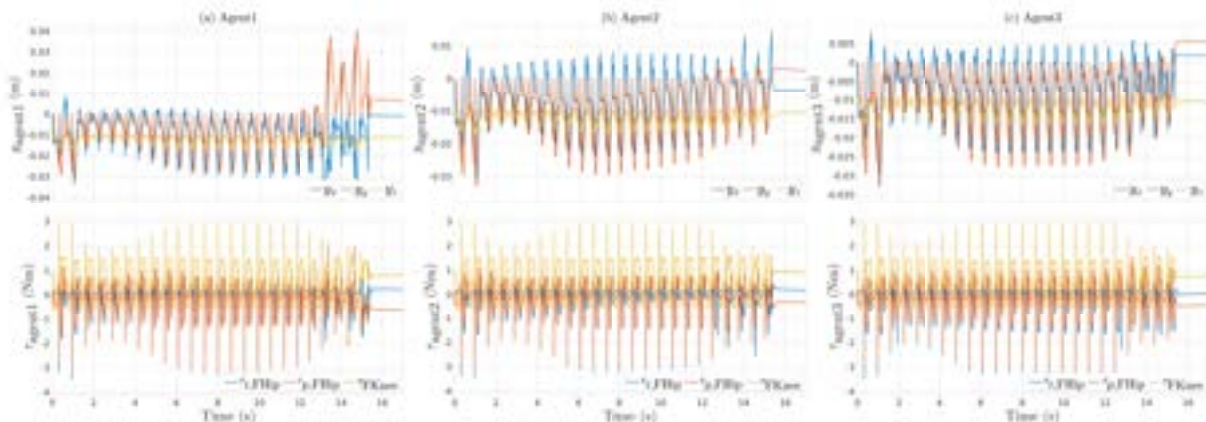


Figure 3.9: Plot of the virtual constraints and torque inputs in RaiSim for robust forward trot gait subject to a payload with $N = 3$ agents. Subplots (a), (b), and (c) correspond to the agents 1, 2, and 3, respectively. Subplots in the first and second rows correspond to the virtual constraints and torque inputs of each agent, respectively.

dynamics. Snapshots of the simulation results for cooperative locomotion of agents with and without the proposed approach of this chapter are depicted in Figs. 3.11, 3.12, and 3.13 to visualize the successes and failures. It is clear that the agents *cannot* have robustly stable cooperative locomotion while using their own MPC without considering the interconnected LIP dynamics.

To show the robustness of the controller against the change in the ground height profile, we

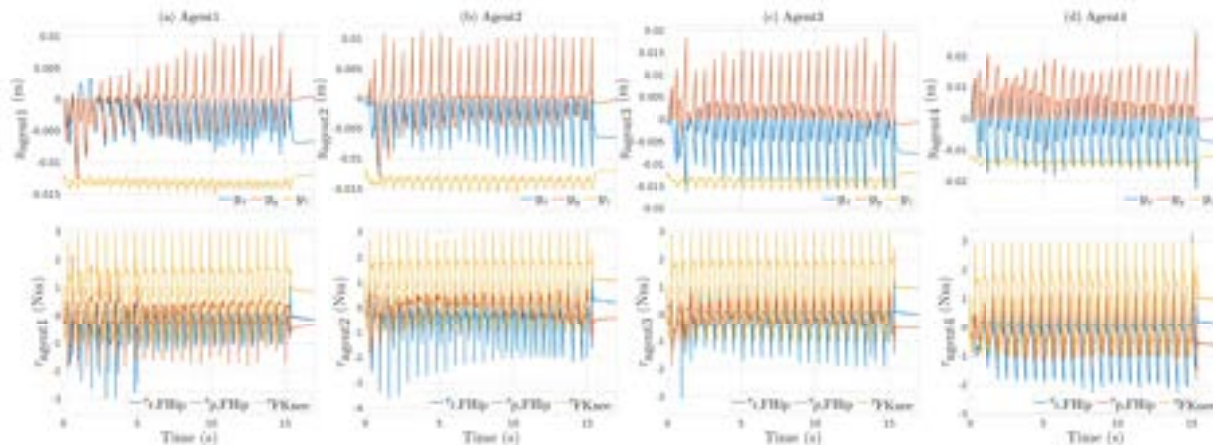


Figure 3.10: Plot of the virtual constraints and torque inputs in RaiSim for robust trot gait subject to a payload with $N = 4$ agents. Subplots (a), (b), (c), and (d) correspond to the agent 1, 2, 3, and 4, respectively. Subplots in the first and second rows correspond to the virtual constraints and torque inputs of each agent, respectively.

study the cooperative locomotion with $N = 2$ and $N = 3$ agents on uneven terrain. Here, we assume that the ground height profile changes in a random manner in the discrete set $\{\pm 1, \pm 2\}$ (cm). The evolution of the virtual constraints and torque inputs together with the convergence of the robots to the target points is depicted in Figs. 3.14 and 3.15 for two and three agents, respectively. From the figures, it is observed that the control inputs and outputs remain bounded during the cooperative locomotion. Figures 3.16 and 3.17 depict the snapshots of the cooperative locomotion patterns with the proposed control algorithm. In addition, Figs. 3.16 and 3.17 compare the robustness and performance of the proposed control solutions with the individual MPC algorithms that do not consider the interaction forces for the path planning. Animations of these simulations can be found online².

3.6 Discussion

The numerical simulations of the reduced- and full-order models show the effectiveness of the proposed supervisory predictive control algorithm in generating stable cooperative locomotion patterns for multi-agent legged robots. The proposed hierarchical control algorithm developed based on the interconnected LIP dynamics allows robustly stable cooperative locomotion of multi-agent legged robots subject to holonomic constraints whereas the same legged machines cannot perform stable cooperative locomotion patterns without the proposed algorithm. The objective of this section is to analyze the results and to discuss the limitations of the proposed control approach.

²<https://youtu.be/8G1tniNW7jg>

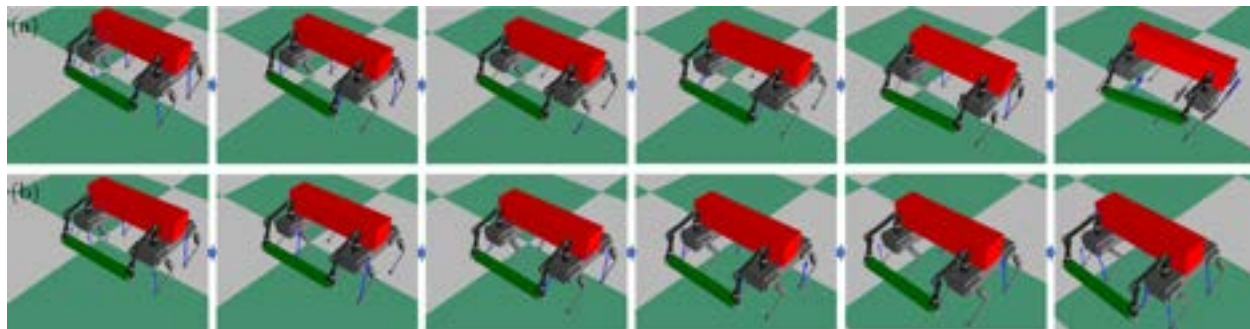


Figure 3.11: (a) Snapshots of the unstable cooperative locomotion of 2 agents with the individual predictive control of Chapter 2 for agents in RaiSim. Here, each agent makes use of MPC for its own LIP dynamics without considering the interaction forces. (b) Snapshots of the robustly stable cooperative locomotion of 2 agents with the proposed supervisory predictive control of this chapter in the presence of a 20 (kg) payload.

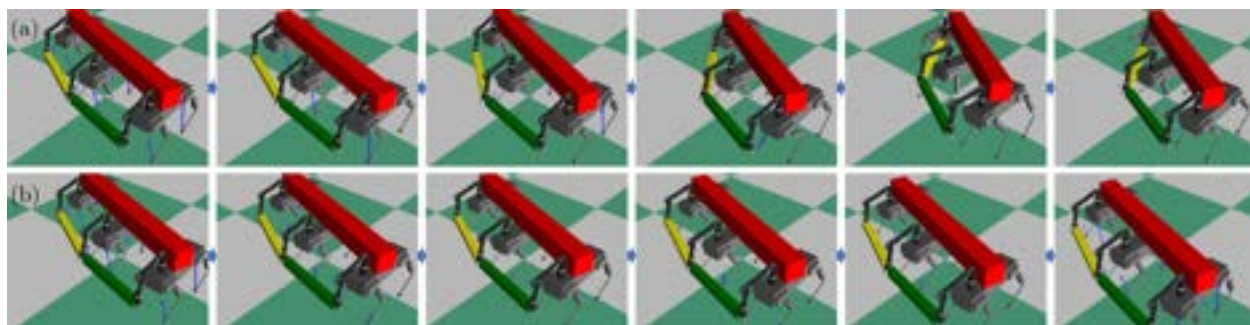


Figure 3.12: (a) Snapshots of the unstable cooperative locomotion of 3 agents in RaiSim, in which each agent makes use of its own MPC without considering the interaction forces between agents in the interconnected LIP dynamics. (b) Snapshots of the robustly stable cooperative locomotion of 3 agents with the proposed supervisory predictive control in the presence of a 32 (kg) payload.

3.6.1 Robustness against Uncertainties

The developed control algorithm enhances the level of robustness of the coupled full-order dynamical systems against uncertainties arising from the unknown payloads as well as ground height profile changes. Here, we make use of the number of steps that the robots can take as metrics to evaluate the performance of the closed-loop system. In particular, success occurs if the robots can reach the target points in a specified number of domains, denoted by m_d . Otherwise, it is a “failure (instability)” (e.g., the robots may fall before reaching the target point or in a number of domains less than m_d).

Unknown payloads: For the payload simulations, we consider cooperative locomotion

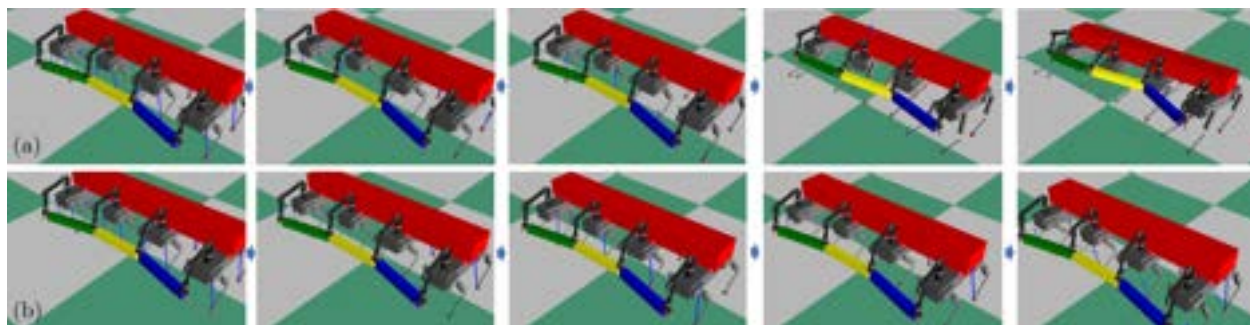


Figure 3.13: (a) Snapshots of the unstable cooperative locomotion of 4 agents in RaiSim, in which each agent makes use of its own MPC without considering the interaction forces in the interconnected LIP dynamics. (b) Snapshots of the robustly stable cooperative locomotion of 4 agents with the proposed supervisory predictive control in the presence of a 48 (kg) payload.

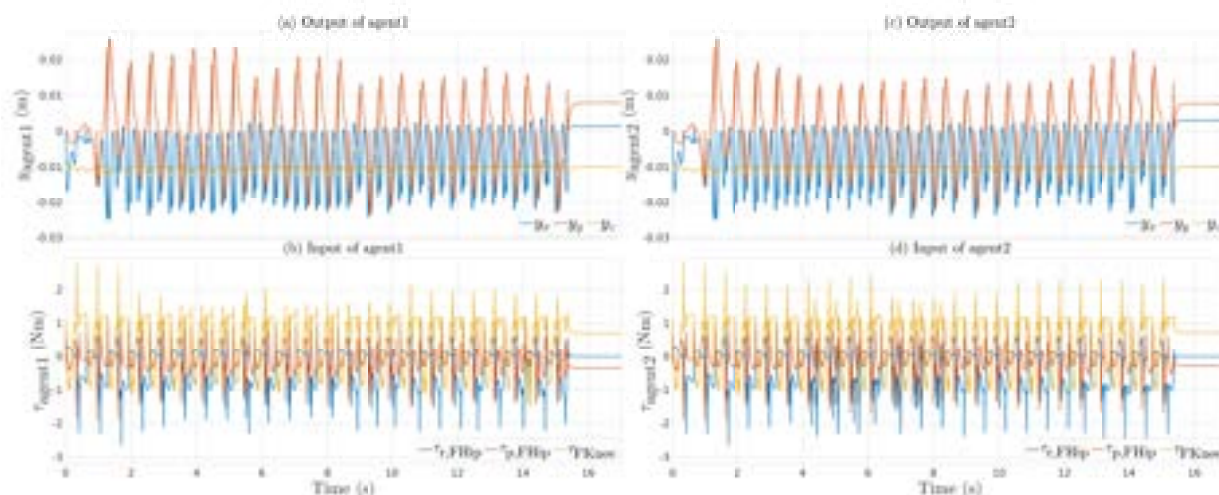


Figure 3.14: Evolution of virtual constraints and control inputs for locomotion of $N = 2$ agents over an unknown terrain. Plots show the inputs and outputs for individual agents.

over $m_d = 50$ continuous-time domains. The objective is to evaluate the performance of cooperative locomotion for a team of $N \in \{2, 3, 4\}$ agents. As described in Section 3.5 and Figs. 3.8-3.13, the developed control algorithms allow transporting unknown and much heavier objects than the maximum payload of a single agent (i.e., 12 (kg)). More specifically, legged co-robots can cooperatively carry the payloads and arrive at the target positions in 50 domains. In contrast, the same interconnected agents without the supervisory MPC cannot depart from the initial positions due to the lack of consideration of the interaction forces at the planner level. Our numerical studies show that the cooperative system with the supervisory MPC algorithm can transport 20 (kg), 34 (kg), and 48 (kg) with two, three,

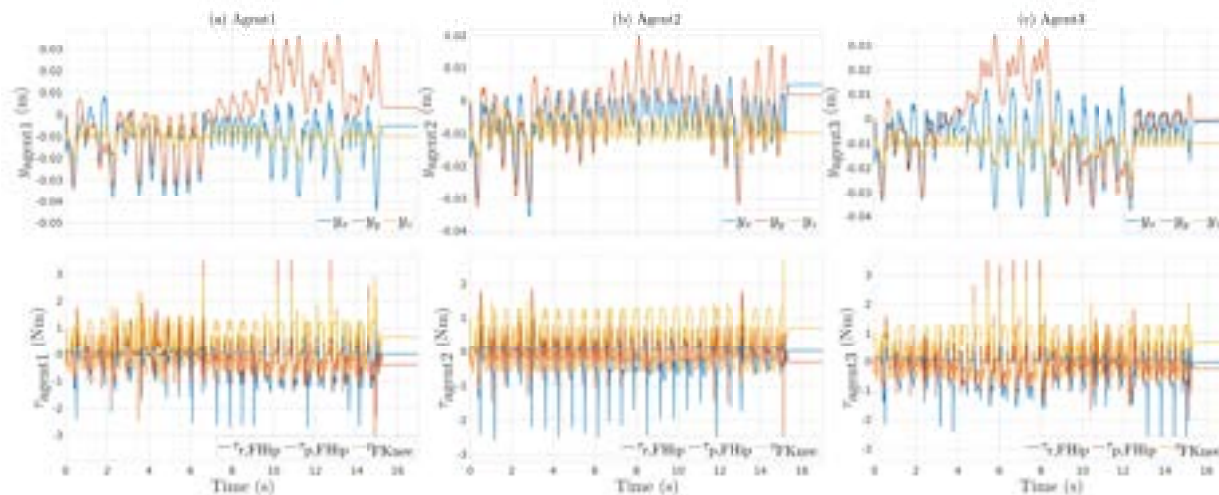


Figure 3.15: Evolution of virtual constraints and control inputs for locomotion of $N = 3$ agents over an unknown terrain.

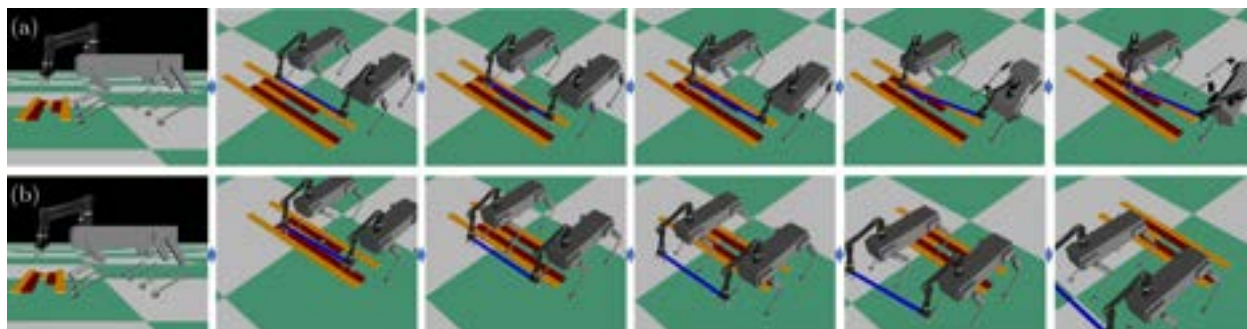


Figure 3.16: (a) Snapshots of the unstable cooperative locomotion of 2 agents over an unknown terrain, where each agent makes use of its own MPC algorithm without considering the interaction forces. (b) Snapshots of the robustly stable cooperative locomotion of 2 agents over the same terrain with the proposed supervisory predictive control based on the interconnected LIP dynamics.

and four agents, respectively. In other words, the agents can transport *unknown* payloads whose masses are up to 57%, 97%, and 137% of a single agent's mass with a team of two, three, and four legged co-robots.

In addition to the payloads mentioned above on the agents' torso, we consider payloads amongst the EEs in Section 3.5. The maximum weight for this load follows the Kinova arm's payload limitation (i.e., 0.5 (kg)). If we do not consider this limitation, our numerical simulations show that the proposed control algorithm can transport payloads of 4.5 (kg), 9 (kg), and 13.5 (kg) between EEs with a team of two, three, and four co-robots, respectively.

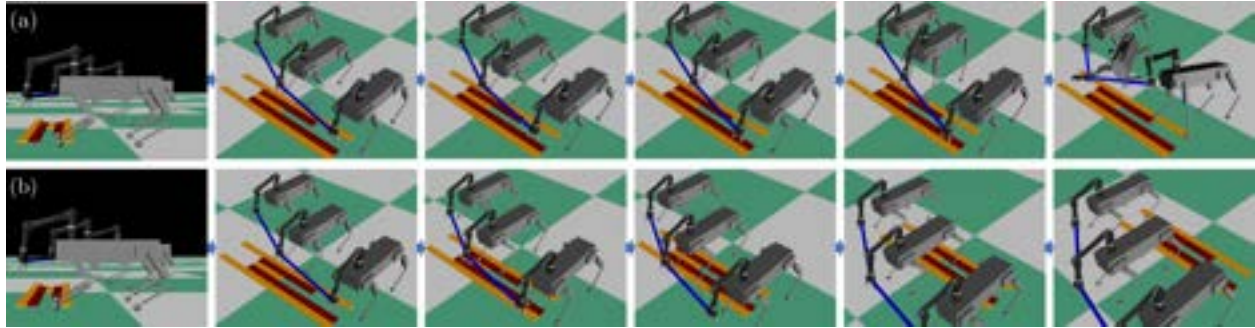


Figure 3.17: (a) Snapshots of the unstable cooperative locomotion of 3 agents, where each agent makes use of its own MPC algorithm without considering the interaction forces. (b) Snapshots of the robustly stable cooperative locomotion of 3 agents over an unknown terrain with the proposed supervisory predictive control.

Varying ground height profiles: For this set of simulations, we study cooperative locomotion on uneven terrains over $m_d = 100$ continuous-time domains. The objective is to evaluate the performance of cooperative locomotion for a team of $N \in \{2, 3\}$ agents. Our numerical studies show that the proposed control algorithm can result in stable cooperative locomotion on unknown terrains with ground height changes in the discrete set $\{\pm 1, \pm 2\}$ (cm). In particular, we simulated 100 different ground height profiles with discontinuities within the above set. In all of these simulations, the agents can successfully reach the final target in the specified number of domains. In contrast, the interconnected system without the supervisory MPC algorithm always fails on these terrains.

3.6.2 Limitations and Analysis of Results

Linearization of the interconnected LIP dynamics: The interconnected LIP dynamics in (3.7) are nonlinear. In order to formulate a convex optimal control problem, the supervisory control algorithm first linearizes the dynamics, and then solves an MPC problem for the linearized dynamics. Our numerical simulations in Fig. 3.4 depict the behavior of the nonlinear dynamics subject to the supervisory MPC. From this figure, we observe that the optimal control problem, formulated for the linearized dynamics, can stabilize the target points for the original and interconnected LIP dynamics. In particular, the states of the nonlinear system remain bounded and asymptotically converge to the target points. We also remark that the supervisory MPC does not use a constant Jacobian linearization for the entire period of locomotion. Instead, it linearizes the dynamics around the current point at the beginning of each continuous-time domain. This makes the linearization error zero (i.e., resets it) at the beginning of each domain, which in turn reduces the gap between the states of the linearized and nonlinear dynamics. Furthermore, the adequacy of this linearization technique is validated in the full-order and complex models of cooperative locomotion. In

particular, the virtual constraint plots in Figs. 3.5 and 3.6 show that the actual COM positions of the agents follow the desired COM trajectories, based on the linearized dynamics, and the error remains bounded. For future research, we will investigate nonlinear MPC algorithms that can address the path planning problem for the interconnected reduced-order models without linearization.

Limitations of the reduced-order LIP dynamics: In this chapter, we make use of the LIP dynamics to form the interconnected reduced-order network. One of the limitations of the LIP model is that it cannot capture moments about the COM. Hence, the arms model is not used in the interconnected LIP dynamics as the forces generated by the grippers due to the holonomic constraints can create moments about the COMs. Consequently, the holonomic constraints are represented amongst the COMs in the reduced-order model. However, we remark that the actual holonomic constraints are imposed between the EEs in the full-order simulations of Section 3.5. In the numerical simulations of Section 3.5, the arm joints are not locked. However, we define some virtual constraints to control the EE’s Cartesian coordinates in the task space. The desired trajectory for the EE’s position is taken as the desired COM trajectory, generated by the supervisory MPC, plus a constant value that represents the relative motion of the EE with respect to the body. Hence, the EE’s relative motion with respect to the body becomes almost static. Consequently, the process of initiating the grasping motion is not addressed in this work. This can limit the general problem of loco-manipulation during cooperative locomotion of multi-agent robots. For future research, we will investigate alternative networks of reduced-order models that can be integrated with simple arm models for manipulation purpose.

The alternative limitation of the LIP model is that it cannot address dynamic locomotion. Furthermore, the height of the COM is assumed to be constant in the LIP dynamics that can limit locomotion on rough terrains. This motivates the use of alternative reduced-order models for future research. However, this may also increase the complexity of the reduced-order models and the computational burden of the supervisory MPC.

Considerations for the real-world implementation: The proposed controllers of this work assume that the agents can share their “reduced-order” states for the path planning purpose. In particular, the higher level of the control algorithm (i.e., supervisory MPC) is assumed to have access to all the reduced-order states of the agents (i.e., positions of the COMs). This can be realized via a direct communication network [191]. However, the low-level controllers for the whole-body motion control are distributed and do *not* require full-order state sharing. The preliminary work [73, Chap. 4] shows that the QP-based low-level controllers can stabilize the locomotion of single-agent legged robots in practice. We will experimentally evaluate the performance of the proposed controllers for multi-agent legged robots in future work.

Dynamic locomotion: The numerical simulations of this chapter have shown that the interconnected LIP dynamics and the event-based supervisory MPC are sufficient to have robustly stable cooperative locomotion of legged robots. Although state-of-the-art single

quadrupedal robots have dynamic gaits, the nature of single-agent locomotion and collaborative locomotion of multi-agent systems for cooperative transportation is completely different. Hence, the proposed control algorithms are validated for cooperative locomotion with quasi-static gaits but not dynamic gaits. The developed control approach would likely need to be altered to address more agile locomotion patterns in complex environments for future work.

3.7 Summary

This chapter presented a hierarchical nonlinear control algorithm for the real-time planning and control of legged robots that collaboratively carry objects. We presented an innovative network of reduced-order models subject to holonomic constraints, referred to as the interconnected LIP dynamics, to address the motion planning problem of collaborative locomotion. The properties of the interconnected LIP dynamics were studied to formulate a supervisory control as the higher-level planner in the proposed control algorithm. The supervisory control is formulated as an event-based predictive control to steer the interconnected LIP dynamics subject to the feasibility of the net GRFs of individual agents. At the lower level of the proposed control scheme, distributed nonlinear controllers, based on QP and virtual constraints, were developed to impose the full-order dynamical model of each agent to asymptotically track the optimal reduced-order trajectories, prescribed by the supervisory predictive control, while having feasible contact forces at the leg ends. The effectiveness and robustness of the proposed nonlinear control scheme were demonstrated and investigated via full-order numerical simulations of a team of two, three, and four collaborative quadrupedal robots, each with a total of 22 DOFs, while carrying different objects in the presence of uncertainties.

In the next chapter, we will investigate the design of centralized and distributed predictive controllers at the higher level of the proposed control scheme with interconnected SRB dynamics. This work also focused on validating the legged robots' cooperative locomotion in numerical simulations and various practical environments subject to unknown disturbances.

Part III

Cooperative Locomotion via Centralized and Distributed MPCs

Chapter 4

Centralized and Distributed MPCs of Cooperative Locomotion

4.1 Introduction

4.1.1 Motivation and Goal

Human-centered communities, including factories, offices, and homes, are typically developed for humans who are bipedal walkers capable of stepping over gaps and walking up/down stairs. This motivates the development of collaborative legged robots that can cooperatively work with each other to assist humans in different aspects of their life, such as labor-intensive tasks, construction, manufacturing, and assembly. One of the most challenging and essential problems in deploying collaborative legged robots is *cooperative locomotion* in complex environments, wherein the collaboration between robots is described by holonomic constraints. Cooperative locomotion with holonomic constraints arises in different applications of legged robots, such as cooperative transportation of payloads like social insects [116] (see Fig. 4.1), human-robot locomotion via prosthetic legs and exoskeletons [1, 5, 90, 213], and human-robot locomotion via guide dog robots [12].

In recent years, important theoretical and technological advances have allowed for the successful control of [multi-robot systems \(MRSs\)](#) [191, 209], including collaborative robotic arms with or without mobility [15, 49, 65, 68, 143, 207], aerial vehicles [38, 41, 119, 122, 134, 137, 146, 156, 184, 187, 202, 211], and ground vehicles [50, 71, 127, 155, 178]. In addition, distributed control algorithms, including distributed receding horizon control approaches, have been developed to address the motion planning of MRSs, see e.g., [33, 63, 128, 138]. Some recent works also address the control and planning of heterogeneous robot teams, including legged robots [2, 190, 210] but without holonomic constraints amongst the agents. However, the capabilities of cooperative legged locomotion have not been fully explored. In particular, collaborating legged robots can be described by *inherently unstable* dynamical systems with *high dimensionality* (i.e., high [degrees of freedom \(DOFs\)](#)), *nonlinear*, and *hybrid* nature, and subject to underactuation and unilateral constraints, as opposed to most of the MRSs where the state-of-the-art algorithms have been deployed [13]. This complicates the design of real-time trajectory planning and control approaches, both in centralized and distributed fashions, to guarantee each agent's dynamic and robust stability while addressing the curse



Figure 4.1: Snapshot illustrating holonomically constrained quadrupedal robots locomoting on gravel while carrying a payload of 4.53 (kg).

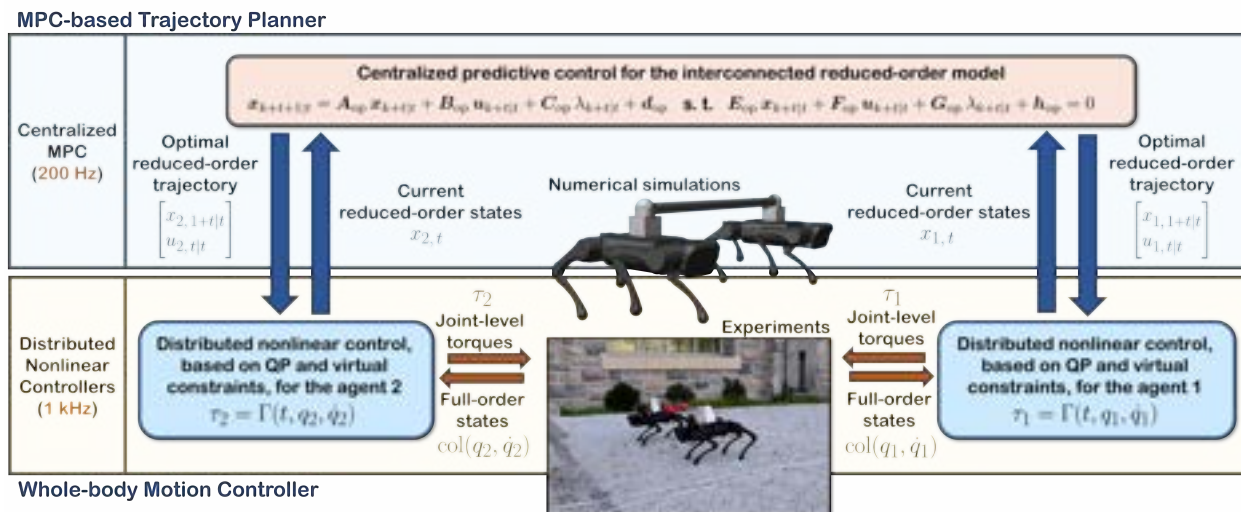


Figure 4.2: Overview of the proposed layered control approach with the centralized MPC algorithm at the high level and distributed nonlinear controllers at the low level for cooperative locomotion.

of dimensionality and respecting the holonomic and unilateral constraints.

Reduced-order (i.e., template) models provide low-dimensional realizations of full-order dynamical models of legged robots [80]. They can be integrated with convex optimization techniques and [model predictive control \(MPC\)](#) approaches to enable gait planning for the existing legged robots. Some popular reduced-order models include the [linear inverted pen-](#)

dulum (LIP) model [110], centroidal dynamics [147], and single rigid body (SRB) dynamics [28, 44, 58]. These template models have been used for real-time planning of different single-agent bipedal [54, 66, 94, 162] and quadrupedal robots [14, 28, 44, 56, 58, 72, 75, 86, 151]. In this chapter, we aim to answer three *fundamental questions* in the context of cooperative locomotion of legged robots. 1) How do we develop effective and interconnected reduced-order models that describe the cooperative locomotion of dynamic legged robots with holonomic constraints? 2) How do we develop computationally tractable predictive control algorithms in centralized and distributed manners for real-time planning of interconnected reduced-order models? In particular, we aim to examine the implementation of centralized and distributed predictive control algorithms for real-time planning to overcome the limitations caused by the curse of dimensionality in cooperative locomotion. And 3) How do we map optimal reduced-order trajectories to full-order and complex dynamical models of cooperative locomotion?

In order to address the above questions, this chapter aims to develop mathematical foundations, experimentally implement, and comprehensively study the cooperative locomotion of two holonomically constrained dynamic legged robots. In particular, the *overarching goal* of this chapter is to develop a layered control algorithm for the real-time trajectory planning and control of dynamic cooperative locomotion for two holonomically constrained legged-robotic systems. The higher layer of the proposed algorithm considers an innovative reduced-order model composed of two interconnected SRB dynamics subject to holonomic constraints for the planning problem. The chapter develops novel centralized and distributed MPC algorithms for the planning purpose of interconnected SRB dynamics (see Figs. 4.2 and 4.3). These MPC algorithms address the real-time planning at the higher layer of the control hierarchy subject to the interaction terms and feasibility of the *ground reaction forces (GRFs)*. The optimal reduced-order trajectories and GRFs, generated by the high-level MPCs, are then mapped to the full-order and complex dynamics via distributed nonlinear controllers at the low level for the whole-body motion control. The low-level nonlinear controllers are developed based on *quadratic programming (QP)* and input-output (I-O) linearization. The efficacy of the proposed layered control approach is validated via extensive experiments for robustly stable locomotion of two holonomically constrained A1 quadrupedal robots that cooperatively transport unknown payloads on different terrains and in the presence of disturbances (see Fig. 4.1). A comprehensive numerical analysis of the performance of the proposed centralized and distributed MPC algorithms is finally presented.

4.1.2 Related Work

Holonomically constrained MRSs, including fixed-based collaborative robotic arms [49, 207], aerial vehicles with payloads [137, 146, 187, 202], and ground vehicles [71, 127, 155, 178] have gained significant attention during the last years. Moreover, MRSs augmented with robotic arms have been studied for more complex cooperative tasks [15, 38, 65, 68, 119, 211]. In contrast to the above-mentioned robotic systems, collaborative legged robots are

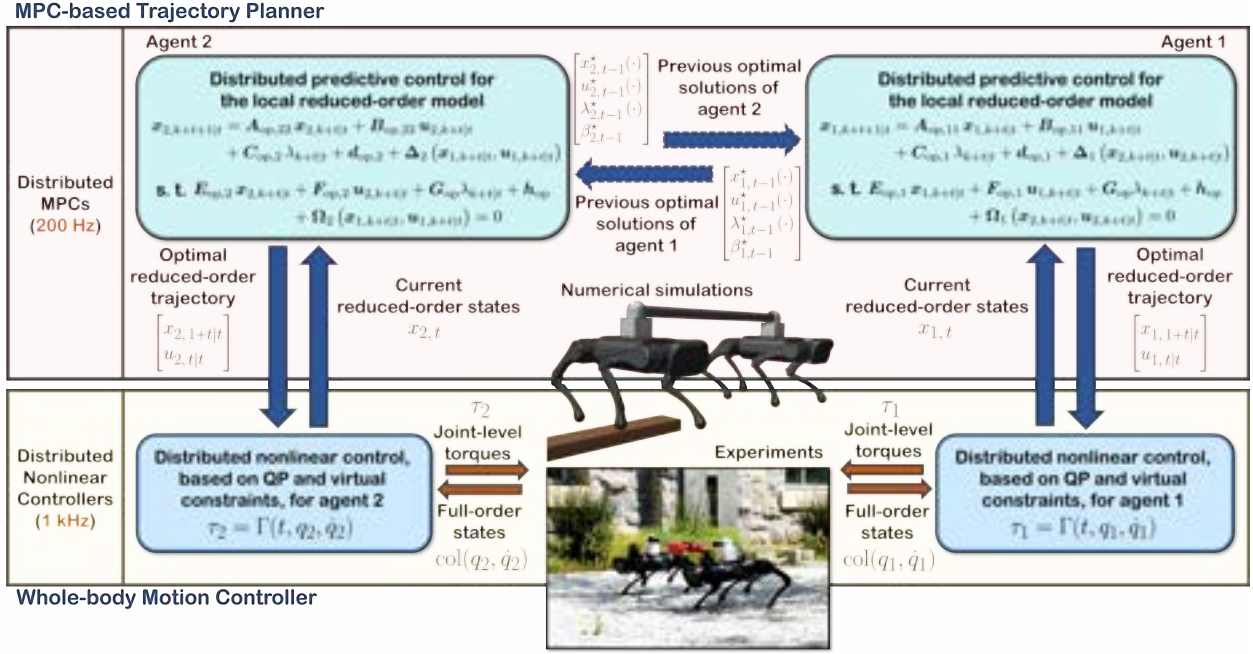


Figure 4.3: Overview of the proposed layered control approach with the distributed MPC algorithms at the high level and distributed nonlinear controllers at the low level for cooperative locomotion.

dynamical systems with high dimensionality, unilateral constraints, and hybrid nature that add further complexity to synthesizing planning and control algorithms. In addition, the strong interacting wrenches (forces/torques) between the agents, arising from holonomic constraints, must be carefully addressed to result in a robustly stable planner for cooperative legged locomotion. As a result, collaborative legged locomotion has not been studied to the same degree as other robotic systems. This paper, there, marks the first experimental implementation in this context.

In the context of legged robots, the trajectory planning and control approaches can be sectioned into two categories: the ones using the full-order models and the others using the reduced-order models. Hybrid systems theory plays an important role in understanding and analyzing full-order dynamical models of legged locomotion [84, 98, 99, 104, 107, 141, 159, 180, 206]. Advanced nonlinear control algorithms such as hybrid reduction [18], controlled symmetries [179], transverse linearization [130], and **hybrid zero dynamics (HZD)** [19, 205] address the hybrid nature of full-order locomotion models. The HZD approach regulates some output functions, referred to as virtual constraints, with I-O linearization techniques [106] to coordinate the robot's links within a stride. This method can systematically address under-actuation and its effectiveness has been validated for stable locomotion of different bipedal [42, 51, 103, 131, 183] and quadrupedal robots [74, 126] as well as powered prosthetic legs [90, 213]. The full-order gait planning is typically formulated as a **nonlinear programming**

(NLP) problem that can be addressed with existing NLP tools and direct collocation techniques [39, 103, 113, 154, 157]. Although the direct-collocation-based approaches generate optimal trajectories for full-order models of legged robots effectively, they *cannot* address real-time trajectory optimization of cooperative legged robots in complex environments.

In contrast to full-order models of legged locomotion, template models present reduced-order representations of legged robots that significantly reduce the computational burden and complexity associated with trajectory optimization. Various template models, including LIP [110], SRB [28, 44, 58], and centroidal dynamics [147], have been successfully integrated with the MPC framework for the real-time planning of bipedal and quadrupedal robots [14, 28, 44, 54, 56, 58, 66, 75, 86, 94, 151, 162]. The main challenge with using template models is bridging the gap between reduced- and full-order models of locomotion arising from abstraction (e.g., ignoring the legs' dynamics in template models). In particular, one needs to translate the optimal reduced-order trajectories to the full-order joint positions and torques. Different hierarchical control algorithms have been proposed in the literature to close this gap, in which a whole-body motion controller is utilized at the low level to map the optimal trajectories, generated by the higher-level MPC, to the full-order dynamics. For instance, [44, 58] have used Jacobian mapping, [14, 116] have used HZD-based controllers, [151] has used robust MPC integrated with reinforcement learning, [76] has used data-driven template models, and [25, 72] have used joint space whole-body controllers.

Despite the success of the above methods on individual robots, it is unknown what reduced-order models can represent multi-agent-legged robots' dynamic and cooperative transportation effectively. In addition, it is unclear if the existing MPC techniques can address the real-time trajectory planning for the reduced-order models of cooperative locomotion with increased dimensionality. Moreover, it is unclear how the centralized MPC algorithms for such complex models can be decomposed into lower-dimensional distributed MPC algorithms considering the strong interaction terms. Our previous work in Chapter 3 employed an interconnected network of LIP models with event-based MPC (introduced in Chapter 2) as a trajectory planner for cooperative locomotion. The simple nature of the LIP model and event-based MPC reduced the computational burden by running the MPC only at the beginning of the continuous-time domains rather than every time sample. However, using the LIP model prohibits us from capturing the interaction torques due to the assumption of a concentrated point mass at the **center of mass (COM)**. This model also restricts the generation of dynamic cooperative gaits because the **center of pressure (COP)** must always remain within the support polygon, limiting the system's full potential. Moreover, the proposed event-based MPC was formulated only in a centralized manner and validated on numerical simulations and without experimental validations. In the current work, we aim to develop a new framework to allow more dynamic cooperative gaits while solving MPC problems faster in both centralized and distributed manners and experimentally validating the approach on two dynamic quadrupedal robots.

4.1.3 Objectives and Contributions

The *objectives* and *key contributions* of this chapter are as follows:

- 1) The chapter presents an innovative network of two holonomically constrained SRB dynamics as an effective reduced-order model to capture the interaction wrenches between agents while dynamically stabilizing the motion during cooperative locomotion. It is numerically shown that the MPC algorithms utilizing a nominal SRB model cannot stabilize cooperative locomotion.
- 2) A layered control approach is proposed to robustly stabilize cooperative locomotion of holonomically constrained quadrupedal robots. At the high level of the control hierarchy, two different MPC algorithms, based on QP, are proposed: centralized MPC and distributed MPC (see Figs. 4.2 and 4.3). The centralized MPC algorithm solves for the optimal state trajectory, GRFs, and interaction wrenches for the interconnected SRB dynamics. The distributed MPC algorithm assumes two local QPs that share their optimal solutions with a one-step communication delay. The distributed MPCs solve for the local states, local GRFs, and estimated local interaction wrenches according to an agreement protocol in the cost function.
- 3) At the low level of the proposed control architecture, distributed and full-order nonlinear controllers are presented for the whole-body motion control of agents. The distributed nonlinear controllers are developed based on QP and virtual constraints to impose the full-order dynamics to track the prescribed and optimal reduced-order trajectories and GRFs, generated by the high-level MPC (centralized or distributed).
- 4) Extensive numerical simulations are presented to evaluate the performance of the cooperative locomotion of two holonomically constrained A1 robots with different payloads on different rough terrains and in the presence of external force disturbances. A comparative analysis of the closed-loop systems with centralized and distributed MPC algorithms with more than 1000 randomly generated rough terrain profiles and external forces is presented. It is shown that the proposed distributed MPC algorithm has a performance similar to that of the centralized one, while the solve time is reduced by 70%. In addition, it is shown that the proposed centralized and distributed MPCs can drastically improve the robust stability of cooperative locomotion subject to a wide range of uncertainties, while the nominal MPCs cannot stabilize it.
- 5) The effectiveness of the proposed layered control algorithms (centralized and distributed) is verified with an extensive set of experiments for the blind and cooperative locomotion of two holonomically constrained A1 quadrupedal robots, each with 18 DOFs. The experiments include cooperative locomotion with different and unknown payloads on different terrains (covered with blocks, gravel, mulch, and slippery surfaces) and in the presence

of external pushes and tethered pulling. Detailed robustness analysis is presented to experimentally evaluate the performance of the closed-loop system against the violations of assumptions made for the synthesis of the controller.

4.1.4 Outline

The chapter is organized as follows. Section 4.2 develops interconnected SRB models as a reduced-order model of cooperative locomotion. Section 4.3 formulates centralized and distributed MPC-based trajectory planning algorithms with the proposed reduced-order model. Section 4.4 presents distributed nonlinear controllers for the whole-body motion control. Section 4.5 provides a detailed and extensive set of numerical and experimental validations of the proposed layer control algorithm. In Section 4.6, we discuss the results and compare the performance of the centralized and distributed MPC algorithms. Section 4.7 finally presents some concluding remarks and future research directions.

4.2 Reduced-Order Model of Cooperative Legged Locomotion

This section aims to address the reduced-order models that describe the cooperative locomotion of two holonomically constrained quadrupedal robots. The section assumes a rigid bar connected via ball joints to two points on the robots for carrying objects (see Fig. 4.1). These two points will be referred to as the *interaction points*. This assumption simplifies the analysis and results in a holonomic constraint, stating that the Euclidean distance between the interaction points is constant. However, the analysis of this section can be extended to more sophisticated connections, such as restricting the pitch or roll angles of the bar/load. In Section 4.6.4, we will experimentally show the robustness of the developed algorithms subject to these additional constraints.

In our notation, the subscript $i \in \mathcal{I} := \{1, 2\}$ represents the i th robot. We assume that $\{B_i\}$ is the local frame rigidly attached to the body of the agent i with its origin on the COM. The orientation of the frame $\{B_i\}$ with respect to the inertial world frame $\{O\}$ is denoted by $R_i \in \text{SO}(3)$, where $\text{SO}(3) := \{R \in \mathbb{R}^{3 \times 3} \mid R^\top R = \mathbb{I}, \det(R) = 1\}$ is the special orthogonal group of order 3, and \mathbb{I} represents the identity matrix. The Cartesian coordinates of the COM of agent i with respect to $\{O\}$ are also represented by $r_{ci} := \text{col}(x_{ci}, y_{ci}, z_{ci}) \in \mathbb{R}^3$, where “col” denotes the column operator. Moreover, $\omega_i^{B_i} \in \mathbb{R}^3$ represents the angular velocity of agent i expressed in the body frame $\{B_i\}$. We assume that $p_i \in \mathbb{R}^3$ for $i \in \mathcal{I}$ represents Cartesian coordinates of the interaction points with respect to the inertial frame $\{O\}$, that is,

$$p_i = r_{ci} + R_i d_i^{B_i}, \quad (4.1)$$

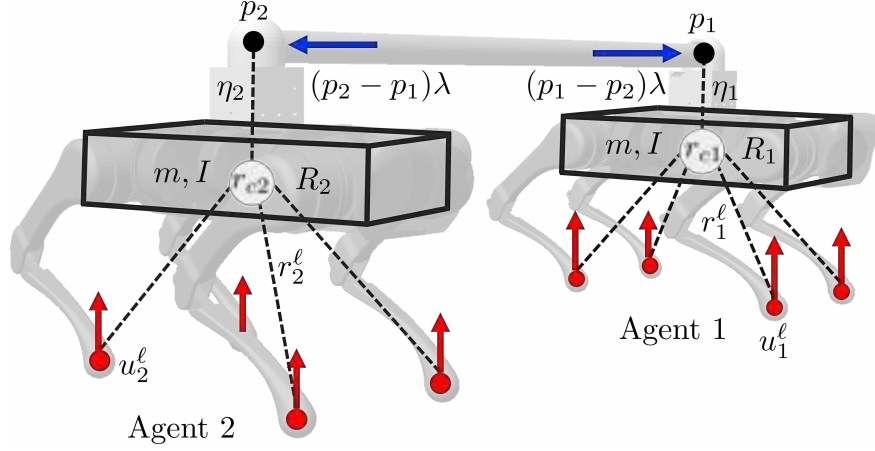


Figure 4.4: Illustration of the interconnected SRB models for the cooperative locomotion of two quadrupedal robots.

where $d_i^{B_i} \in \mathbb{R}^3$ is a constant vector denoting the coordinates of the interaction points in the body frame $\{B_i\}$. For future purposes, we define $\eta_i := R_i d_i^{B_i}$ (see Fig. 4.4). We remark that the holonomic constraint between two agents can be described as a constraint on the Euclidean distance between the interaction points as follows:

$$\psi(r_{c1}, r_{c2}, R_1, R_2) := \frac{1}{2} \|p_1 - p_2\|^2 = \psi_0, \quad (4.2)$$

in which $\|\cdot\|$ denotes the 2-norm, and ψ_0 is a constant number, determined based on the length of the bar.

According to the principle of virtual work, one can consider $(p_1 - p_2)\lambda \in \mathbb{R}^3$ as the interaction force applied to agent 1 for some Lagrange multiplier $\lambda \in \mathbb{R}$ to be determined later (see again Fig. 4.4). Consequently, the net external wrench applied to agent $i \in \mathcal{I}$ can be expressed as follows:

$$\begin{bmatrix} f_i^{\text{net}} \\ \tau_i^{\text{net}} \end{bmatrix} = \sum_{\ell \in \mathcal{C}_i} \begin{bmatrix} \mathbb{I} \\ \widehat{r}_i^\ell \end{bmatrix} u_i^\ell + \begin{bmatrix} \mathbb{I} \\ \widehat{\eta}_i \end{bmatrix} (p_i - p_j)\lambda, \quad (4.3)$$

where $j \neq i \in \mathcal{I}$ denotes the index of the other agent and the hat map $\widehat{(\cdot)} : \mathbb{R}^3 \rightarrow \mathfrak{so}(3)$ represents the skew-symmetric operator with the property $\widehat{x}y = x \times y$ for all $x, y \in \mathbb{R}^3$. In (4.3), the superscript $\ell \in \mathcal{C}_i$ denotes the index of the contacting legs with the ground, \mathcal{C}_i represents the set of contacting legs for the agent i , and $u_i^\ell \in \mathbb{R}^3$ denotes the GRF at the contacting leg ℓ for the agent i . In addition, $r_i^\ell \in \mathbb{R}^3$ represents the position of each contacting leg with respect to the COM of agent i , that is, $r_i^\ell = r_{\text{foot},i}^\ell - r_{ci}$, where $r_{\text{foot},i}^\ell$ is the position of the contacting foot ℓ of the agent i with respect to the world frame $\{O\}$.

By taking the *local state variables* for the agent $i \in \mathcal{I}$ as

$$\mathbf{x}_i := \text{col}(r_{ci}, \dot{r}_{ci}, \text{vec}(R_i), \omega_i^{B_i}) \in \mathbb{R}^{18}, \quad (4.4)$$

the *global state variables* can be defined as

$$\mathbf{x} := \text{col}(\mathbf{x}_1, \mathbf{x}_2), \quad (4.5)$$

where “vec” represents the vectorization operator. Similarly, the *global control inputs* can be defined as $\mathbf{u} := \text{col}(\mathbf{u}_1, \mathbf{u}_2)$, where \mathbf{u}_i denotes the *local control inputs* (i.e., GRFs) for the agent i , that is,

$$\mathbf{u}_i := \text{col} \{u_i^\ell \mid \ell \in \mathcal{C}_i\}. \quad (4.6)$$

By differentiating the holonomic constraint (4.2), one can get

$$\dot{\psi}(\mathbf{x}) = (p_1 - p_2)^\top (\dot{p}_1 - \dot{p}_2) = 0, \quad (4.7)$$

and hence, the *state manifold* for the interconnected SRB dynamics can be expressed as

$$\mathcal{X} := \left\{ \mathbf{x} \in \mathbb{R}^{36} \mid R_i \in \text{SO}(3), i \in \mathcal{I}, \psi(\mathbf{x}) = \psi_0, \dot{\psi}(\mathbf{x}) = 0 \right\}.$$

Finally, the interconnected SRB dynamics can be expressed as

$$\dot{\mathbf{x}} = \mathbf{f}(\mathbf{x}, \mathbf{u}, \lambda) := \begin{bmatrix} \dot{r}_{c1} \\ \frac{f_1^{\text{net}}}{m} - g \\ \text{vec}(R_1 \widehat{\omega}_1^{B_1}) \\ I^{-1} \left(R_1^\top \tau_1^{\text{net}} - \widehat{\omega}_1^{B_1} I \omega_1^{B_1} \right) \\ \dot{r}_{c2} \\ \frac{f_2^{\text{net}}}{m} - g \\ \text{vec}(R_2 \widehat{\omega}_2^{B_2}) \\ I^{-1} \left(R_2^\top \tau_2^{\text{net}} - \widehat{\omega}_2^{B_2} I \omega_2^{B_2} \right) \end{bmatrix}, \quad (4.8)$$

where m and $I \in \mathbb{R}^{3 \times 3}$ denote the total mass and the fixed moment of inertia in the body frame for each agent, respectively, and g represents the constant gravitational vector. We remark that the kinematics relations in (4.8) are expressed as $\dot{R}_i = R_i \widehat{\omega}_i^{B_i}$ for $i \in \mathcal{I}$. The rotational dynamics can be further expressed as Euler’s equation $I \dot{\omega}_i^{B_i} + \widehat{\omega}_i^{B_i} I \omega_i^{B_i} = R_i^\top \tau_i^{\text{net}}$. We also note that in (4.8), $\mathbf{f} : \mathcal{X} \times \mathcal{U} \times \mathbb{R} \rightarrow \text{T}\mathcal{X}$ is smooth with

$$\mathcal{U} := \underbrace{\mathcal{FC} \times \dots \times \mathcal{FC}}_{m_u \text{-times}} \subset \mathbb{R}^{3m_u} \quad (4.9)$$

being the *admissible set of control inputs*, where m_u denotes the total number of contacting legs with the ground (e.g., $m_u = 4$ for cooperative trot), $\mathcal{FC} := \{\text{col}(f_x, f_y, f_z) \mid f_z > 0, |f_x| \leq \frac{\mu}{\sqrt{2}} f_z, |f_y| \leq \frac{\mu}{\sqrt{2}} f_z\}$ represents the linearized friction cone for some friction coefficient μ , and $\text{T}\mathcal{X}$ is the tangent bundle of the state manifold \mathcal{X} .

In order to make the manifold \mathcal{X} invariant under the flow of (4.8), one would need to choose the Lagrange multiplier λ to satisfy the holonomic constraint. In particular, differentiating (4.7) according to (4.1) and $\dot{R}_i = R_i \widehat{\omega}_i^{B_i}$ results in

$$\begin{aligned} \ddot{\psi}(\mathbf{x}, \mathbf{u}, \lambda) &= (p_1 - p_2)^\top (\ddot{p}_1 - \ddot{p}_2) + \|\dot{p}_1 - \dot{p}_2\|^2 \\ &= (p_1 - p_2)^\top \left\{ \ddot{r}_{c1} - \ddot{r}_{c2} + R_1 \left(\widehat{\omega}_1^{B_1} \right)^2 d_1^{B_1} - R_2 \left(\widehat{\omega}_2^{B_2} \right)^2 d_2^{B_2} \right. \\ &\quad \left. + R_1 \widehat{\omega}_1^{B_1} d_1^{B_1} - R_2 \widehat{\omega}_2^{B_2} d_2^{B_2} \right\} + \|\dot{p}_1 - \dot{p}_2\|^2 = 0. \end{aligned} \quad (4.10)$$

This latter equation, together with the equations of motion (4.8) and (4.3), results in λ being a function of (\mathbf{x}, \mathbf{u}) . However, replacing this nonlinear expression for λ in (4.8) can make the original dynamics (4.8) more nonlinear and complex. Furthermore, this can numerically complicate the Jacobian linearization of $\dot{\mathbf{x}} = \mathbf{f}(\mathbf{x}, \mathbf{u}, \lambda(\mathbf{x}, \mathbf{u}))$ when formulating the trajectory planning problem as a convex MPC in Section 4.3. Alternatively, we pursue a computationally effective approach by considering $\dot{\mathbf{x}} = \mathbf{f}(\mathbf{x}, \mathbf{u}, \lambda)$ subject to the equality constraint $\ddot{\psi}(\mathbf{x}, \mathbf{u}, \lambda) = 0$ within the optimal control problem formulation. More specifically, the decision variables for the MPC include the trajectories of $(\mathbf{x}, \mathbf{u}, \lambda)$ over the control horizon, and the MPC will satisfy the equality constraint. The other advantage of this technique is that the interconnected SRB dynamics can be integrated with the variational-based approach of [44, 58] to linearize and then discretize the dynamics such that the rotation matrices $R_i, i \in \mathcal{I}$ evolve on $\text{SO}(3)$.

To clarify this latter point, following [58], we introduce a new set of local state variables for the agent $i \in \mathcal{I}$ with the abuse of notation as

$$\mathbf{x}_i := \text{col}(r_{ci}, \dot{r}_{ci}, \xi_i, \omega_i^{B_i}) \in \mathbb{R}^{12}. \quad (4.11)$$

Here, $\xi_i \in \mathbb{R}^3$ is a vector used to approximate the rotation matrix R_i around an operating point $R_{i,\text{op}}$ as follows:

$$R_i = R_{i,\text{op}} \exp(\widehat{\xi}_i) \approx R_{i,\text{op}} \left(\mathbb{I} + \widehat{\xi}_i \right). \quad (4.12)$$

The approach of [58] has linearized the SRB dynamics subject to GRFs without interaction forces. Hence, one must extend the technique to write down the Taylor series expansion for the additional wrench terms in (4.3) arising from the interaction. This results in a discrete and linear time-varying (LTV) system to predict the future states as follows:

$$\mathbf{x}_{k+t+1|t} = \mathbf{A}_{\text{op}} \mathbf{x}_{k+t|t} + \mathbf{B}_{\text{op}} \mathbf{u}_{k+t|t} + \mathbf{C}_{\text{op}} \lambda_{k+t|t} + \mathbf{d}_{\text{op}}, \quad (4.13)$$

for all $k = 0, 1, \dots, N-1$ and with the initial condition $\mathbf{x}_{t|t} = \mathbf{x}_t$. Here, $\mathbf{x} \in \mathbb{R}^{24}$ denotes the global state variables, N represents the control horizon, and $(\mathbf{x}_{k+t|t}, \mathbf{u}_{k+t|t}, \lambda_{k+t|t})$ denotes the tuple of the predicted global states, global inputs (i.e., GRFs), and Lagrange multiplier at time $k+t$ computed at time t . Furthermore, $\mathbf{A}_{\text{op}} \in \mathbb{R}^{24 \times 24}$, $\mathbf{B}_{\text{op}} \in \mathbb{R}^{24 \times 3m_u}$, $\mathbf{C}_{\text{op}} \in \mathbb{R}^{24}$, and $\mathbf{d}_{\text{op}} \in \mathbb{R}^{24}$ are the Jacobian matrices and offset term evaluated around the current operating

point $(\mathbf{x}_t, \mathbf{u}_{t-1}, \lambda_{t-1})$.

The approximation in (4.12) only ensures that the rotation matrices evolve on $\text{SO}(3)$. To guarantee that the state predictions in (4.13) belong to the tangent space of the state manifold at the operating point (i.e., $\mathbf{T}_{\text{op}}\mathcal{X}$), we first define the following equality constraint

$$\Psi(\mathbf{x}, \mathbf{u}, \lambda) := \begin{bmatrix} \psi(\mathbf{x}) - \psi_0 \\ \dot{\psi}(\mathbf{x}) \\ \ddot{\psi}(\mathbf{x}, \mathbf{u}, \lambda) \end{bmatrix} = 0. \quad (4.14)$$

Then, analogous to the technique used for the linearization of the interconnected dynamics, the equality constraint (4.14) can be approximated around the operating point as follows:

$$\mathbf{E}_{\text{op}} \mathbf{x}_{k+t|t} + \mathbf{F}_{\text{op}} \mathbf{u}_{k+t|t} + \mathbf{G}_{\text{op}} \lambda_{k+t|t} + \mathbf{h}_{\text{op}} = 0 \quad (4.15)$$

to ensure that $\Psi(\mathbf{x}_{k+t|t}, \mathbf{u}_{k+t|t}, \lambda_{k+t|t}) \equiv 0$. Here, $\mathbf{E}_{\text{op}} \in \mathbb{R}^{3 \times 24}$, $\mathbf{F}_{\text{op}} \in \mathbb{R}^{3 \times 3m_u}$, $\mathbf{G}_{\text{op}} \in \mathbb{R}^3$, and $\mathbf{h}_{\text{op}} \in \mathbb{R}^3$ are proper matrices and vectors that can be either computed via the approach of [58] or symbolic calculus.

Remark 4.1. As the nature of the holonomic constraints between the agents becomes more complex, the procedure for obtaining the corresponding prediction model and equality constraints becomes computationally expensive. However, our experimental results in Section 4.5 will indicate that the proposed layered control approach, developed based on the assumption of holonomic constraints in (4.2), can robustly stabilize cooperative locomotion subject to uncertainties in the constraints (e.g., limiting the pitch angles of the ball joints). In addition, Section 4.5.2 will show that ignoring the holonomic constraints (4.2) for the reduced-order model and trajectory planner can *destabilize* cooperative locomotion.

4.3 MPC-Based Trajectory Planning

This section aims to formulate the real-time trajectory planning problem for cooperative locomotion as centralized and distributed MPC algorithms.

4.3.1 Centralized MPC

We will consider a locomotion pattern for the agents, described by the directed cycle $\mathcal{G}(\mathcal{V}, \mathcal{E})$, where \mathcal{V} and $\mathcal{E} \subset \mathcal{V} \times \mathcal{V}$ represent the sets of vertices and edges, respectively. The vertices denote the continuous-time domains of locomotion, and the edges represent the discrete-time transitions between the continuous-time domains.

Assumption 4.2. At every time sample t , the higher-level MPC is aware of the current stance legs, assuming that the stance leg configuration does not change throughout the prediction horizon.

Remark 4.3. Assumption 4.2 is *not* restrictive and simplifies the optimal control problem of (4.13) subject to (4.15) over the control horizon. Otherwise, one would need to consider the optimal control problem for a piecewise affine (PWA) system [29, Chap. 16] subject to different switching times.

We are now in a position to present the following real-time centralized MPC algorithm for the cooperative locomotion

$$\begin{aligned}
& \min_{(\mathbf{x}(\cdot), \mathbf{u}(\cdot), \lambda(\cdot))} p(\mathbf{x}_{t+N|t}) + \sum_{k=0}^{N-1} \mathcal{L}(\mathbf{x}_{k+t|t}, \mathbf{u}_{k+t|t}, \lambda_{k+t|t}) \\
& \text{s.t.} \quad \text{Prediction model (4.13)} \\
& \quad \text{Equality constraints (4.15)} \\
& \quad \mathbf{u}_{k+t|t} \in \mathcal{U}, \quad k = 0, 1, \dots, N-1,
\end{aligned} \tag{4.16}$$

where the equality constraints for the MPC arise from a) the prediction model (4.13) to address the interconnected SRB dynamics with the initial condition of $\mathbf{x}_{t|t} = \mathbf{x}_t$, and b) the holonomic constraints (4.15) (see Fig. 4.2). Here, the centralized MPC solves for the optimal trajectories of the global states, global inputs, and the Lagrange multiplier encoded in $(\mathbf{x}(\cdot), \mathbf{u}(\cdot), \lambda(\cdot))$ to retain the sparsity structure of [201], where $\mathbf{x}(\cdot) := \text{col}\{\mathbf{x}_{k+t|t} \mid k = 1, \dots, N\}$, $\mathbf{u}(\cdot) := \text{col}\{\mathbf{u}_{k+t|t} \mid k = 0, 1, \dots, N-1\}$, and $\lambda(\cdot) := \text{col}\{\lambda_{k+t|t} \mid k = 0, 1, \dots, N-1\}$. The terminal and stage cost functions in (4.16) are then taken as $p(\mathbf{x}_{t+N|t}) := \|\mathbf{x}_{t+N|t} - \mathbf{x}_{t+N|t}^{\text{des}}\|_{\mathbf{P}}^2$ and $\mathcal{L}(\mathbf{x}_{k+t|t}, \mathbf{u}_{k+t|t}, \lambda_{k+t|t}) := \|\mathbf{x}_{k+t|t} - \mathbf{x}_{k+t|t}^{\text{des}}\|_{\mathbf{Q}}^2 + \|\mathbf{u}_{k+t|t}\|_{\mathbf{R}_u}^2 + \|\lambda_{k+t|t}\|_{\mathbf{R}_\lambda}^2$ for some desired trajectory $\mathbf{x}^{\text{des}}(\cdot)$ and some positive definite matrices \mathbf{Q} and \mathbf{R}_u , and a positive scalar \mathbf{R}_λ . Finally, the inequality constraints of (4.16) represent the feasibility of the GRFs for two agents.

Remark 4.4. The MPC in (4.16) addresses the trajectory planning problem over the current continuous-time domain. In particular, we do not include the following domain for prediction purposes. This is mainly due to the fact that the actual footholds for the following domain are *not* known *a priori*. More specifically, we employ Raibert's heuristic [165, Eq. (2.4), pp. 46] to plan for the upcoming footholds of each agent. Assuming pre-planned footholds, one can extend the MPC to include other domains. However, our experimental results in Section 4.5 suggest that planning over the current domain is sufficient for robustly stable cooperative locomotion. This is in agreement with most of the existing MPC approaches for single SRB dynamics. We also remark that the centralized MPC has $(25 + 3m_u)N$ decision variables, where m_u represents the total number of contacting legs with the ground. Finally, the MPC problem (4.16) solves for the optimal trajectories of the state variables $\mathbf{x}^*(\cdot)$, control inputs $\mathbf{u}^*(\cdot)$, and Lagrange multiplier $\lambda^*(\cdot)$. However, the high-level MPC only applies the first element of the optimal state and control sequence, i.e., $(\mathbf{x}_{t+1|t}^*, \mathbf{u}_{t|t}^*)$, to the low-level nonlinear controller for tracking while discarding $\lambda_{t|t}^*$ (see Fig. 4.2).

4.3.2 Distributed MPC

This section aims to develop a network of distributed MPCs with a smaller number of decision variables that plan for the cooperative locomotion of two holonomically constrained quadrupedal robots. From (4.13), the local dynamics of the agent $i \in \mathcal{I}$ can be expressed as follows:

$$\mathbf{x}_{i,k+t+1|t} = \mathbf{A}_{\text{op},ii} \mathbf{x}_{i,k+t|t} + \mathbf{B}_{\text{op},ii} \mathbf{u}_{i,k+t|t} + \mathbf{C}_{\text{op},i} \lambda_{k+t|t} + \mathbf{d}_{\text{op},i} + \Delta_i(\mathbf{x}_{j,k+t|t}, \mathbf{u}_{j,k+t|t}), \quad (4.17)$$

for $j \neq i \in \mathcal{I}$, where $\mathbf{A}_{\text{op},ii}, \mathbf{A}_{\text{op},ij} \in \mathbb{R}^{12 \times 12}$, $\mathbf{B}_{\text{op},ii}, \mathbf{B}_{\text{op},ij} \in \mathbb{R}^{12 \times \frac{3}{2}m_u}$, $\mathbf{C}_{\text{op},i} \in \mathbb{R}^{12}$, and $\mathbf{d}_{\text{op},i} \in \mathbb{R}^{12}$ denote the corresponding partitioning of $(\mathbf{A}_{\text{op}}, \mathbf{B}_{\text{op}}, \mathbf{C}_{\text{op}}, \mathbf{d}_{\text{op}})$. In addition,

$$\Delta_i(\mathbf{x}_{j,k+t|t}, \mathbf{u}_{j,k+t|t}) := \mathbf{A}_{\text{op},ij} \mathbf{x}_{j,k+t|t} + \mathbf{B}_{\text{op},ij} \mathbf{u}_{j,k+t|t} \quad (4.18)$$

represents the interaction term on the agent i . Similarly, the equality constraints (4.15) can be rewritten as follows:

$$\mathbf{E}_{\text{op},i} \mathbf{x}_{i,k+t|t} + \mathbf{F}_{\text{op},i} \mathbf{u}_{i,k+t|t} + \mathbf{G}_{\text{op}} \lambda_{k+t|t} + \mathbf{h}_{\text{op}} + \Omega_i(\mathbf{x}_{j,k+t|t}, \mathbf{u}_{j,k+t|t}) = 0, \quad (4.19)$$

in which $\mathbf{E}_{\text{op},i} \in \mathbb{R}^{3 \times 12}$ and $\mathbf{F}_{\text{op},i} \in \mathbb{R}^{3 \times \frac{3}{2}m_u}$ are the corresponding columns of $(\mathbf{E}_{\text{op}}, \mathbf{F}_{\text{op}})$, and

$$\Omega_i(\mathbf{x}_{j,k+t|t}, \mathbf{u}_{j,k+t|t}) := \mathbf{E}_{\text{op},j} \mathbf{x}_{j,k+t|t} + \mathbf{G}_{\text{op},j} \mathbf{u}_{j,k+t|t}$$

for $j \neq i$. Motivated by the inherent limitation of the distributed QP problems, one would need to estimate the interaction terms Δ_i and Ω_i , $i \in \mathcal{I}$ to solve for local QPs. For this purpose, we make the following assumption.

Assumption 4.5 (One-Step Communication Protocol). At every time sample t , each local MPC has access to the optimal solution of the other local MPC at time $t-1$. More specifically, the local MPCs share their previous optimal solutions over the network.

From Assumption 4.5, we can estimate the interaction terms Δ_i and Ω_i in (4.17) and (4.19) using the previous optimal solutions, that is,

$$\begin{aligned} \Delta_i(\mathbf{x}_{j,k+t|t}, \mathbf{u}_{j,k+t|t}) &\approx \Delta_i(\mathbf{x}_{j,k+t|t-1}^*, \mathbf{u}_{j,k+t|t-1}^*) \\ \Omega_i(\mathbf{x}_{j,k+t|t}, \mathbf{u}_{j,k+t|t}) &\approx \Omega_i(\mathbf{x}_{j,k+t|t-1}^*, \mathbf{u}_{j,k+t|t-1}^*), \end{aligned} \quad (4.20)$$

in which $\mathbf{x}_{j,k+t|t-1}^*$ and $\mathbf{u}_{j,k+t|t-1}^*$ denote the optimal solution from the local QP j for time $k+t$ computed at time $t-1$ for $k = 0, 1, \dots, N-1$. We remark that as the QP j does not plan for $\mathbf{u}_{N-1+t|t-1}$, we let $\mathbf{u}_{N-1+t|t-1}^* = 0$. The assumption in (4.20) estimates the interaction terms in the local dynamics and equality constraints based on the optimal values from the local QP j at the previous time sample. With this assumption, the local MPC i needs to optimally solve for its own local state trajectory $\mathbf{x}_i(\cdot)$, local control trajectory $\mathbf{u}_i(\cdot)$, and the Lagrange multiplier trajectory $\lambda(\cdot)$. However, as the Lagrange multiplier λ is

common between the decision variables of two local MPCs, they need to reach a consensus over time for the optimal λ value.

To address the consensus problem, we develop an agreement protocol as follows. The cost function of the centralized MPC (4.16) can be written as the sum of individual terms, i.e.,

$$\mathcal{J}_1(\mathbf{x}_1(\cdot), \mathbf{u}_1(\cdot)) + \mathcal{J}_2(\mathbf{x}_2(\cdot), \mathbf{u}_2(\cdot)) + \mathcal{J}_\lambda(\lambda(\cdot)). \quad (4.21)$$

We assume that each local QP estimates its own trajectory of the Lagrange multiplier, denoted by $\lambda_i(\cdot)$. We then propose the following real-time distributed MPC for agent $i \in \mathcal{I}$

$$\begin{aligned} \min_{(\mathbf{x}_i(\cdot), \mathbf{u}_i(\cdot), \lambda_i(\cdot))} & \mathcal{J}_i(\mathbf{x}_i(\cdot), \mathbf{u}_i(\cdot)) + \mathcal{J}_\lambda(\lambda_i(\cdot)) + w \sum_{k=0}^{N-1} \|\lambda_{i,k+t|t} - a_{ii} \lambda_{i,k+t|t-1}^* - a_{ij} \lambda_{j,k+t|t-1}^*\|^2 \\ & + \beta_{j,t-1}^{*\top} \mathcal{K}_{j,i} \begin{bmatrix} \mathbf{x}_i(\cdot) \\ \mathbf{u}_i(\cdot) \end{bmatrix} + \beta_{j,t-1}^{*\top} \mathcal{K}_{j,\lambda} \lambda_i(\cdot) \\ \text{s.t.} & \text{Local prediction model (4.17) with (4.20)} \\ & \text{Local equality constraints (4.19) with (4.20)} \\ & \mathbf{u}_{i,k+t|t} \in \mathcal{U}_i, \quad k = 0, 1, \dots, N-1, \end{aligned} \quad (4.22)$$

where w is a positive weighting factor added to introduce a new term in the local cost function to address the agreement protocol. In particular, the agreement term penalizes the difference between the local predicted values of $\lambda_{i,k+t|t}$ and the average of the previously computed optimal values $\lambda_{i,k+t|t-1}^*$ and $\lambda_{j,k+t|t-1}^*$ by the local MPCs i and j at time $t-1$. Here, a_{ii} and a_{ij} are the weighting factors for averaging with the property $a_{ii}, a_{ij} \in [0, 1]$ and $a_{ii} + a_{ij} = 1$, where $i \neq j \in \mathcal{I}$. The last two terms in the cost functions will be described shortly. The distributed MPC (4.22) has two sets of equality constraints arising from a) the local dynamics (4.17), and b) the holonomic constraint (4.19) with the assumption (4.20).

The proposed local MPC for the agent i does not consider the local dynamics of the other agent (i.e., agent j). Instead, motivated by our previous work [112], it uses the Karush–Kuhn–Tucker (KKT) Lagrange multipliers that correspond to the equality constraint arising from the local dynamics of the agent j in the QP j at time $t-1$. This set of *KKT Lagrange multipliers* is denoted by $\beta_{j,t-1}^*$. In addition, $\mathcal{K}_{j,i}$ and $\mathcal{K}_{j,\lambda}$ represent the *sensitivity* (i.e., gradient) of the local dynamics j with respect to the local variables $(\mathbf{x}_i(\cdot), \mathbf{u}_i(\cdot))$ and $\lambda(\cdot)$, respectively. In particular, $\mathcal{K}_{j,i}$ can be computed in a straightforward manner by taking the gradient of the local interaction terms Δ_j with respect to $(\mathbf{x}_{i,k+t|t}, \mathbf{u}_{i,k+t|t})$ over the entire control horizon and stacking the results together, that is,

$$\mathcal{K}_{j,i} := \frac{\partial \text{col}\{\Delta_j(\mathbf{x}_{i,k+t|t}, \mathbf{u}_{i,k+t|t}) \mid k = 0, 1, \dots, N-1\}}{\partial(\mathbf{x}_i(\cdot), \mathbf{u}_i(\cdot))}.$$

An analogous approach can be used to compute the sensitivity matrix $\mathcal{K}_{j,\lambda}$. We then add the last two linear terms to the cost function of the local MPC (4.22). Our previous work [112,

Theorem 1] has shown that the inclusion of the KKT Lagrange multipliers $\beta_{j,t-1}^*$ together with the sensitivity matrices $(\mathcal{K}_{j,i}, \mathcal{K}_{j,\lambda})$ in the cost function can result in a set of local KKT conditions that have a similar structure to that of the KKT equations for the centralized problem. Finally, \mathbf{u}_i in (4.22) represents the local feasibility set for the GRFs (i.e., inputs).

Remark 4.6. We remark that local MPCs in the proposed structure (4.22) share their optimal local state trajectory $\mathbf{x}_i^*(\cdot)$, local control trajectory $\mathbf{u}_i^*(\cdot)$, local estimates of the Lagrange multiplier trajectory $\lambda_i^*(\cdot)$, and the KKT Lagrange multipliers corresponding to the local dynamics in the QP structure β_i^* with the other agent and according to the one-step communication delay protocol (see Fig. 4.3). Finally, the number of decision variables for each local MPC becomes $(13 + \frac{3}{2} m_u) N$. Section 4.6.2 will numerically study and show the consensus problem of the estimated Lagrange multipliers.

4.4 Distributed Nonlinear Controllers for Full-Order Models

The objective of this section is to present the low-level and distributed nonlinear controllers for the whole-body motion control of each agent. The full-order and floating-based model of the agent i can be described by the Euler-Lagrange equations and principle of virtual work as follows:

$$D(q_i) \ddot{q}_i + H(q_i, \dot{q}_i) = \Upsilon \tau_i + \sum_{\ell \in \mathcal{C}_i} J_\ell^\top(q_i) f_i^\ell + J_{\text{int}}^\top(q_i) (p_i - p_j) \lambda, \quad (4.23)$$

where $q_i \in \mathcal{Q} \subset \mathbb{R}^{n_q}$ represents the generalized coordinates of the robot i , \mathcal{Q} and n_q denote the configuration space and number of DOFs, respectively, $\tau_i \in \mathcal{T} \subset \mathbb{R}^{n_\tau}$ represents the joint-level torques at the actuated joints, \mathcal{T} is a closed and convex set of admissible torques, and \mathcal{C}_i represents the set of contacting legs with the environment. In addition, f_i^ℓ denotes the GRF at the contacting leg $\ell \in \mathcal{C}_i$ of the full-order model for the agent i . We remark that the GRF at the contacting leg $\ell \in \mathcal{C}_i$ of the reduced-order model for the agent i was denoted by u_i^ℓ in Section 4.2. This is due to the possible gap between the reduced- and full-order models arising from abstraction (i.e., ignoring legs' dynamics). Moreover, $D(q_i) \in \mathbb{R}^{n_q \times n_q}$ denotes the positive definite mass-inertia matrix, $H(q_i, \dot{q}_i) \in \mathbb{R}^{n_q}$ represents the Coriolis, centrifugal, and gravitational terms, $\Upsilon \in \mathbb{R}^{n_q \times n_\tau}$ is the input distribution matrix, $J_\ell(q_i)$ denotes the contact Jacobin matrix at the leg ℓ , $J_{\text{int}}(q_i)$ represents the Jacobian of the interaction point p_i , and $(p_i - p_j) \lambda$ denotes the interaction force between the two agents as described in the reduced-order model of Section 4.2. The local and full-order state variables for the agent i is defined as $z_i := \text{col}(q_i, \dot{q}_i) \in \mathcal{Q} \times \mathbb{R}^{n_q}$. For future purposes, the vector of GRFs for the agent i is shown by $f_i := \text{col}\{f_i^\ell \mid \ell \in \mathcal{C}_i\}$.

For the whole-body motion control of each agent, we develop a QP-based nonlinear controller that maps the desired optimal trajectories and GRFs, generated by the high-level MPC, to

the full-order model. For this purpose, we consider the following time-varying and holonomic output functions, referred to as *virtual constraints* [74], to be regulated:

$$y_i(t, z_i) := y_a(q_i) - y_{\text{des}}(t), \quad (4.24)$$

where $y_a(q_i)$ represents a set of controlled variables and $y_{\text{des}}(t)$ denotes the desired evolution of the controlled variables in terms of a time-based phasing variable. In this chapter, the controlled variables include the Cartesian coordinates of the robot's COM, the absolute orientation of the robot's body (i.e., Euler angles), and Cartesian coordinates of the swing leg ends. The desired evolution of the COM position and Euler angles are generated by the high-level MPC. In addition, the desired evolution of the swing leg ends' coordinates are taken as a Bézier polynomial connecting the current footholds to the upcoming ones, computed based on Raibert's heuristic [165, Eq. (2.4), pp. 46].

We next implement the standard I-O linearization technique [106] to differentiate the local outputs (4.24) twice along the full-order dynamics (4.23) while ignoring the interaction forces between the agents. This results in the following output dynamics

$$\ddot{y}_i = \Phi_\tau(z_i) \tau_i + \Phi_f(z_i) f_i + \phi(z_i) = -K_P y_i - K_D \dot{y}_i + \delta_i, \quad (4.25)$$

where $\Phi_\tau(z_i)$, $\Phi_f(z_i)$, and $\phi(z_i)$ are proper matrices and vectors computed based on I-O linearization and Lie derivatives similar to [116, Appendix A]. Moreover, K_P and K_D are positive definite matrices, and δ_i is a slack variable to be used later for the feasibility of the QP-based nonlinear controller. Unlike the high-level trajectory planner of Section 4.3 that takes into account the interaction terms, the low-level nonlinear controller ignores the interaction forces. In particular, our numerical results in Section 4.5 suggest that considering holonomic constraints for trajectory planning is crucial for stabilizing cooperative locomotion. However, the optimal trajectories, generated by the high-level MPC, can be robustly mapped to the full-order model without considering the interaction terms at the low level. This reduces the complexity of the distributed and full-order model controllers.

By stacking together the Cartesian coordinates of the stance leg ends and then differentiating them twice, one can get an additional constraint to express zero acceleration for the stance leg ends. In particular, we have

$$\ddot{r}_{\text{foot},i} = \Theta_\tau(z_i) \tau_i + \Theta_f(z_i) f + \theta(z_i) = 0, \quad (4.26)$$

where $r_{\text{foot},i} := \text{col}\{r_{\text{foot},i}^\ell \mid \ell \in \mathcal{C}_i\}$ is a vector containing the Cartesian coordinates of the stance feet for the agent i . Moreover, $\Theta_\tau(z_i)$, $\Theta_f(z_i)$, and $\theta(z_i)$ are proper matrices and vectors computed based on I-O linearization. We then employ the following real-time and strictly convex QP [74] to solve for feasible (τ_i, f_i, δ_i) at 1kHz to meet the output dynamics

(4.17) and the contact equation (4.26)

$$\begin{aligned}
& \min_{(\tau_i, f_i, \delta_i)} \frac{\gamma_1}{2} \|\tau_i\|^2 + \frac{\gamma_2}{2} \|f_i - f_{\text{des},i}\|^2 + \frac{\gamma_3}{2} \|\delta_i\|^2 \\
& \text{s.t. } \Phi_\tau(z_i) \tau_i + \Phi_f(z_i) f_i + \phi(z_i) = -K_P y_i - K_D \dot{y}_i + \delta_i \\
& \quad \Theta_\tau(z_i) \tau_i + \Theta_f(z_i) f_i + \theta(z_i) = 0 \\
& \quad \tau_i \in \mathcal{T}, \quad f_i^\ell \in \mathcal{FC}, \quad \forall \ell \in \mathcal{C}_i,
\end{aligned} \tag{4.27}$$

where γ_1 , γ_2 , and γ_3 are positive weighting factors, and $f_{\text{des},i}$ represents the desired evolution of the GRFs generated by the high-level MPC. The cost function of (4.27) tries to minimize the effect of the slack variable δ_i in the output dynamics (4.25) via a high weighting factor γ_3 while 1) imposing the actual GRFs of the full-order model f_i to follow the prescribed force profile $f_{\text{des},i}$ with the weighting factor γ_2 , and 2) having the minimum-power torques with the weighting factor γ_1 .

4.5 Numerical and Experimental Validations

This section aims to validate the proposed layered control architecture composed of the high-level centralized and distributed MPC algorithms and the low-level distributed nonlinear controllers via extensive numerical simulations and experiments. We study both the reduced- and full-order models of cooperative locomotion in numerical simulations to show the robust stability of the collaborative gaits. We further experimentally investigate the robustness of the trajectories with a team of two holonomically constrained A1 robots, as shown in Fig. 4.1.

4.5.1 Closed-Loop System

Robot hardware and gait

The hardware platform considered here, the A1 robot, is a torque-controlled quadrupedal robot platform with 18 DOFs and 12 actuators. More specifically, 12 DOFs of the system represent the actuated DOFs of the legs' joints. Each leg consists of a 2-DOF hip joint (roll and pitch) and a 1-DOF knee joint (knee pitch). The remaining 6 DOFs describe the unactuated position and orientation of the body with respect to the inertial world frame. The robot is approximately 12.45 (kg) and stands up to about 0.3 (m) off the ground. This work considers a standing height of 0.26 (m) for all experiments. Here, the position of the interactions points with respect to COMs in the body frames $\{B_i\}$ is taken as $d_i^{B_i} = \text{col}(0, 0, 0.15)$ (m) for all $i \in \mathcal{I}$ (see (4.1)). Different mechanisms are designed to holonomically constrain the motion of two robots with ball joints and an adjustable bar length between the agents (see Fig. 4.5). Furthermore, the mechanisms can limit the ball joints to add further constraints

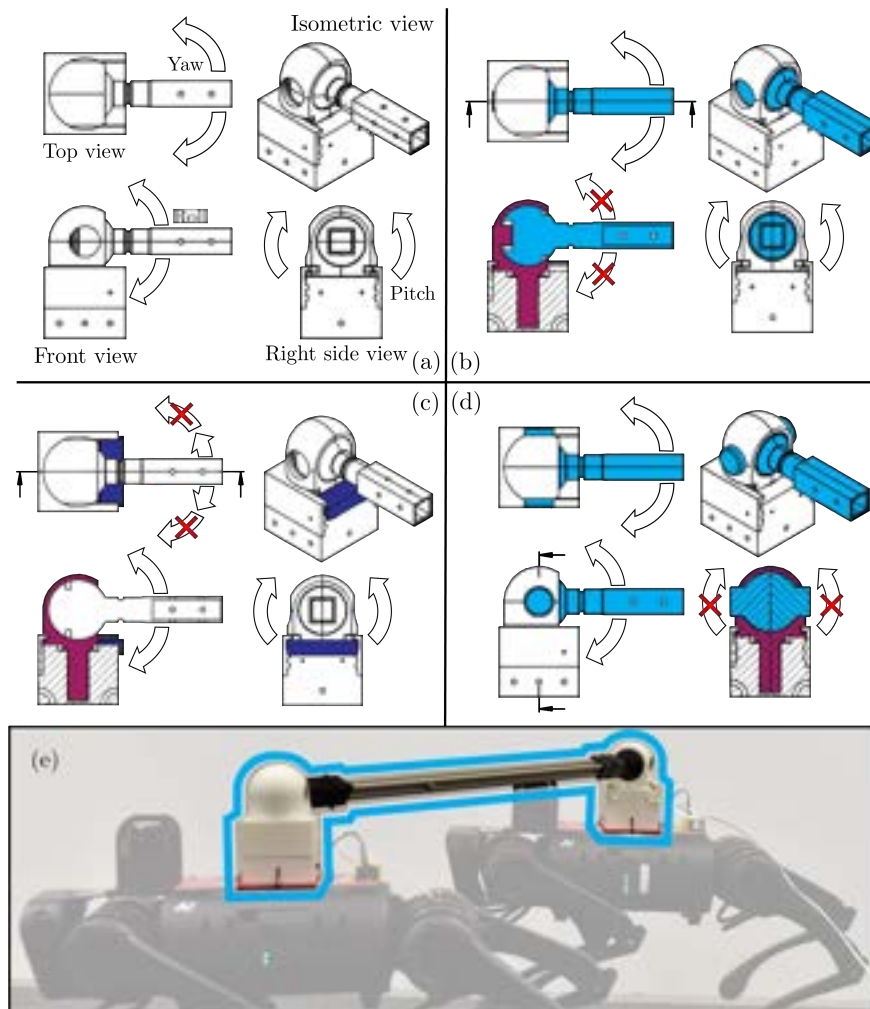


Figure 4.5: Illustration of the mechanisms designed to be mounted on the torso of each robot to holonomically constrain the motion of agents. The mechanism in (a) can implement the holonomic constraint (4.2) with free ball joints. The mechanisms in (b), (c), and (d) implement the constraint (4.2) while also restricting the roll, yaw, and pitch motions, respectively. The mechanism implemented on top of the robots is illustrated in (e).

on their Euler angles. For numerical and experimental studies in Sections 4.5.2 and 4.5.3, the nominal length of the bar is 1 (m) (see Fig. 4.1). However, we will alter it to 0.75 (m) and 1.5 (m) for the robustness analysis.

In the following sections, we study a cooperative trot gait with a swing time of 0.2 (s) and at different speeds up to 0.5 (m/s) and subject to external disturbances, uncertainties in holonomic constraints, unknown payloads up to 55% uncertainty in one robot’s mass, and on different terrains (e.g., slippery surfaces, wooden blocks, gravel, mulch, and grass).

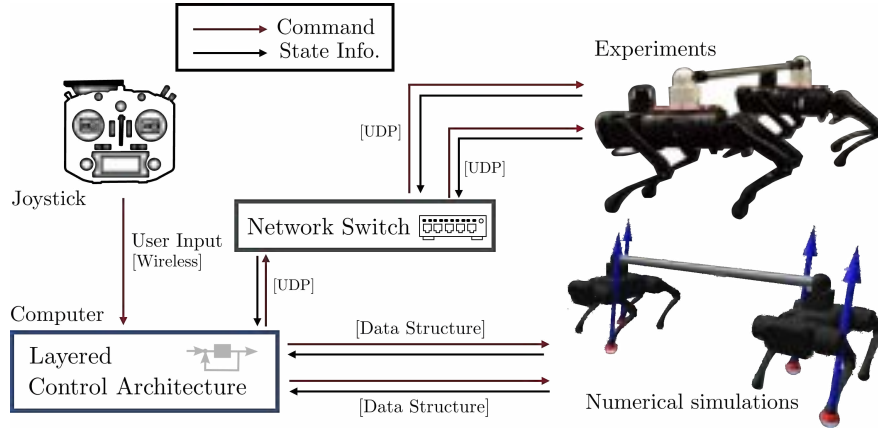


Figure 4.6: Numerical and experimental validation system setup. Here, the joystick commands the desired velocity trajectories to the trajectory planner of each agent. Both agents are controlled by one joystick. Joystick sends out the desired trajectories on both numerical simulations and experimental validations. The network switch is used to build the connection between the computer and two agents without IP address collision. UDP communication protocol through Ethernet cables is used in experimental validations.

Computation, control loop, and network

We use RaiSim [105] to simulate both the interconnected reduced- and full-order models numerically. The proposed high-level centralized and distributed MPC algorithms for trajectory planning and the low-level distributed nonlinear controllers for whole-body motion control are solved using qpSWIFT [150] at 200 Hz and 1 kHz, respectively. A joystick is used to command the desired velocity trajectories to the high-level trajectory planner. The joystick includes two 2-DOFs gimbals, six auxiliary switches, and two knobs for the controlling purpose (see Fig. 4.6). The gimbals are used to command the desired speed, whereas the switches allow us to simultaneously control both agents or individually command them. This control scheme allows us to coordinate the agents during cooperative locomotion and unexpected scenarios effectively. This will be discussed further in Section 4.6.5. Moreover, we remark that the joystick commands the desired trajectories for both the numerical simulations and experimental validations. The joystick connects with the computer through a 2.4 GHz wireless channel as described in Fig. 4.6.

The proposed layered controller, including the MPC-based trajectory planners and distributed nonlinear controllers, is solved on an off-board laptop computer with an i7-10750H CPU running at 2.60 GHz and 16 GB RAM. For the experiment, we use a network switch in the connection between the robotic team and the computer. The connection diagram is illustrated in Fig. 4.6. The switch supports 1000 Mbps gigabit Ethernet with five ports. The robot IP addresses are redefined to avoid IP collision during communication. Here, we also define the IP routing table and proper IP address on the computer to communicate with both

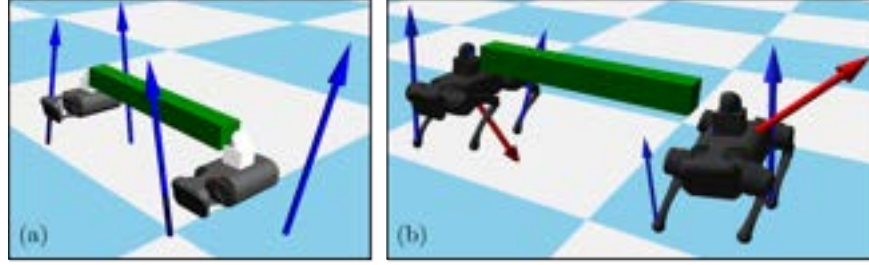


Figure 4.7: Snapshots demonstrating the performance of the proposed control approach in numerical simulations. The left plot shows the snapshot of the numerical simulation with the interconnected reduced-order model (torso dynamics) and subject to a 5 (kg) payload (40% uncertainty in one robot’s mass) between the agents. The right plot shows the snapshot of the numerical simulation with the full-order model and subject to a 5 (kg) payload between agents and unknown time-varying external disturbances applied to the robots. Arrows at the leg ends describe the GRFs, and the ones on the torso represent the external disturbance forces. The payload is illustrated with a box.

agents without data packet confusion. Internally, a UDP protocol through Ethernet cables is used to communicate between the computer and the robots. The data structure in C++ is used for numerical simulations to communicate between the layered control architecture and the simulation environment.

Tuning controllers

The control horizon for both the centralized and distributed MPC is taken as $N = 5$ discrete-time samples, where the time discretization at the high level is 5 (ms). The centralized and distributed MPC algorithms in (4.16) and (4.22) have 245 and 125 decision variables, respectively. The stage cost gain of the centralized MPC is tuned as $\mathbf{Q} = \text{diag}\{Q_{rc1} Q_{rc2} Q_{rc1} Q_{rc2} Q_{\xi1} Q_{\xi2} Q_{\omega1} Q_{\omega2}\} \in \mathbb{R}^{24 \times 24}$, where $Q_{rci} = 10^5 \times \text{diag}\{3 \ 300 \ 30\}$, $Q_{rci} = 10^4 \mathbb{I}_{3 \times 3}$, $Q_{\xi i} = 10^8 \mathbb{I}_{3 \times 3}$, and $Q_{\omega i} = 5 \times 10^3 \mathbb{I}_{3 \times 3}$, $i \in \mathcal{I}$. The terminal cost gain of the centralized MPC is also tuned as $\mathbf{P} = 10^{-1} \mathbf{Q} \in \mathbb{R}^{24 \times 24}$. The input gains of the centralized MPC are chosen as $\mathbf{R}_u = 10^{-2} \mathbb{I}_{24 \times 24}$ and $\mathbf{R}_\lambda = 10^4$. In a similar manner, the stage cost gain and terminal cost gain of the distributed MPC on the i -th agent are tuned as $\mathbf{Q}_i = \text{diag}\{Q_{rci} Q_{rci} Q_{\xi i} Q_{\omega i}\} \in \mathbb{R}^{12 \times 12}$ and $\mathbf{P}_i = 10^{-1} \mathbf{Q}_i \in \mathbb{R}^{12 \times 12}$. The input gains of the distributed MPC are finally chosen as $\mathbf{R}_u = 10^{-2} \mathbb{I}_{12 \times 12}$ and $\mathbf{R}_\lambda = 10^4$. Additionally, we choose the weighting factor for the agreement protocol in (4.22) as $w = 10$, and the averaging factors in (4.22) are chosen as $a_{ii} = a_{ij} = 0.5$ for all $i \neq j \in \mathcal{I}$. The friction coefficient for both the centralized MPC and distributed MPC algorithms is assumed to be $\mu = 0.6$. However, the experiments on slippery surfaces assume a lower friction coefficient of $\mu = 0.3$. For the low-level and distributed nonlinear controllers in (4.27), the weighting factors for the joint-level torques, force tracking error, and slack variables are chosen as $\gamma_1 = 10^2$, $\gamma_2 = 10^4$,

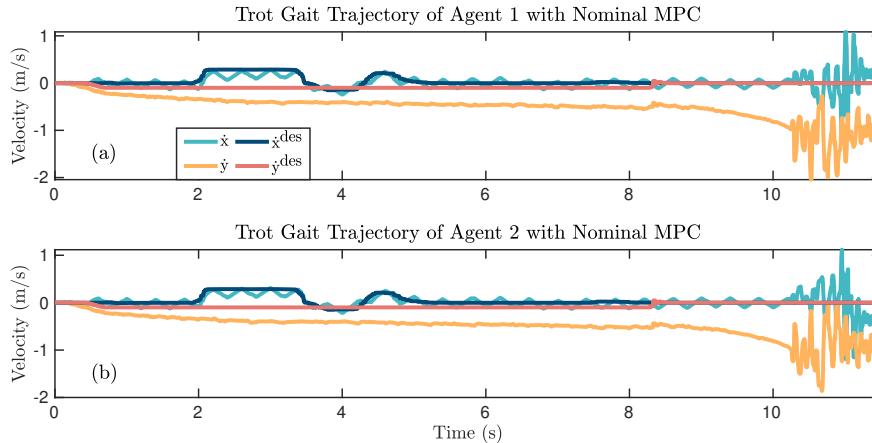


Figure 4.8: Plots of the desired and actual velocities of the closed-loop interconnected reduced-order model for two agents in the numerical simulation. Here, two nominal MPCs are applied to the reduced-order models of agents to generate optimal GRFs *without* considering the holonomic constraints between them. The joystick provides desired trajectories. The instability of the cooperative gait is evident.

and $\gamma_3 = 10^6$, respectively. We finally remark that the low-level controller uses the same friction coefficient values from the high-level MPC.

The computation time of the centralized and distributed MPC algorithms under nominal conditions is approximately 1.38 (ms) and 0.41 (ms), respectively. This shows that the solve time with the proposed distributed MPC is reduced by 70%. Furthermore, the computation time of the low-level distributed nonlinear controllers is about 0.12 (ms).

4.5.2 Numerical Validation

Simulation with the reduced-order model

We model the interconnected SRB dynamics in the RaiSim environment for numerical validation and apply the optimal GRFs generated from the proposed centralized (4.16) and distributed MPC (4.22) algorithms. In addition, for comparison purposes, we apply the GRFs generated from the nominal MPC that considers a standard SRB model *without* the holonomic constraints to this interconnected model. An overview of the numerical simulation environment for the interconnected reduced-order model is illustrated in Fig. 4.7(a). The evolution of the desired and actual COM velocities using the nominal MPC is depicted in Fig. 4.8. It is evident that the nominal MPC, which does not consider the holonomic constraint between agents, *cannot* stabilize the interconnected reduced-order system. On the other hand, the interconnected SRB model performs stable cooperative locomotion when integrated with the GRFs generated from the proposed centralized and distributed MPCs as shown in Figs. 4.9 and 4.10, respectively. In these simulations, an unknown payload of

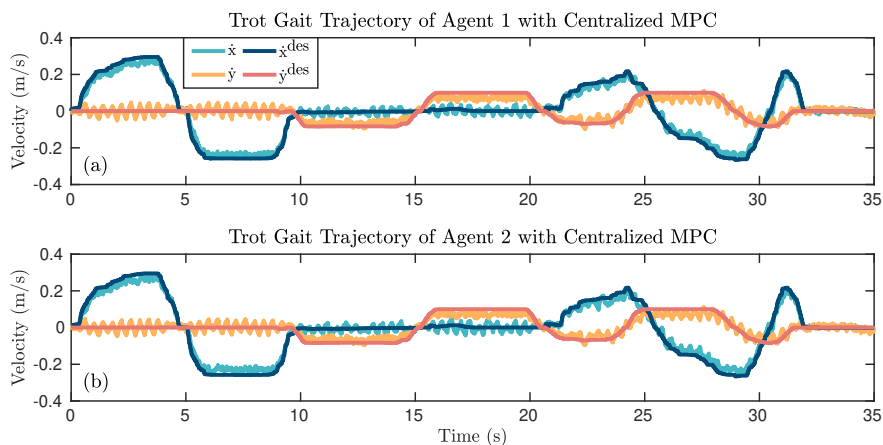


Figure 4.9: Plots of the desired and actual velocities of the closed-loop interconnected reduced-order model for two agents in the numerical simulation. Here, the optimal GRFs are generated by the centralized MPC (4.16) and are applied to the reduced-order models subject to an unknown payload of 5 (kg) between agents. A joystick provides desired trajectories. The robust tracking is evident.

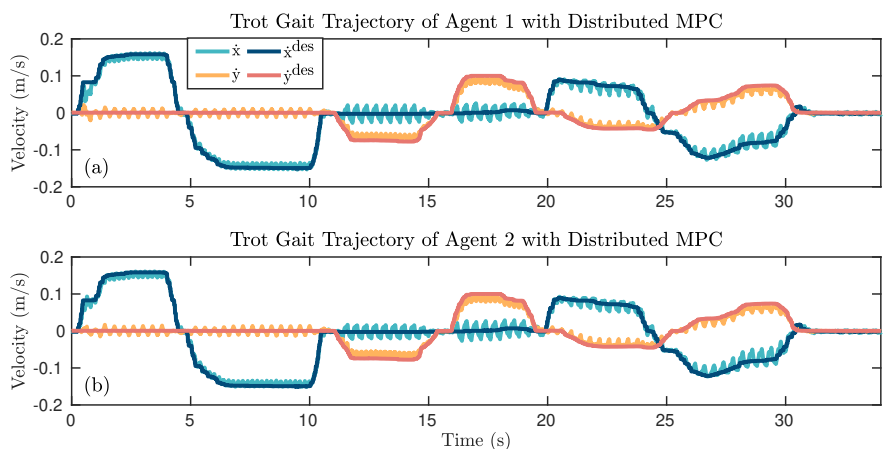


Figure 4.10: Plots of the desired and actual velocities of the closed-loop interconnected reduced-order model for two agents in the numerical simulation. Here, the optimal GRFs are generated by the distributed MPCs (4.22) and are applied to the reduced-order models subject to an unknown payload of 5 (kg) between agents. A joystick provides desired trajectories. The robust tracking is evident.

5 (kg) (40% uncertainty in one robot's mass) is considered between the agents (i.e., in the middle of the bar), and the joystick provides the desired trajectories. Figures 4.9 and 4.10 illustrate that the closed-loop interconnected reduced-order model robustly tracks the time-varying desired trajectories subject to unknown payloads. Animations of all simulations can

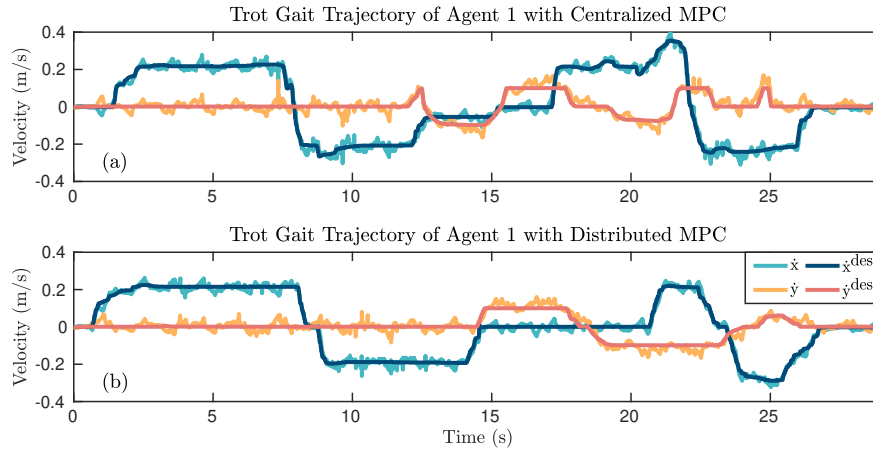


Figure 4.11: Comparison between the desired velocities and optimal velocities, generated with the high-level centralized and distributed MPCs, for the closed-loop interconnected full-order model in RaiSim. The joystick provides time-varying reference trajectories. The figure depicts the optimal trajectories generated by (a) the centralized MPC (4.16) and (b) the distributed MPC (4.22) for agent 1. Here, we consider a trot gait over rough terrain with an unknown payload of 5 (kg) between the agents and subject to unknown, time-varying, and external disturbance forces applied to the robots.

be found online ¹.

Simulation with the full-order model

We next numerically study the performance of the closed-loop system with the interconnected full-order dynamical model in RaiSim. Here, the proposed layered control approach is employed, including the centralized and distributed MPC algorithms for trajectory planning and nonlinear controllers for whole-body motion control. The desired time-varying trajectories are generated using the joystick. The high-level MPC then generates optimal GRFs and reduced-order trajectories from the centralized and distributed algorithms. The distributed low-level controller computes the corresponding joint-level torques to impose the full-order model to track the optimal trajectories. An overview of the numerical simulation environment for the full-order model is illustrated in Fig. 4.7(b). The desired trajectories provided by the joystick together with the optimal trajectories computed by the centralized and distributed MPC are depicted in Figs. 4.11(a) and 4.11(b). Due to the similarity of the plots for agents, Fig. 4.11 only includes the trajectories for agent 1. Here, we consider the trot gait over a randomly generated rough terrain with a maximum height of 5 (cm) (19% uncertainty in the robot’s nominal height). The gait is also subject to an unknown payload of 5 (kg) and unknown sinusoidal external disturbance force with the magnitude of 20 (N)

¹<https://youtu.be/mzAFemO0XeI>

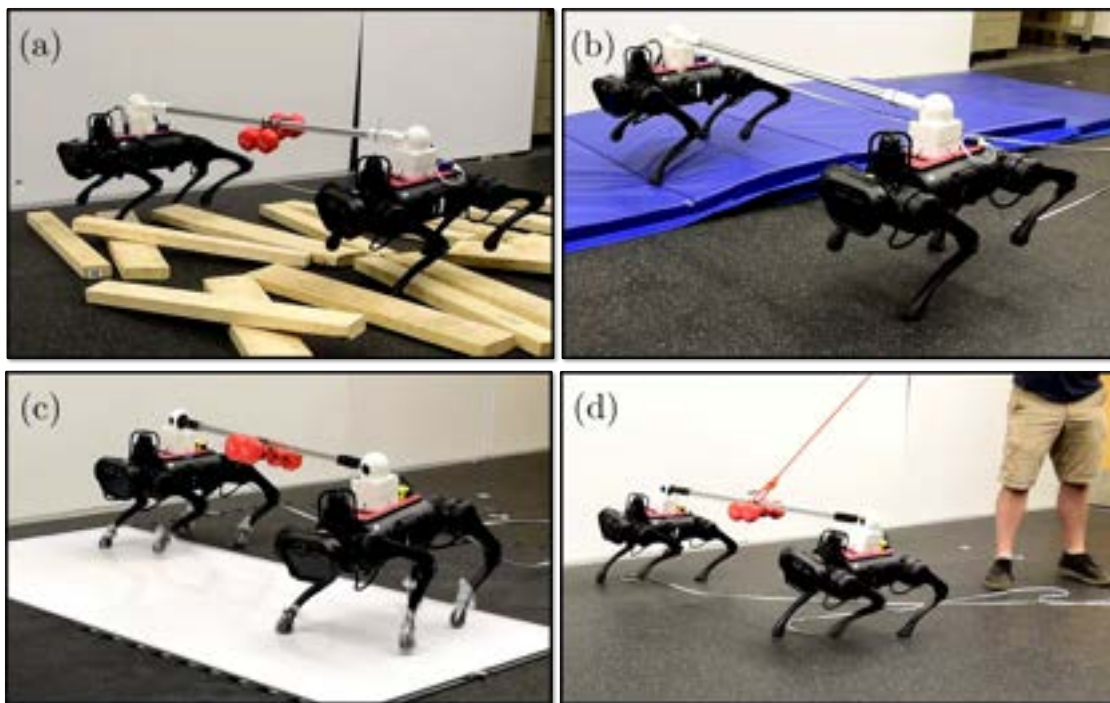


Figure 4.12: Snapshots demonstrating the performance of the proposed layered control algorithm for a series of cooperative locomotion experiments. Indoor experiments: (a) rough terrain with the agents traversing arbitrarily displaced wooden blocks, (b) asymmetrical terrain with one agent being on a compliant surface and elevated by 10 (cm), (c) slippery surface covered by a cooking spray, and (d) tethered pulling. The robots are loaded with a payload of 4.53 (kg) (36% uncertainty in one robot’s mass) in (a), (c), and (d). The friction coefficient is taken as $\mu = 0.3$ in (c) and $\mu = 0.6$ in (a), (b), and (d). Here, (a) and (b) show the snapshots where the centralized MPC is applied, while (c) and (d) show the snapshots where the distributed MPC is employed. Videos of all experiments are available online [<https://youtu.be/mzAFemO0XeI>].

and the period of 1.0 (s), 0.7 (s), and 0.4 (s) along the x -, y -, and z -directions, respectively. It is evident that the closed-loop system robustly tracks the desired trajectories.

4.5.3 Experimental Validation and Robustness Analysis

This section experimentally validates the proposed layered control approach with the high-level centralized and distributed MPC algorithms and the low-level distributed nonlinear controllers. The robustness of the cooperative gaits on different indoor and outdoor terrains and subject to unknown payloads and external disturbances is evaluated.

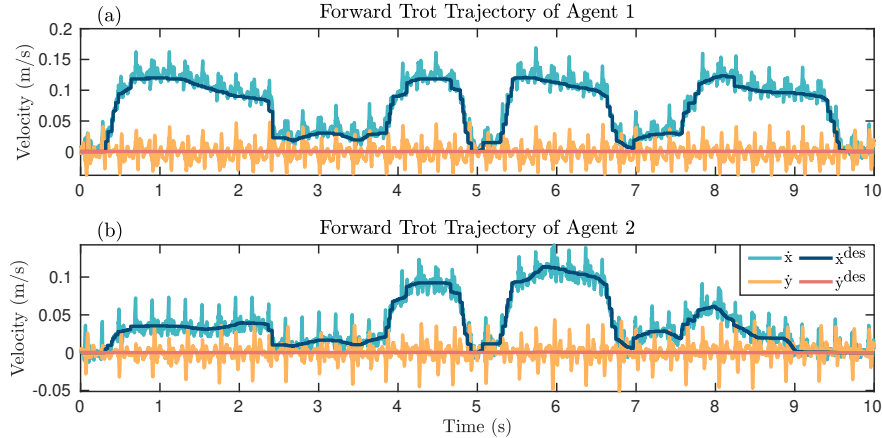


Figure 4.13: Comparison between the desired and optimal velocities of the robots for the nominal trot experiment on flat ground. Optimal velocities are provided from the high-level centralized MPC. Time-varying desired trajectories are provided by the joystick to coordinate the robots’ motions. It is observed that the centralized MPC’s outputs can successfully track the desired trajectories.

Indoor experiments with the centralized MPC

In the indoor experiments, we employ the proposed layered control algorithm on two A1 robots subject to holonomic constraints, where ball joints are applied at the interaction points (see Fig. 4.12). We first investigate the nominal and cooperative trot gait with the centralized MPC algorithm on flat ground and without unknown disturbances. The desired and optimal COM trajectories, generated by the high-level MPC, together with the generated optimal GRFs, are illustrated in Fig. 4.13 and Fig. 4.14, respectively. It is evident that the team of two A1 robots performs stable cooperative locomotion while the trajectory planner effectively tracks the time-varying desired trajectories. Furthermore, the optimal GRFs generated by the centralized MPC are feasible, with the vertical component value being close to 60 (N), which is approximately the force required by each stance leg to support the total mass of each robot during trotting.

We further investigate the robustness of the proposed layered control approach by studying the tracking performance of the closed-loop system with different experiments, including locomotion on rough terrain (see Fig. 4.12(a)), locomotion on a slippery surface (see Fig. 4.12(c)), and locomotion subject to unknown external disturbances (see Fig. 4.12(d)), as shown in Figs. 4.15(a), 4.15(b), and 4.15(c), respectively. In these experiments, the rough terrain is made of randomly displaced wooden blocks with a maximum height of 5 (cm) (19% of the robot’s height). Moreover, the slippery surface is a whiteboard covered with cooking spray. The unknown external disturbances are further applied by a human user, including pushes and tethered pulls on both agents. The robots cooperatively transport an unknown payload of 4.53 (kg) (36% uncertainty in one robot’s mass) in all these experiments. The

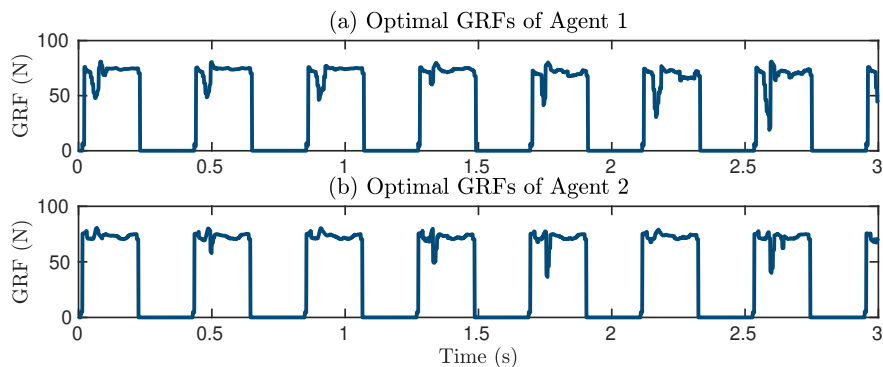


Figure 4.14: Plots of the optimal GRFs generated from the centralized MPC for agents 1 and 2 during the nominal trot experiment on flat ground. The figure depicts the z components of the optimal GRFs for the left front leg of each agent. We remark that the GRFs in the z -direction are close to 60 (N) since the trot gait is adopted and the total mass of the robot is 12.45 (kg).

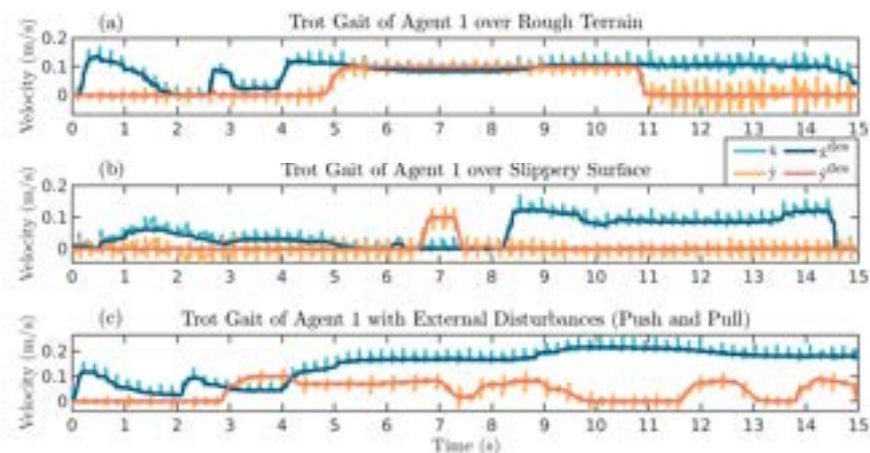


Figure 4.15: Plots of the desired and optimal velocities for cooperative locomotion experiments on (a) rough terrain, (b) a slippery surface, and (c) subject to external disturbances with the centralized MPC. Time-varying desired trajectories are provided by the joystick. It is clear that the centralized MPC's outputs can robustly track the desired trajectories in the presence of uncertainties and disturbances.

optimal GRFs computed by the MPC on rough terrain, on the slippery surface, and subject to external disturbances are depicted in Figs. 4.16(a), 4.16(b), and 4.16(c), respectively. We remark that despite the uncertainties, the GRFs are in the feasible range, and the MPC's outputs robustly track the desired and time-varying trajectories. Furthermore, the phase portraits of the body's roll and pitch motions (i.e., unactuated DOFs) during these cooperative trot gaits are shown in Figs. 4.17(a) and 4.17(b). Figure 4.17 indicates that the A1 robots can perform robustly stable cooperative locomotion in the presence of various

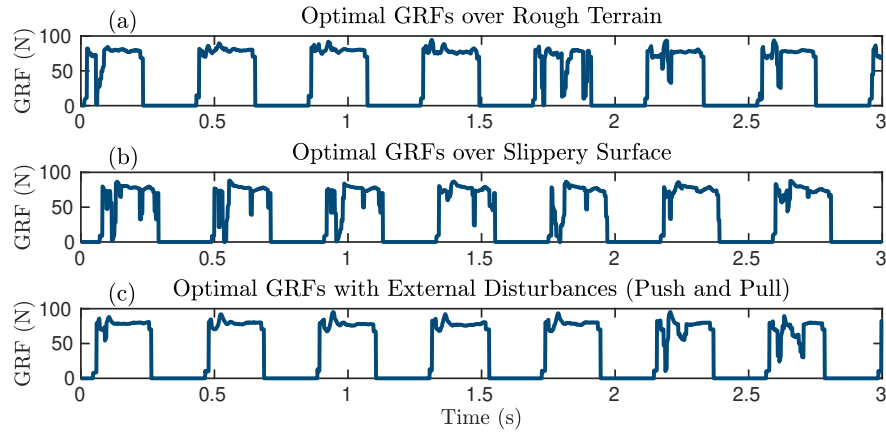


Figure 4.16: Plots of the optimal GRFs, generated by the centralized MPC, for cooperative locomotion experiments on (a) rough terrain, (b) a slippery surface, and (c) subject to external disturbances. The figure depicts the optimal GRFs for the left front leg of agent 1 along the z -direction.

unknown terrains and disturbances. Videos of all experiments are available online ².

Indoor experiments with the distributed MPC

In this part, we evaluate the performance of the closed-loop system with the proposed distributed MPC algorithm in similar indoor experiments (see Fig. 4.12). The evolution of the optimal trajectories generated from the distributed MPC and time-varying desired trajectories during the cooperative transportation of the same payload over rough terrain, the slippery surface, and subject to unknown disturbances are illustrated in Figs. 4.18(a), 4.18(b), and 4.18(c), respectively. The optimal GRFs are also shown in Fig. 4.19. The phase portraits of the body's roll and pitch motions during the cooperative gait with the distributed MPC algorithm and subject to these uncertainties are depicted in Figs. 4.17(c) and 4.17(d). It is evident that the optimal GRFs, generated by the MPC, remain feasible, and the MPC's outputs robustly track the desired trajectories in the presence of unknown terrains and external disturbances.

Outdoor experiments with centralized and distributed MPCs

We next investigate the performance and robustness of the closed-loop system with the centralized and distributed MPC algorithms in different outdoor experiments, as shown in Fig. 4.20. These experiments include cooperative locomotion on gravel, concrete, mulch, and grass subject to unknown payloads. In these studies, we investigate two different payloads:

²<https://youtu.be/mzAFemO0XeI>

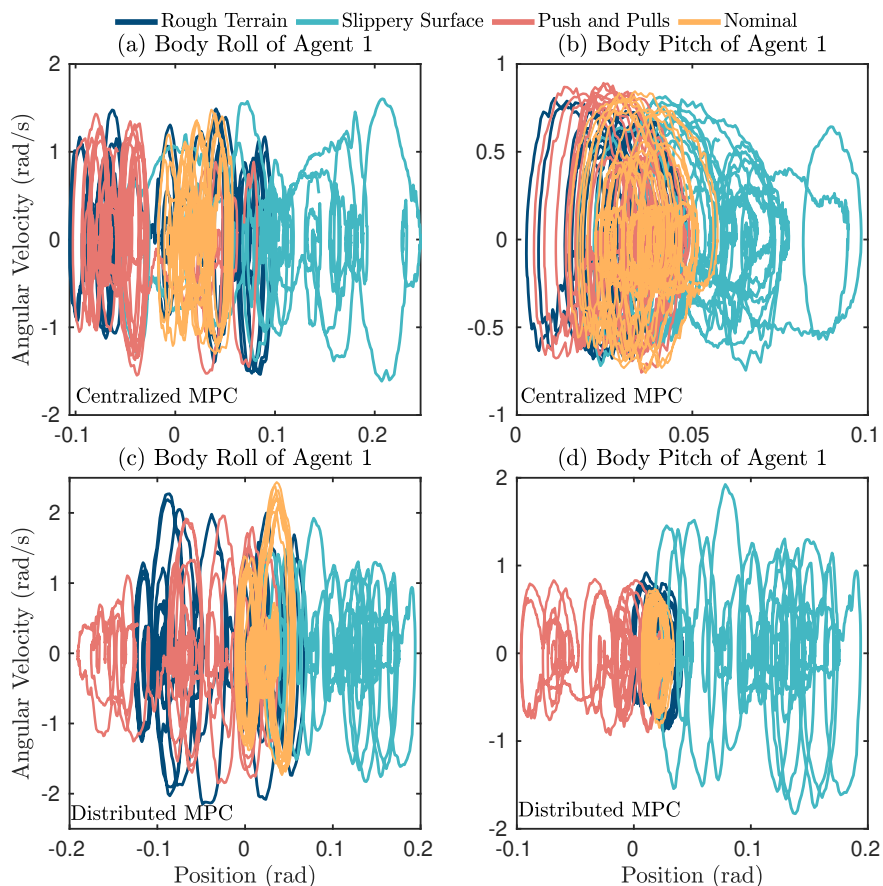


Figure 4.17: Phase portraits for (a) the body roll and (b) the body pitch of agent 1 with the centralized MPC and (c) the body roll and (d) the body pitch of agent 1 with the distributed MPCs during different experiments. The plots show the robustness of the cooperative locomotion over rough terrain covered with randomly dispersed wooden blocks, the slippery surface, and subject to unknown external disturbances.

a payload of 4.53 (kg) (36% uncertainty) in Figs. 4.20(b) and 4.20(c) and a payload of 6.80 (kg) (55% uncertainty) in Figs. 4.20(a) and 4.20(d). The evolution of the virtual constraints (4.24) for trotting over the gravel and transitioning from concrete to grass with the centralized MPC and trotting over mulch and grass with the distributed MPC is shown in Fig. 4.21. As the virtual constraint plots stay close to zero, we can conclude that the full-order system effectively tracks the optimal reduced-order trajectories generated by the high-level MPCs. Furthermore, it is evident that the proposed layered control approach with both centralized and distributed MPCs can robustly stabilize cooperative gaits in the presence of payloads on unknown outdoor terrains.

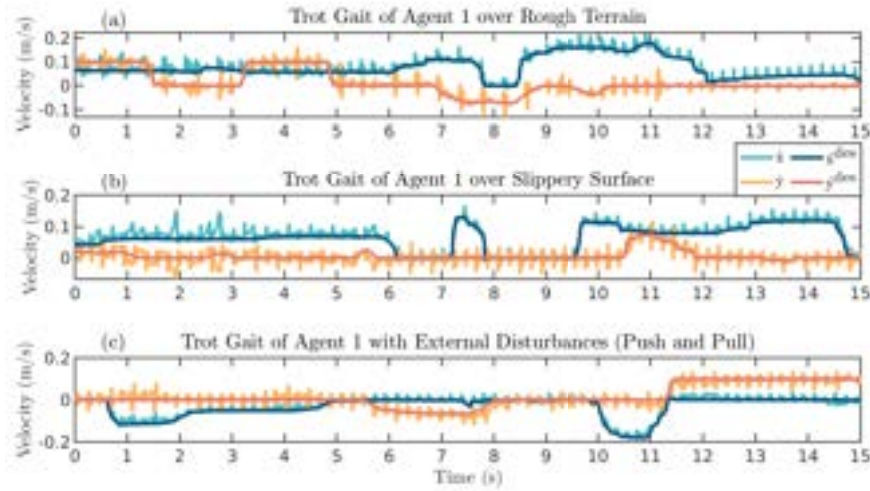


Figure 4.18: Plots of the desired and optimal velocities for cooperative locomotion experiments on (a) rough terrain, (b) a slippery surface, and (c) subject to external disturbances with the distributed MPC. Time-varying desired trajectories are provided by the joystick. It is clear that the distributed MPC’s outputs can robustly track the desired trajectories in the presence of uncertainties and disturbances.

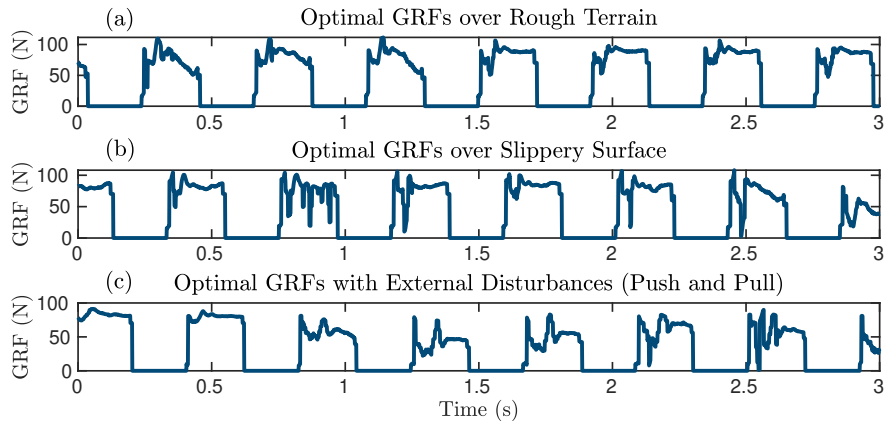


Figure 4.19: Plots of the optimal GRFs, generated by the distributed MPC, for cooperative locomotion experiments on (a) rough terrain, (b) a slippery surface, and (c) subject to external disturbances. The figure depicts the optimal GRFs for the left front leg of agent 1 along the z -direction.

4.6 Discussion and Comparison

Numerical simulations and experimental validations in Section 4.5 show the effectiveness of the proposed centralized and distributed MPC algorithms for cooperative locomotion. This section aims to analyze and compare the performance of the proposed MPCs while discussing



Figure 4.20: Snapshots demonstrate the proposed layered controller’s performance for a series of cooperative locomotion experiments. Outdoor experiments: (a) cooperative locomotion on gravel, (b) transitioning from concrete surface to grass, (c) cooperative locomotion on mulch, and (d) cooperative locomotion on grass. The robots cooperatively transport a payload of 4.53 (kg) (36% uncertainty) in (b) and (c) and 6.80 (kg) (55% uncertainty) in (a) and (d). Here, (a) and (c) show the snapshots where the distributed MPC is adopted, while (b) and (d) show the snapshots where the centralized MPC is employed.

their limitations.

4.6.1 Comparison of the Centralized and Distributed MPCs

The robustness of the cooperative locomotion with the proposed centralized and distributed MPC algorithms in the presence of various uncertainties and disturbances is studied numerically and experimentally in Section 4.5. To compare the performance and robustness of the proposed trajectory planners, we apply the nominal, centralized, and distributed MPCs over 1500 randomly generated rough terrains in the simulation environment of RaiSim, as shown in Fig. 4.22(a). Here, the randomly generated landscapes’ maximum height is 12 (cm) (46% uncertainty in the robot’s height). Furthermore, the total length of the terrain is assumed to be 10 (m). In these simulations, we evaluate the cooperative locomotion as a success if the agents reach 10 (m) without losing stability. We assess the locomotion as a failure if at least one of the agents’ bodies touches the ground before reaching 10 (m). The success rate

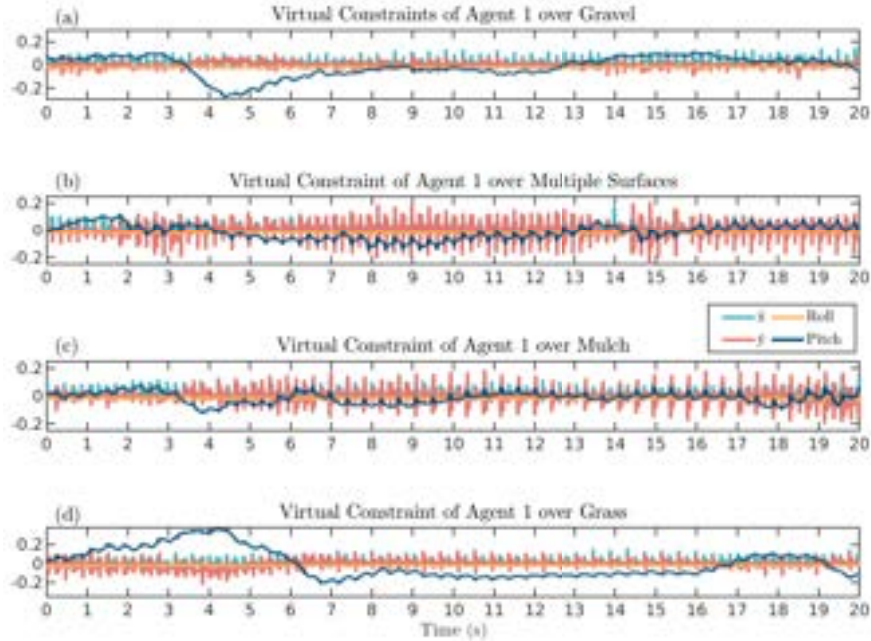


Figure 4.21: Plots of the virtual constraints of agent 1 during cooperative locomotion with unknown payloads and on various outdoor terrains, including (a) locomotion on gravel, (b) transitioning from concrete to grass, (c) locomotion on mulch, and (d) locomotion on grass. The payload is 4.53 (kg) in (b) and (c) and 6.80 (kg) in (a) and (d). Here, (a) and (c) depict the evolution of virtual constraints with the distributed MPC at the high level. In addition, (b) and (d) illustrate the evolution of the virtual constraints with the centralized MPC at the high level. Here, we plot the components of virtual constraints in (4.24) that correspond to the COM position along the x and y axes (m) (i.e., COM position tracking) and the body’s roll and pitch angles (rad) (i.e., angle tracking). It is clear that the full-order system tracks the prescribed optimal and reduced-order trajectories generated by the MPCs.

versus the length of the terrain is depicted in Fig. 4.22(b). The overall success rate of the nominal, centralized, and distributed MPCs is 0%, 54.2%, and 53.8%, respectively.

Similarly, we compare the performance and robustness of the nominal, centralized, and distributed MPCs subject to 1200 randomly generated external forces and payloads, as shown in Fig. 4.22(c). The external force is taken as sinusoidal with a maximum amplitude of 80 (N) (65% of one robot’s weight) and a maximum period of 4 (s) on the x -, y -, and z -directions. The maximum mass of the payload is also assumed to be 5 (kg). We evaluate the cooperative locomotion as a success if the agents sustain the stability until 60 seconds. We assess the locomotion as a failure if at least one of the agents’ bodies touches the ground before 60 (s). The success rate versus time is depicted in Fig. 4.22(d). The overall success rate of the nominal, centralized, and distributed MPCs is 0%, 55.6%, and 53.9%, respectively.

Our experimental studies in Figs. 4.13-4.19 and Fig. 4.21 suggest that the proposed cen-

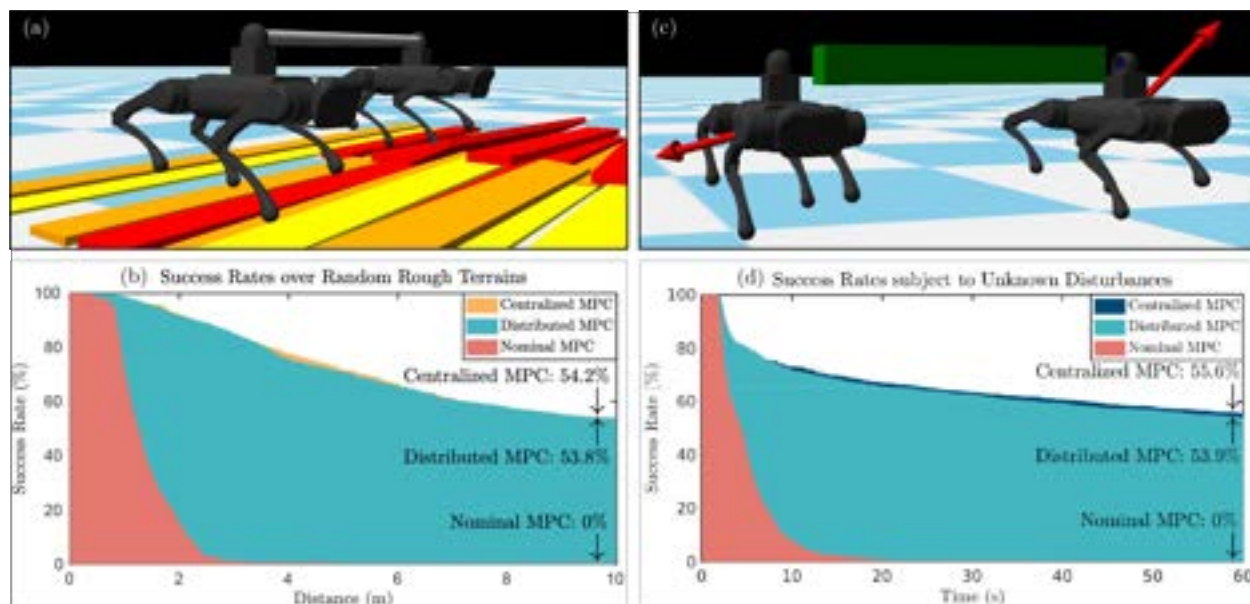


Figure 4.22: Illustration of the comparison results between the nominal, centralized, and distributed MPCs. (a) The snapshot shows the RaiSim simulation environment with one of the randomly generated rough terrains. The maximum height of the generated terrains is 12 (cm) (46% uncertainty in robots' height). (b) The plot describes the success rate of the proposed trajectory planners over 1500 randomly generated rough terrains in numerical simulations. The overall success rate of the nominal, centralized, and distributed MPCs over randomly generated rough terrain is 0%, 54.2%, and 53.8%, respectively. (c) The snapshot shows the RaiSim simulation environment with one of the randomly generated external forces and a randomly generated payload. The arrows illustrate the applied external forces on each agent. The maximum external force is 80 (N) (65% of one robot's weight) on the x -, y -, and z -directions. The evolution of the forces in each direction is sinusoidal with a maximum random period of 4 (s). External forces are applied from 1 (s) to 60 (s). The maximum payload mass is 5 (kg). (d) The plot describes the success rate of the proposed trajectory planners with 1200 randomly applied external forces and payloads in numerical simulations. The overall success rate of the nominal, centralized, and distributed MPCs subject to unknown external forces and payloads is 0%, 55.6%, and 53.9%, respectively.

tralized and distributed trajectory planners show similar robustness in indoor and outdoor experiments. Slightly better robustness has been observed in numerical simulations of Fig. 4.22 when employing the centralized MPC at the high level. Still, the success rate between the centralized and distributed MPCs does not significantly differ. These comparisons suggest that the proposed centralized and distributed MPCs can robustly stabilize dynamic cooperative locomotion. However, the distributed MPC has substantially less computational time.

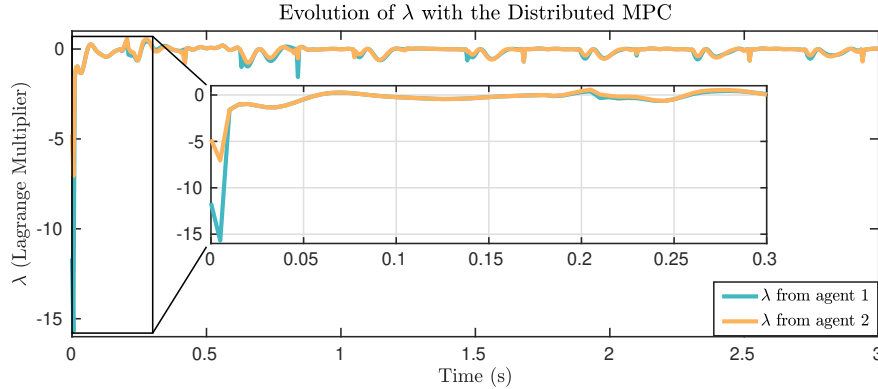


Figure 4.23: Plots of the locally estimated Lagrange multiplier λ by two agents using the distributed MPC algorithm. It is clear that the local values reach an agreement and stay close to each other.

4.6.2 Evolution of the Lagrange Multiplier in Distributed MPC

Section 4.6.1 demonstrated a similar success rate for the centralized and distributed MPC algorithms with the randomly generated terrains and disturbances. To further study this similar robust stability behavior, Fig. 4.23 illustrates the evolution of the estimated Lagrange multiplier, λ , for each agent when the agents cooperatively walk with the distributed MPC. In formulating the distributed MPC, each agent locally estimates the Lagrange multiplier according to the one-step communication delay and the agreement protocol. Therefore, λ on each distributed MPC evolves differently. We introduced the consensus protocol in the cost function of (4.22) to mitigate the divergence of the local estimates and to impose the agreement. The magnified portion of the plot in Fig. 4.23 shows that the initial λ values on each agent are different while converging after a short amount of time according to the consensus protocol. The plot also shows that each agent's λ values are not precisely the same during cooperative locomotion. However, we can observe that both λ values stay close.

4.6.3 Synchronization and Asynchronization

We aim to study the robustness of the layered control approach against possible phase differences between agents that can easily occur on rough terrain, where the discrete-time transitions (i.e., impacts) happen earlier or later than anticipated times on normal gaits. To further investigate this point, we study the estimated height of the agents' front right legs over rough terrain in Fig. 4.24. Both agents are synchronized at the beginning of the locomotion. After encountering the rough terrain, the asynchrony is observed in Fig. 4.24. However, the proposed centralized and distributed MPCs show robust cooperative gaits over unknown rough terrains, as shown in Figs. 4.12(a), 4.17, 4.20, and Fig. 4.21. Moreover, the robustness subject to more than 1000 randomly generated rough terrains is also validated in Fig. 4.22.

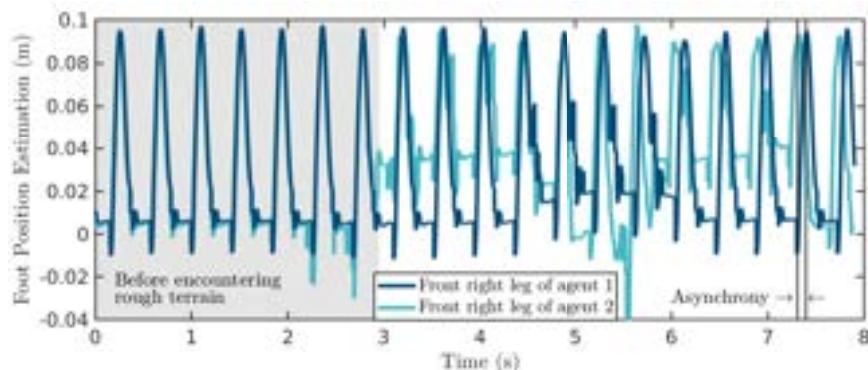


Figure 4.24: Plots of the estimated height of agents’ front right legs. Initial locomotion has complete synchrony before encountering the rough terrain described in the gray area in the plot. After engaging the rough terrain, it is clear that asynchrony happens between agents. However, the layered control approach robustly stabilizes the cooperative gait.

4.6.4 Robustness Against Unknown Holonomic Constraints

The holonomic constraint of Section 4.2 assumes a distance constraint between the interaction points of agents. In particular, we take no additional rotational constraints at the interaction points. This assumption simplifies the interconnected SRB model and, thereby, the centralized and distributed MPC algorithms. However, more sophisticated connections could exist, such as limited DOFs on both ends of the holonomic constraint. Here, we study the robustness of the proposed MPCs subject to uncertainties arising from rotational restrictions at the interaction points. These constraints can arise from cooperative locomanipulation in various applications. Figure 4.25 depicts the body roll and pitch evolution during cooperative locomotion over rough terrain with different holonomic constraints at the interaction points, including restrictions on ball joints’ pitch-yaw, yaw-roll, roll-pitch, and roll-pitch-yaw. These restrictions are implemented with the different mechanisms designed in Fig 4.5. The robust stability of the cooperative locomotion with the proposed centralized MPC is shown in the phase portraits of the body roll and body pitch in Figs. 4.25(a) and 4.25(b). The robust stability of the proposed distributed MPC is also illustrated in Figs. 4.25(c) and 4.25(d). We observe that the cooperative locomotion over rough terrain with different and unknown holonomic constraints has robust stability similar to the one illustrated in Fig. 4.17. However, the phase portraits in Fig. 4.25 show that the unknown additional interactions from the limited DOFs on both ends of the holonomic constraint can induce aggressive angular positions and velocity changes.

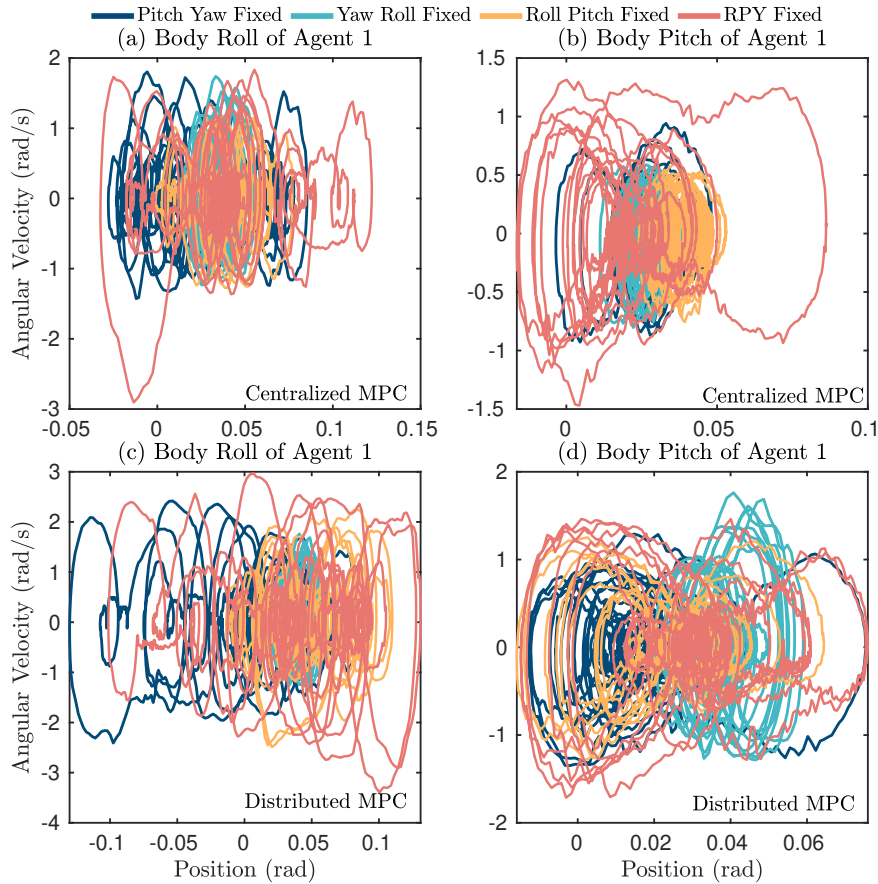


Figure 4.25: Phase portraits for (a) the body roll and (b) the body pitch of agent 1 with the centralized MPC and (c) the body roll and (d) the body pitch of agent 1 with the distributed MPC during different experiments. The plots show the robustness of the cooperative locomotion over rough terrain with fixed DOFs in holonomic constraints on the roll, pitch, and yaw directions.

4.6.5 Limitations and Future Study

Optimal control with switching

The proposed MPC approaches for cooperative locomotion were shown to be very robust to various unknown terrains and subject to unknown disturbances. However, the gait presented here does not exhibit extremely dynamic or highly agile maneuvers. One of the reasons for this is the relatively small planning horizon (25 (ms)). While the distributed approach provides an interesting avenue to explore longer horizons in future work due to the considerable decrease in computation time, long horizons suffer when only considering the current domain. For this reason, future work should not only explore increased planning lengths but should also consider a PWA optimal control formulation [29, Chap. 16] such that the change

in stance leg configurations can be considered directly by the planner.

Sophisticated constraints between agents

We assumed the holonomic constraint (4.2) with a ball joint on agents to simplify the development of the interconnected reduced-order model and the synthesis of centralized and distributed MPCs. We further studied the robustness of the proposed layered control approach subject to the unknown restrictions on the ball joints in Section 4.6.4. However, more sophisticated cooperative tasks may require dexterous manipulation during cooperative locomotion. For instance, quadrupedal robots can be equipped with robotic arms for loco-manipulation. Our future work will investigate the development of robust control algorithms that systematically address the gap between simplified reduced-order models and complex dynamical models of cooperative loco-manipulation.

Extension to multi-agents

Our previous work [116] presented quasi-statically stable cooperative gaits for $M \geq 2$ agents. In particular, a closed-form expression for the interconnected LIP models was developed to address the real-time trajectory planning based on a centralized MPC algorithm. The interconnected LIP model *cannot* address interaction torques between the agents. Furthermore, the gait is *not* dynamic. The current chapter presents an interconnected reduced-order model, based on the SRB dynamics, that addresses interaction torques between the agents while allowing dynamic cooperative gaits. In addition, centralized and distributed MPC algorithms are developed for the cooperative locomotion of two agents. However, a closed-form expression for the Jacobian matrices in (4.13) and (4.15) may not be easily computed for $M \geq 3$ interconnected SRB dynamics with sophisticated holonomic constraints. Our future work will investigate the extension of the approach for dynamic cooperative locomotion of $M \geq 3$ agents with complex holonomic constraints. One possible way is to develop robust distributed MPC algorithms integrated with reinforcement learning and data-driven techniques [76, 151] to bridge the gap between interconnected reduced-order models and full-order models.

Coordination between agents

In numerical simulations, each agent's global coordinates can be easily used without sensor limitations or unexpected noises. However, experimental evaluations estimate the agents' global coordinates via kinematic estimators. The estimation errors may result in unexpected coordination changes. This chapter addresses this issue by the human operator who coordinates the agents with the corresponding speed commands from the joystick. For example, the user commands a higher or lower desired speed to the lagging or leading agent, respec-

tively. Our future work will investigate the design of algorithms that robustly estimate the global coordinates of the agents in the presence of noisy measurements.

4.7 Summary

This chapter presented a layered control algorithm for real-time trajectory planning and robust control for cooperative locomotion of two holonomically constrained quadrupedal robots. An innovative reduced-order model of cooperative locomotion is developed and studied based on interconnected SRB dynamics. At the high level of the layered control algorithm, the real-time trajectory planning problem is formulated as an optimal control problem of the interconnected reduced-order model with two different schemes: centralized and distributed MPCs. The centralized MPC plans for the global reduced-order states, global GRFs, and the interaction wrenches between agents. The distributed MPC is developed based on a one-step communication delay and an agreement protocol to solve for the local reduced-order states, local GRFs, and the local estimated wrenches. At the low level of the control scheme, distributed nonlinear controllers, based on QP and virtual constraints, are developed to impose the full-order model of each agent to track the optimal reduced-order trajectories and GRFs prescribed by the high-level MPCs.

The effectiveness of the proposed layered control approach was verified with extensive numerical simulations and experiments for the blind and robust cooperative locomotion of two holonomically constrained A1 robots with different payloads on different terrains and subject to external disturbances. A detailed study was presented to compare the performance of the proposed centralized and distributed MPCs over more than 1000 randomly generated landscapes and external pushes. It was shown that the distributed MPC is robustly stable, similar to that of the centralized MPC, while the computation time is reduced significantly. The results also show that both the centralized and distributed MPCs integrated with the interconnected SRB dynamics can drastically improve the robust stability of cooperative locomotion compared to the individual nominal MPCs. The experimental results suggest that the proposed control algorithm can result in robustly stable cooperative locomotion on different terrains (e.g., wooden blocks, slippery surfaces, grass, mulch, and concrete) subject to unknown payloads and external disturbances at different speeds. The robustness of the control approach was also studied against uncertainties in holonomic constraints and assumptions.

Chapter 5

Conclusions and Future Works

The objective of this chapter is to present a concise summary and possible future works with final thoughts. In Section 5.1, we will briefly summarize the contributions of Chapters 2, 3, and 4. Section 5.2 will provide brief discussions about possible future works. Finally, the dissertation will be concluded with final thoughts in Section 5.3.

5.1 Summary of the Contributions

5.1.1 Event-based MPC and QP-based low-level nonlinear controllers for single-agent legged robots

Chapter 2 developed a hierarchical control algorithm based on nonlinear control, MPC, and QP, to generate and stabilize locomotion trajectories for complex dynamical models of quadrupedal robots in a real-time manner. The proposed hierarchical control algorithm consists of a high-level planner and a low-level nonlinear controller. The high-level planner generates an optimal COM trajectory according to the LIP dynamics to steer the robot from an initial state to a final one. The constraints applied to the MPC formulation help to generate feasible COM trajectories for the reduced-order model. Furthermore, MPC is solved at the beginning of each continuous-time domain (i.e., event-based MPC) to reduce the computational burden. A QP-based nonlinear controller was solved at the lower level of the proposed approach to impose the full-order dynamics to track the optimal trajectories while keeping all individual GRFs feasible. The effectiveness of the proposed hierarchical control algorithm with the event-based MPC was evaluated with extensive numerical simulations of the full-order locomotion model subject to disturbances and uncertainties.

5.1.2 Hierarchical control algorithms with supervisory MPC for multi-agent legged robots

Chapter 3 developed a hierarchical computational algorithm to enable the real-time planning and control of collaborative locomotion for multi-agent legged robotic systems that carry objects. The higher level of the proposed algorithm employs supervisory control, based on event-based MPC, to generate optimal and reduced-order trajectories for individual agents.

In particular, we proposed an innovative network of reduced-order models subject to holonomic constraints, referred to as the interconnected LIP dynamics, for path planning. Unlike the LIP model, interconnected LIP dynamics have a nonlinear nature. To address this nonlinearity, we made use of Jacobian linearizations of the interconnected LIP dynamics in the supervisory MPC. Distributed nonlinear controllers were then implemented at the lower level of the proposed algorithm to impose the full-order dynamics of each agent to asymptotically track the optimal trajectories while keeping GRFs at all contacting leg ends in the friction cone. The proposed hierarchical control algorithm bridges the gap between the network of reduced- and full-order complex models of cooperative locomotion. It has been numerically shown that the proposed control approach can generate and robustly stabilize collaborative locomotion patterns for multi-agent quadrupedal robotic systems in the presence of model uncertainties arising from unknown payloads and ground height variations.

5.1.3 Layered control architecture with centralized and distributed approaches for cooperative locomotion of legged robots

Chapter 4 developed a layered control architecture for real-time trajectory planning and control of the two holonomically constrained quadrupedal robots. At the higher level of the control architecture, centralized and distributed MPCs are proposed to address the optimal control problem of the interconnected SRB dynamics. The MPCs compute the reduced-order states, GRFs, and interaction wrenches between the agents. Additionally, the distributed MPC approach assumes two local QPs that share their optimal solutions according to a one-step communication delay and an agreement protocol. In the lower levels of the control architecture, distributed nonlinear controllers, based on QP and virtual constraints, impose full-order dynamics to track the prescribed optimal reduced-order trajectories and GRFs. Based on extensive numerical simulations and experiments, the proposed layered control approach is shown to be effective for blind, robust, and cooperative locomotion of two A1 robots with different payloads on different terrains and in the presence of external disturbances. We remark that the distributed MPC performs similarly to the centralized MPC, while the computation time is significantly reduced.

5.2 Directions of Future Work

The dissertation addressed layered control algorithms for real-time trajectory planning of a various number of legged robots. The layered control algorithms' development contributed to the robust control for cooperative locomotion of holonomically constrained quadrupedal robots. However, as highlighted in Chapters 3 and 4, there are some limitations, and this section introduces the available future works to address those limitations.

In the real-time trajectory planner implementation, we considered a short period as a planning horizon, which helps mitigate the violation of the assumption that the MPC formulation

is not considering the PWA system. In future work, long planning horizons have a big possibility to address highly agile and dynamic gaits without suffering from the computational burden due to the significant decrease in computational time from distributed MPC. PWA system control formulation should be addressed together when elongating the planning horizon for managing highly dynamic gaits.

In applying holonomic constraints, we assumed the ball joints on both ends to simplify the development of the interconnected reduced-order model, which also helps run centralized and distributed MPCs in real time. However, more sophisticated collaborative tasks can easily require dexterous manipulation during locomotion. Considering more sophisticated constraints between agents for representing dexterous manipulation can systematically address the gap between simplified reduced-order model and complex full-order models in a streamlined manner.

Chapter 3 presented quasi-statically stable cooperative gaits for $M \geq 2$ agents with a closed-form expression for the interconnected LIP models to address the real-time trajectory planning based on a centralized MPC algorithm. One limitation of the interconnected LIP model was that it *could not* capture interaction torques. Furthermore, the gait was not dynamic due to the inherent limitation of the LIP model. Chapter 4 presented interconnected SRB dynamics that address interaction torques between the agents while allowing dynamic cooperative gaits. However, a closed-form expression for the Jacobian matrices in MPC formulation may not be easily computed for $M \geq 3$ interconnected SRB dynamics with sophisticated holonomic constraints. In our future work, we will investigate the extension of the approach for dynamic cooperative locomotion of $M \geq 3$ with holonomic constraints amongst agents. Here we expect the proposed distributed MPC to mitigate the computational burden when comparing the centralized MPC. We can imagine the other possible way under the model-free approach aspect. More specifically, developing robust distributed MPC algorithms integrated with reinforcement learning or data-driven techniques [76, 151] to bridge the gap between interconnected reduced-order models and full-order models can be an answer to the robust control for cooperative locomotion.

One limitation was the difference between numerical simulations and experiments. In every numerical simulation, each agent's global coordinates can be determined without sensor limitations or unexpected noises. However, experimental evaluations estimate the agents' global coordinates via kinematic estimators. The estimation errors may result in unexpected coordination changes during locomotion. This dissertation, especially in Chapter 4, addresses this issue by the human operator who coordinates the agents with the corresponding speed commands from the joystick. Our future work will investigate the design of algorithms that robustly estimate the global coordinates of the agents in the presence of noisy measurements.

5.3 Conclusion

This dissertation has contributed to synthesizing layered control architectures with innovative interconnected reduced-order models integrated with high-level centralized and distributed MPC algorithms for real-time trajectory planning and low-level distributed nonlinear controllers for whole-body motion control. We have shown numerically and experimentally that the proposed layered architectures can address the dynamic cooperative locomotion of holonomically constrained legged robots with unknown payloads and on rough terrains and subject to external disturbances. We hope this work shows the blueprint of the application of legged robots in collaborative works or as a member of cooperative teams. The steps in developing the hierarchical control algorithms we introduced could inspire the extension of control schemes for other high-dimensional complex dynamical systems with underactuation and hybrid nature.

Bibliography

- [1] A. Agrawal, O. Harib, A. Hereid, S. Finet, M. Masselin, L. Praly, A. Ames, K. Sreenath, and J. Grizzle. First steps towards translating HZD control of bipedal robots to decentralized control of exoskeletons. *IEEE Access*, 5:9919–9934, 2017.
- [2] Mohamadreza Ahmadi, Andrew Singletary, Joel W Burdick, and Aaron D Ames. Safe policy synthesis in multi-agent pomdps via discrete-time barrier functions. In *2019 IEEE 58th Conference on Decision and Control (CDC)*, pages 4797–4803, 2019.
- [3] Zakia Ahmed, Sevak Tahmasian, and Craig A Woolsey. Vibrational control of a 2-link mechanism. In *Dynamic Systems and Control Conference*, volume 84287, page V002T38A005. American Society of Mechanical Engineers, 2020.
- [4] K. Akbari Hamed and R. D. Gregg. Decentralized feedback controllers for robust stabilization of periodic orbits of hybrid systems: Application to bipedal walking. *IEEE Transactions on Control Systems Technology*, 25(4):1153–1167, July 2017.
- [5] K. Akbari Hamed and R. D. Gregg. Decentralized event-based controllers for robust stabilization of hybrid periodic orbits: Application to underactuated 3D bipedal walking. *IEEE Transactions on Automatic Control*, 64(6):2266–2281, June 2019.
- [6] K. Akbari Hamed and J. W. Grizzle. Reduced-order framework for exponential stabilization of periodic orbits on parameterized hybrid zero dynamics manifolds: Application to bipedal locomotion. *Nonlinear Analysis: Hybrid Systems*, 25:227–245, August 2017.
- [7] K. Akbari Hamed and J.W. Grizzle. Event-based stabilization of periodic orbits for underactuated 3-D bipedal robots with left-right symmetry. *Robotics, IEEE Transactions on*, 30(2):365–381, April 2014.
- [8] K. Akbari Hamed, N. Sadati, W.A. Gruver, and G.A. Dumont. Exponential stabilization of periodic orbits for running of a three-dimensional monopodal robot. *Control Theory Applications, IET*, 5(11):1304–1320, July 2011.
- [9] K. Akbari Hamed, N. Sadati, W.A. Gruver, and G.A. Dumont. Stabilization of periodic orbits for planar walking with noninstantaneous double-support phase. *Systems, Man and Cybernetics, Part A: Systems and Humans, IEEE Transactions on*, 42(3):685–706, May 2012.
- [10] K. Akbari Hamed, B.G. Buss, and J.W. Grizzle. Exponentially stabilizing continuous-time controllers for periodic orbits of hybrid systems: Application to bipedal locomotion.

- tion with ground height variations. *The International Journal of Robotics Research*, 35(8):977–999, 2016.
- [11] K. Akbari Hamed, W. Ma, and A. D. Ames. Dynamically stable 3D quadrupedal walking with multi-domain hybrid system models and virtual constraint controllers. In *2019 American Control Conference (ACC)*, pages 4588–4595, July 2019.
- [12] K. Akbari Hamed, V. R. Kamidi, W. Ma, A. Leonessa, and A. D. Ames. Hierarchical and safe motion control for cooperative locomotion of robotic guide dogs and humans: A hybrid systems approach. *IEEE Robotics and Automation Letters*, 5(1):56–63, Jan 2020.
- [13] K. Akbari Hamed, V. R. Kamidi, A. Pandala, W. Ma, and A. D. Ames. Distributed feedback controllers for stable cooperative locomotion of quadrupedal robots: A virtual constraint approach. In *2020 American Control Conference (ACC)*, pages 5314–5321, 2020.
- [14] Kaveh Akbari Hamed, Jeeseop Kim, and Abhishek Pandala. Quadrupedal locomotion via event-based predictive control and QP-based virtual constraints. *IEEE Robotics and Automation Letters*, 5(3):4463–4470, 2020.
- [15] Javier Alonso-Mora, Stuart Baker, and Daniela Rus. Multi-robot formation control and object transport in dynamic environments via constrained optimization. *The International Journal of Robotics Research*, 36(9):1000–1021, 2017.
- [16] A. D. Ames. Human-inspired control of bipedal walking robots. *Automatic Control, IEEE Transactions on*, 59(5):1115–1130, May 2014.
- [17] A. D. Ames, R. D. Gregg, and M. W. Spong. A geometric approach to three-dimensional hipped bipedal robotic walking. In *Decision and Control, 46th IEEE Conference on*, pages 5123–5130, Dec 2007.
- [18] A. D. Ames, R. D. Gregg, E. D. B. Wendel, and S. Sastry. On the geometric reduction of controlled three-dimensional bipedal robotic walkers. In *Lagrangian and Hamiltonian Methods for Nonlinear Control 2006*, pages 183–196, Berlin, Heidelberg, 2007. Springer.
- [19] A. D. Ames, K. Galloway, K. Sreenath, and J. W. Grizzle. Rapidly exponentially stabilizing control Lyapunov functions and hybrid zero dynamics. *IEEE Transactions on Automatic Control*, 59(4):876–891, April 2014.
- [20] A.D. Ames and S. Sastry. Hybrid geometric reduction of hybrid systems. In *Decision and Control, 45th IEEE Conference on*, pages 923–929, Dec 2006.
- [21] A.D. Ames, R. W. Sinnet, and E. D.B. Wendel. Three-dimensional kneed bipedal walking: A hybrid geometric approach. In Rupak Majumdar and Paulo Tabuada, editors, *Hybrid Systems: Computation and Control*, volume 5469 of *Lecture Notes in*

- Computer Science*, pages 16–30. Springer Berlin Heidelberg, 2009. ISBN 978-3-642-00601-2.
- [22] ANYbotics. <https://www.anybotics.com/>.
- [23] T. Başar and P. Bernhard. *\mathcal{H}_∞ -Optimal Control and Related Minimax Design Problems: A Dynamic Game Approach*. Birkhauser, 2008.
- [24] D. D. Bainov and P. S. Simeonov. *Systems With Impulse Effect: Stability, Theory and Applications*. Ellis Horwood Ltd, June 1989.
- [25] C Dario Bellicoso, Christian Gehring, Jemin Hwangbo, Péter Fankhauser, and Marco Hutter. Perception-less terrain adaptation through whole body control and hierarchical optimization. In *2016 IEEE-RAS International Conference on Humanoid Robots*, pages 558–564, 2016.
- [26] D. S. Bernstein and W. M. Haddad. LQG control with an \mathcal{H}_∞ performance bound: A Riccati equation approach. *IEEE Transactions on Automatic Control*, 34(3):293–305, March 1989.
- [27] G. Bledt, P. M. Wensing, and S. Kim. Policy-regularized model predictive control to stabilize diverse quadrupedal gaits for the MIT Cheetah. In *2017 IEEE/RSJ International Conference on Intelligent Robots and Systems (IROS)*, pages 4102–4109, Sep. 2017.
- [28] G. Bledt, M. J. Powell, B. Katz, J. Di Carlo, P. M. Wensing, and S. Kim. MIT Cheetah 3: Design and control of a robust, dynamic quadruped robot. In *2018 IEEE/RSJ International Conference on Intelligent Robots and Systems (IROS)*, pages 2245–2252, Oct 2018.
- [29] F. Borrelli, A. Bemporad, and Morari M. *Predictive Control for Linear and Hybrid Systems*. Cambridge University Press, 2017.
- [30] F. Borrelli, A. Bemporad, and M. Morari. *Predictive control for linear and hybrid systems*. Cambridge University Press, 2017.
- [31] S. Boyd, L. E. Ghaoui, E. Feron, and V. Balakrishnan. *Linear Matrix Inequalities in System and Control Theory*. Society for Industrial and Applied Mathematics, June 1997.
- [32] R. P. Braatz, P. M. Young, J. C. Doyle, and M. Morari. Computational complexity of μ calculation. *IEEE Transactions on Automatic Control*, 39(5):1000–1002, May 1994.
- [33] F. Bullo, J. Cortés, and Martinez. S. *Distributed Control of Robotic Networks: A Mathematical Approach to Motion Coordination Algorithms*. Princeton University Press, 2009.

- [34] S. A. Burden, H. Gonzalez, R. Vasudevan, R. Bajcsy, and S. S. Sastry. Metrization and simulation of controlled hybrid systems. *IEEE Transactions on Automatic Control*, 60(9):2307–2320, Sept 2015.
- [35] S.A. Burden, S. Revzen, and S. Sastry. Model reduction near periodic orbits of hybrid dynamical systems. *Automatic Control, IEEE Transactions on*, 60(10):2626–2639, Oct 2015.
- [36] K. Byl and R. Tedrake. Approximate optimal control of the compass gait on rough terrain. In *Robotics and Automation. IEEE International Conference on*, pages 1258–1263, May 2008.
- [37] Katie Byl and Russ Tedrake. Metastable walking machines. *The International Journal of Robotics Research*, 28(8):1040–1064, 2009.
- [38] Fabrizio Caccavale, Gerardo Giglio, Giuseppe Muscio, and Francesco Pierri. Cooperative impedance control for multiple uavs with a robotic arm. In *2015 IEEE/RSJ International Conference on Intelligent Robots and Systems (IROS)*, pages 2366–2371, 2015.
- [39] J. Carpentier, S. Tonneau, M. Naveau, O. Stasse, and N. Mansard. A versatile and efficient pattern generator for generalized legged locomotion. In *2016 IEEE International Conference on Robotics and Automation (ICRA)*, pages 3555–3561, May 2016.
- [40] MIT Mini Cheetah. <https://robots.ieee.org/robots/minicheetah/>.
- [41] Yuxiao Chen, Andrew Singletary, and Aaron D Ames. Guaranteed obstacle avoidance for multi-robot operations with limited actuation: A control barrier function approach. *IEEE Control Systems Letters*, 5(1):127–132, 2020.
- [42] C. Chevallereau, G. Abba, Y. Aoustin, F. Plestan, E. R. Westervelt, C. Canudas-de Wit, and J.W. Grizzle. RABBIT: A testbed for advanced control theory. *IEEE Control Systems Magazine*, 23(5):57–79, Oct 2003.
- [43] C. Chevallereau, J.W. Grizzle, and C.-L. Shih. Asymptotically stable walking of a five-link underactuated 3-D bipedal robot. *Robotics, IEEE Transactions on*, 25(1):37–50, Feb 2009.
- [44] M. Chignoli and P. M. Wensing. Variational-based optimal control of underactuated balancing for dynamic quadrupeds. *IEEE Access*, 8:49785–49797, 2020.
- [45] M. Chilali and P. Gahinet. \mathcal{H}_∞ design with pole placement constraints: An LMI approach. *IEEE Transactions on Automatic Control*, 41(3):358–367, March 1996.
- [46] S. Collins, A. Ruina, R. Tedrake, and M. Wisse. Efficient bipedal robots based on passive-dynamic walkers. *Science*, 307(5712):1082–1085, 2005.

- [47] Sebastien Corner, Corina Sandu, and Adrian Sandu. Modeling and sensitivity analysis methodology for hybrid dynamical system. *Nonlinear Analysis: Hybrid Systems*, 31: 19–40, 2019.
- [48] Sebastien Corner, Adrian Sandu, and Corina Sandu. Adjoint sensitivity analysis of hybrid multibody dynamical systems. *Multibody System Dynamics*, 49(4):395–420, 2020.
- [49] Preston Culbertson, Jean-Jacques Slotine, and Mac Schwager. Decentralized adaptive control for collaborative manipulation of rigid bodies. *IEEE Transactions on Robotics*, 37(6):1906–1920, 2021.
- [50] M. Turpin D. Panagou and V. Kumar. Decentralized goal assignment and trajectory generation in multi-robot networks: A multiple Lyapunov functions approach. In *Proc. of the 2014 IEEE Int. Conf. on Robotics and Automation*, Hong Kong, China, June 2014.
- [51] Xingye Da and Jessy Grizzle. Combining trajectory optimization, supervised machine learning, and model structure for mitigating the curse of dimensionality in the control of bipedal robots. *The International Journal of Robotics Research*, 38(9):1063–1097, 2019.
- [52] H. Dai and R. Tedrake. Optimizing robust limit cycles for legged locomotion on unknown terrain. In *IEEE 51st Annual Conference on Decision and Control*, pages 1207–1213, Dec 2012.
- [53] H. Dai and R. Tedrake. \mathcal{L}_2 -gain optimization for robust bipedal walking on unknown terrain. In *Robotics and Automation, IEEE International Conference on*, pages 3116–3123, May 2013.
- [54] Hongkai Dai, Andrés Valenzuela, and Russ Tedrake. Whole-body motion planning with centroidal dynamics and full kinematics. In *2014 IEEE-RAS International Conference on Humanoid Robots*, pages 295–302. IEEE, 2014.
- [55] C.C. De Wit, H. Olsson, K.J. Astrom, and P. Lischinsky. A new model for control of systems with friction. *IEEE Transactions on Automatic Control*, 40(3):419–425, Mar 1995.
- [56] J. Di Carlo, P. M. Wensing, B. Katz, G. Bleedt, and S. Kim. Dynamic locomotion in the MIT Cheetah 3 through convex model-predictive control. In *2018 IEEE/RSJ International Conference on Intelligent Robots and Systems (IROS)*, pages 1–9, Oct 2018.
- [57] Y. Ding, A. Pandala, and H. Park. Real-time model predictive control for versatile dynamic motions in quadrupedal robots. In *2019 International Conference on Robotics and Automation (ICRA)*, pages 8484–8490, May 2019.

- [58] Y. Ding, A. Pandala, C. Li, Y-H. Shin, and H-W. Park. Representation-free model predictive control for dynamic motions in quadrupeds. *IEEE Transactions on Robotics*, 37(4):1154–1171, 2021.
- [59] A. Domahidi, E. Chu, and S. Boyd. ECOS: An SOCP solver for embedded systems. In *2013 European Control Conference (ECC)*, pages 3071–3076, July 2013.
- [60] M.D. Donner. *Real-Time Control of Walking*. Birkhäuser Boston, 1987.
- [61] J. Doyle, A. Packard, and K. Zhou. Review of LFTs, LMIs, and μ ; . In *Decision and Control, 1991., Proceedings of the 30th IEEE Conference on*, pages 1227–1232 vol.2, Dec 1991.
- [62] J. C. Doyle, K. Glover, P. P. Khargonekar, and B. A. Francis. State-space solutions to standard \mathcal{H}_2 and \mathcal{H}_∞ control problems. *IEEE Transactions on Automatic Control*, 34(8):831–847, Aug 1989.
- [63] William B. Dunbar and Richard M. Murray. Distributed receding horizon control for multi-vehicle formation stabilization. *Automatica*, 42(4):549–558, 2006.
- [64] Boston Dynamics. <https://www.bostondynamics.com/>.
- [65] Matthew L Elwin, Billie Strong, Randy A Freeman, and Kevin M Lynch. Human-multirobot collaborative mobile manipulation: The omnid mocobots. *arXiv preprint arXiv:2206.14293*, 2022.
- [66] J. Engelsberger, C. Ott, M. A. Roa, A. Albu-Schäffer, and G. Hirzinger. Bipedal walking control based on capture point dynamics. In *2011 IEEE/RSJ International Conference on Intelligent Robots and Systems*, pages 4420–4427, Sep. 2011.
- [67] Johannes Engelsberger, Christian Ott, and Alin Albu-Schäffer. Three-dimensional bipedal walking control based on divergent component of motion. *Ieee transactions on robotics*, 31(2):355–368, 2015.
- [68] Sebastian Erhart, Dominik Sieber, and Sandra Hirche. An impedance-based control architecture for multi-robot cooperative dual-arm mobile manipulation. In *2013 IEEE/RSJ International Conference on Intelligent Robots and Systems*, pages 315–322, 2013.
- [69] M. A. Estrada, S. Mintchev, D.L. Christensen, M. R. Cutkosky, and D. Floreano. Forceful manipulation with micro air vehicles. *Science Robotics*, 3(23), 2018.
- [70] S. Fahmi, C. Mastalli, M. Focchi, and C. Semini. Passive whole-body control for quadruped robots: Experimental validation over challenging terrain. *IEEE Robotics and Automation Letters*, 4(3):2553–2560, July 2019.

- [71] Hamed Farivarnejad, Sean Wilson, and Spring Berman. Decentralized sliding mode control for autonomous collective transport by multi-robot systems. In *2016 IEEE 55th conference on decision and control (CDC)*, pages 1826–1833, 2016.
- [72] Farbod Farshidian, Michael Neunert, Alexander W Winkler, Gonzalo Rey, and Jonas Buchli. An efficient optimal planning and control framework for quadrupedal locomotion. In *2017 IEEE International Conference on Robotics and Automation*, pages 93–100, 2017.
- [73] R. T. Fawcett. *Real-Time Planning and Nonlinear Control for Robust Quadrupedal Locomotion with Tails*. MS thesis, Virginia Tech, 2021.
- [74] Randall T. Fawcett, Abhishek Pandala, Aaron D. Ames, and Kaveh Akbari Hamed. Robust stabilization of periodic gaits for quadrupedal locomotion via QP-based virtual constraint controllers. *IEEE Control Systems Letters*, pages 1736–1741, 2021.
- [75] Randall T Fawcett, Abhishek Pandala, Jeeseop Kim, and Kaveh Akbari Hamed. Real-time planning and nonlinear control for quadrupedal locomotion with articulated tails. *Journal of Dynamic Systems, Measurement, and Control*, 143(7):071004, July 2021.
- [76] Randall T. Fawcett, Kereshmeh Afsari, Aaron D. Ames, and Kaveh Akbari Hamed. Toward a data-driven template model for quadrupedal locomotion. *IEEE Robotics and Automation Letters*, 7(3):7636–7643, 2022.
- [77] Siyuan Feng, X Xinjilefu, Weiwei Huang, and Christopher G Atkeson. 3d walking based on online optimization. In *2013 13th IEEE-RAS International Conference on Humanoid Robots (Humanoids)*, pages 21–27. IEEE, 2013.
- [78] Siyuan Feng, X Xinjilefu, Christopher G Atkeson, and Joohyung Kim. Optimization based controller design and implementation for the atlas robot in the darpa robotics challenge finals. In *2015 IEEE-RAS 15th International Conference on Humanoid Robots (Humanoids)*, pages 1028–1035. IEEE, 2015.
- [79] R.A. Freeman and P. V. Kokotović. *Robust Nonlinear Control Design*. Birkhauser, 1996.
- [80] R.J. Full and D.E. Koditschek. Templates and anchors: Neuromechanical hypotheses of legged locomotion on land. *Journal of Experimental Biology*, 202(23):3325–3332, 1999.
- [81] P. Gahinet. Explicit controller formulas for LMI-based \mathcal{H}_∞ synthesis. *Automatica*, 32(7):1007 – 1014, 1996.
- [82] P. Gahinet and P. Apkarian. A linear matrix inequality approach to \mathcal{H}_∞ control. *International Journal of Robust & Nonlinear Control*, 4(4):421–448, 1994.

- [83] P. E. Gill, W. Murray, and M. A. Saunders. Snopt: An sqp algorithm for large-scale constrained optimization. *SIAM review*, 47(1):99–131, 2005.
- [84] R. Goebel, R.G. Sanfelice, and A.R. Teel. *Hybrid Dynamical Systems: Modeling, Stability, and Robustness*. Princeton University Press, March 2012.
- [85] R. Goedel, Ricardo G. S., and A. R. Teel. Hybrid dynamical systems: modeling stability, and robustness.
- [86] Ruben Grandia, Farbod Farshidian, Alexey Dosovitskiy, René Ranftl, and Marco Hutter. Frequency-aware model predictive control. *IEEE Robotics and Automation Letters*, 4(2):1517–1524, 2019.
- [87] R. D. Gregg and M. W. Spong. Reduction-based control of three-dimensional bipedal walking robots. *The International Journal of Robotics Research*, 29(6):680–702, May 2010.
- [88] R. D. Gregg, T. Lenzi, L. J. Hargrove, and J. W. Sensinger. Virtual constraint control of a powered prosthetic leg: From simulation to experiments with transfemoral amputees. *IEEE Transactions on Robotics*, 30(6):1455–1471, 2014.
- [89] R.D. Gregg and L. Righetti. Controlled reduction with unactuated cyclic variables: Application to 3D bipedal walking with passive yaw rotation. *Automatic Control, IEEE Transactions on*, 58(10):2679–2685, Oct 2013.
- [90] R.D. Gregg and J.W. Sensinger. Towards biomimetic virtual constraint control of a powered prosthetic leg. *IEEE Transactions on Control Systems Technology*, 22(1): 246–254, Jan 2014.
- [91] R.D. Gregg and M.W. Spong. Reduction-based control with application to three-dimensional bipedal walking robots. In *American Control Conference*, pages 880–887, June 2008.
- [92] R.D. Gregg, A.K. Tilton, S. Candido, T. Bretl, and M.W. Spong. Control and planning of 3-D dynamic walking with asymptotically stable gait primitives. *Robotics, IEEE Transactions on*, 28(6):1415–1423, Dec 2012.
- [93] R.D. Gregg, T. Lenzi, L.J. Hargrove, and J.W. Sensinger. Virtual constraint control of a powered prosthetic leg: From simulation to experiments with transfemoral amputees. *IEEE Transactions on Robotics*, 30(6):1455–1471, Dec 2014.
- [94] R. J. Griffin, G. Wiedebach, S. Bertrand, A. Leonessa, and J. Pratt. Walking stabilization using step timing and location adjustment on the humanoid robot, Atlas. In *2017 IEEE/RSJ International Conference on Intelligent Robots and Systems (IROS)*, pages 667–673, Sep. 2017.

- [95] R. J. Griffin, G. Wiedebach, S. Bertrand, A. Leonessa, and J. Pratt. Straight-leg walking through underconstrained whole-body control. In *2018 IEEE International Conference on Robotics and Automation (ICRA)*, pages 5747–5754. IEEE, 2018.
- [96] Robert J Griffin, Alexander Leonessa, and Alan Asbeck. Disturbance compensation and step optimization for push recovery. In *2016 IEEE/RSJ International Conference on Intelligent Robots and Systems (IROS)*, pages 5385–5390. IEEE, 2016.
- [97] J. W. Grizzle, C. Chevallereau, R. W. Sinnet, and A. D. Ames. Models, feedback control, and open problems of 3D bipedal robotic walking. *Automatica*, 50(8):1955–1988, 2014.
- [98] J.W. Grizzle, G. Abba, and F. Plestan. Asymptotically stable walking for biped robots: Analysis via systems with impulse effects. *IEEE Transactions on Automatic Control*, 46(1):51–64, Jan 2001.
- [99] W.M. Haddad, V. Chellaboina, and S.G. Nersesov. *Impulsive and Hybrid Dynamical Systems: Stability, Dissipativity, and Control*. Princeton University Press, July 2006.
- [100] K. Akbari Hamed and A. D. Ames. Nonholonomic hybrid zero dynamics for the stabilization of periodic orbits: Application to underactuated robotic walking. *IEEE Transactions on Control Systems Technology*, Under Review, 2018.
- [101] A. Hereid, E. A. Cousineau, C. M. Hubicki, and A. D. Ames. 3D dynamic walking with underactuated humanoid robots: A direct collocation framework for optimizing hybrid zero dynamics. In *2016 IEEE International Conference on Robotics and Automation (ICRA)*, pages 1447–1454, May 2016.
- [102] A. Hereid, E. A. Cousineau, C. M. Hubicki, and A. D. Ames. 3D dynamic walking with underactuated humanoid robots: A direct collocation framework for optimizing hybrid zero dynamics. In *2016 IEEE International Conference on Robotics and Automation (ICRA)*, pages 1447–1454, May 2016.
- [103] A. Hereid, C. M. Hubicki, E. A. Cousineau, and A. D. Ames. Dynamic humanoid locomotion: A scalable formulation for HZD gait optimization. *IEEE Transactions on Robotics*, pages 1–18, 2018.
- [104] Y. Hurmuzlu and D. B. Marghitu. Rigid body collisions of planar kinematic chains with multiple contact points. *The International Journal of Robotics Research*, 13(1): 82–92, 1994.
- [105] J. Hwangbo, J. Lee, and M. Hutter. Per-contact iteration method for solving contact dynamics. *IEEE Robotics and Automation Letters*, 3(2):895–902, April 2018.
- [106] A. Isidori. *Nonlinear Control Systems*. Springer; 3rd edition, 1995.

- [107] A. M. Johnson, S. A. Burden, and D. E. Koditschek. A hybrid systems model for simple manipulation and self-manipulation systems. *The International Journal of Robotics Research*, 35(11):1354–1392, 2016.
- [108] S. Kajita, F. Kanehiro, K. Kaneko, K. Yokoi, and H. Hirukawa. The 3d linear inverted pendulum mode: A simple modeling for a biped walking pattern generation. In *Proceedings 2001 IEEE/RSJ International Conference on Intelligent Robots and Systems. Expanding the Societal Role of Robotics in the the Next Millennium (Cat. No. 01CH37180)*, volume 1, pages 239–246. IEEE, 2001.
- [109] S. Kajita, F. Kanehiro, K. Kaneko, K. Fujiwara, K. Harada, K. Yokoi, and H. Hirukawa. Biped walking pattern generation by using preview control of zero-moment point. In *2003 IEEE International Conference on Robotics and Automation*, volume 2, pages 1620–1626 vol.2, Sep. 2003.
- [110] Shuuji Kajita and Kazuo Tani. Study of dynamic biped locomotion on rugged terrain-derivation and application of the linear inverted pendulum mode. In *1991 IEEE International Conference on Robotics and Automation*, pages 1405–1406, 1991.
- [111] Shuuji Kajita, Fumio Kanehiro, Kenji Kaneko, Kiyoshi Fujiwara, Kensuke Harada, Kazuhito Yokoi, and Hirohisa Hirukawa. Resolved momentum control: Humanoid motion planning based on the linear and angular momentum. In *Proceedings 2003 IEEE/RSJ International Conference on Intelligent Robots and Systems (IROS 2003)(Cat. No. 03CH37453)*, volume 2, pages 1644–1650. IEEE, 2003.
- [112] Vinay R. Kamidi, Jeeseop Kim, Randall T. Fawcett, Aaron D. Ames, and Kaveh Akbari Hamed. Distributed quadratic programming-based nonlinear controllers for periodic gaits on legged robots. *IEEE Control Systems Letters*, 6:2509–2514, 2022.
- [113] M. Kelly. An introduction to trajectory optimization: How to do your own direct collocation. *SIAM Review*, 59(4):849–904, 2017.
- [114] H. K. Khalil. *Nonlinear Systems*. Pearson, 3rd edition, 2001.
- [115] D. Kim, J. D. Carlo, B. Katz, G. Bleedt, and S. Kim. Highly dynamic quadruped locomotion via whole-body impulse control and model predictive control. *arXiv: 1909.06586*, 2019.
- [116] Jeeseop Kim and Kaveh Akbari Hamed. Cooperative locomotion via supervisory predictive control and distributed nonlinear controllers. *Journal of Dynamic Systems, Measurement, and Control*, 144(3):031005, Mar. 2022.
- [117] T. Koolen, T. de Boer, J. Rebula, A. Goswami, and J. Pratt. Capturability-based analysis and control of legged locomotion, part 1: Theory and application to three simple gait models. *The International Journal of Robotics Research*, 2012.

- [118] S. Kuindersma, F. Permenter, and R. Tedrake. An efficiently solvable quadratic program for stabilizing dynamic locomotion. In *2014 IEEE International Conference on Robotics and Automation (ICRA)*, pages 2589–2594, May 2014.
- [119] Hyeonbeom Lee, Hyoin Kim, Woojin Kim, and H Jin Kim. An integrated framework for cooperative aerial manipulators in unknown environments. *IEEE Robotics and Automation Letters*, 3(3):2307–2314, 2018.
- [120] Sung-Hee Lee and Ambarish Goswami. A momentum-based balance controller for humanoid robots on non-level and non-stationary ground. *Autonomous Robots*, 33(4):399–414, 2012.
- [121] D. Lehmann, E. Henriksson, and K. H. Johansson. Event-triggered model predictive control of discrete-time linear systems subject to disturbances. In *2013 European Control Conference (ECC)*, pages 1156–1161, 2013.
- [122] Guanrui Li, Rundong Ge, and Giuseppe Loianno. Cooperative transportation of cable suspended payloads with MAVs using monocular vision and inertial sensing. *IEEE Robotics and Automation Letters*, 6(3):5316–5323, 2021.
- [123] Dylan P Losey, Craig G McDonald, Edoardo Battaglia, and Marcia K O’Malley. A review of intent detection, arbitration, and communication aspects of shared control for physical human–robot interaction. *Applied Mechanics Reviews*, 70(1), 2018.
- [124] W. Ma, K. Akbari Hamed, and A. D. Ames. First steps towards full model based motion planning and control of quadrupeds: A hybrid zero dynamics approach. In *2019 IEEE/RSJ International Conference on Intelligent Robots and Systems (IROS)*, pages 5498–5503, Nov 2019.
- [125] W. Ma, K. Akbari Hamed, and A. D. Ames. First steps towards full model based motion planning and control of quadrupeds: A hybrid zero dynamics approach. In *2019 IEEE/RSJ International Conference on Intelligent Robots and Systems (IROS)*, pages 5498–5503. IEEE, 2019.
- [126] Wen-Loong Ma, Noel Csomay-Shanklin, Shishir Kolathaya, Kaveh Akbari Hamed, and Aaron D. Ames. Coupled control Lyapunov functions for interconnected systems, with application to quadrupedal locomotion. *IEEE Robotics and Automation Letters*, 6(2):3761–3768, 2021.
- [127] Toni Machado, Tiago Malheiro, Sérgio Monteiro, Wolfram Erlhagen, and Estela Bicho. Multi-constrained joint transportation tasks by teams of autonomous mobile robots using a dynamical systems approach. In *2016 IEEE international conference on robotics and automation (ICRA)*, pages 3111–3117, 2016.
- [128] José M Maestre and Rudy R Negenborn. *Distributed Model Predictive Control Made Easy*. Springer, 2014.

- [129] M. Maggiore and L. Consolini. Virtual holonomic constraints for Euler Lagrange systems. *Automatic Control, IEEE Transactions on*, 58(4):1001–1008, April 2013.
- [130] I. R. Manchester, U. Mettin, F. Iida, and R. Tedrake. Stable dynamic walking over uneven terrain. *The International Journal of Robotics Research*, 30(3):265–279, 2011.
- [131] A. E. Martin, D. C. Post, and J. P. Schmiedeler. The effects of foot geometric properties on the gait of planar bipeds walking under HZD-based control. *The International Journal of Robotics Research*, 33(12):1530–1543, 2014.
- [132] A. E. Martin, D. C. Post, and J. P. Schmiedeler. Design and experimental implementation of a hybrid zero dynamics-based controller for planar bipeds with curved feet. *The International Journal of Robotics Research*, 33(7):988–1005, 2014.
- [133] S. Martinez, J. Cortes, and F. Bullo. Motion coordination with distributed information. *IEEE Control Systems Magazine*, 27(4):75–88, Aug 2007.
- [134] Carlo Masone, Heinrich H Bülthoff, and Paolo Stegagno. Cooperative transportation of a payload using quadrotors: A reconfigurable cable-driven parallel robot. In *2016 IEEE/RSJ International Conference on Intelligent Robots and Systems (IROS)*, pages 1623–1630, 2016.
- [135] MATLAB. Matlab optimization toolbox.
- [136] A. S. Matveev, Savkin A. V., Hoy M., and Wang C. *Safe Robot Navigation Among Moving and Steady Obstacles 1st Edition*. Butterworth-Heinemann, 2016.
- [137] Daniel Mellinger, Michael Shomin, Nathan Michael, and Vijay Kumar. Cooperative grasping and transport using multiple quadrotors. In *Distributed autonomous robotic systems*, pages 545–558. Springer, 2013.
- [138] M. Mesbahi and Egerstedt. M. *Graph Theoretic Methods in Multiagent Networks*. Princeton University Press, 2010.
- [139] N. Michael, J. Fink, and V. Kumar. Cooperative manipulation and transportation with aerial robots. *Autonomous Robots*, 30(1):73–86, January 2011.
- [140] A. Mohammadi, M. Maggiore, and L. Consolini. Dynamic virtual holonomic constraints for stabilization of closed orbits in underactuated mechanical systems. *Automatica*, 94:112 – 124, 2018.
- [141] B. Morris and J.W. Grizzle. Hybrid invariant manifolds in systems with impulse effects with application to periodic locomotion in bipedal robots. *Automatic Control, IEEE Transactions on*, 54(8):1751–1764, Aug 2009.

- [142] R. M. Murray, D. C. Deno, K. S. J. Pister, and S. S. Sastry. Control primitives for robot systems. *IEEE Transactions on Systems, Man, and Cybernetics*, 22(1):183–193, Jan 1992.
- [143] R.M. Murray, Z. Li, and Sastry S.S. *A Mathematical Introduction to Robotic Manipulation*. Taylor & Francis/CRC, 1994.
- [144] M. Neunert, M. Stäuble, M. Gifftthaler, C. D. Bellicoso, J. Carius, C. Gehring, M. Hut-ter, and J. Buchli. Whole-body nonlinear model predictive control through contacts for quadrupeds. *IEEE Robotics and Automation Letters*, 3(3):1458–1465, July 2018.
- [145] M. Neunert, M. Stäuble, M. Gifftthaler, C. D. Bellicoso, J. Carius, C. Gehring, M. Hut-ter, and J. Buchli. Whole-body nonlinear model predictive control through contacts for quadrupeds. *IEEE Robotics and Automation Letters*, 3(3):1458–1465, July 2018.
- [146] Hai-Nguyen Nguyen, Sangyul Park, Junyoung Park, and Dongjun Lee. A novel robotic platform for aerial manipulation using quadrotors as rotating thrust generators. *IEEE Transactions on Robotics*, 34(2):353–369, 2018.
- [147] D. E. Orin, A. Goswami, and S. Lee. Centroidal dynamics of a humanoid robot. *Autonomous robots*, 35(2):161–176, 2013.
- [148] Jun Ota. Multi-agent robot systems as distributed autonomous systems. *Advanced Engineering Informatics*, 20(1):59 – 70, 2006.
- [149] D. Panagou, M. Turpin, and V. Kumar. Decentralized goal assignment and trajectory generation in multi-robot networks: A multiple lyapunov functions approach. In *2014 IEEE International Conference on Robotics and Automation (ICRA)*, pages 6757–6762. IEEE, 2014.
- [150] A. G. Pandala, Y. Ding, and H. Park. qpSWIFT: A real-time sparse quadratic program solver for robotic applications. *IEEE Robotics and Automation Letters*, 4(4):3355–3362, Oct 2019.
- [151] Abhishek Pandala, Randall T Fawcett, Ugo Rosolia, Aaron D Ames, and Kaveh Akbari Hamed. Robust predictive control for quadrupedal locomotion: Learning to close the gap between reduced-and full-order models. *IEEE Robotics and Automation Letters*, 7(3):6622–6629, 2022.
- [152] H.-W. Park, A. Ramezani, and J.W. Grizzle. A finite-state machine for accommodating unexpected large ground-height variations in bipedal robot walking. *Robotics, IEEE Transactions on*, 29(2):331–345, April 2013.
- [153] A. Patel, S. Shield, S. Kazi, A. M. Johnson, and L. T. Biegler. Contact-implicit trajectory optimization using orthogonal collocation. *arXiv preprint arXiv:1809.06436*, 2018.

- [154] Amir Patel, Stacey Leigh Shield, Saif Kazi, Aaron M Johnson, and Lorenz T Biegler. Contact-implicit trajectory optimization using orthogonal collocation. *IEEE Robotics and Automation Letters*, 4(2):2242–2249, 2019.
- [155] Guilherme AS Pereira, Mario FM Campos, and Vijay Kumar. Decentralized algorithms for multi-robot manipulation via caging. *The International Journal of Robotics Research*, 23(7-8):783–795, 2004.
- [156] Pedro O Pereira and Dimos V Dimarogonas. Collaborative transportation of a bar by two aerial vehicles with attitude inner loop and experimental validation. In *2017 IEEE 56th Annual Conference on Decision and Control (CDC)*, pages 1815–1820, 2017.
- [157] M. Posa, S. Kuindersma, and R. Tedrake. Optimization and stabilization of trajectories for constrained dynamical systems. In *2016 IEEE International Conference on Robotics and Automation (ICRA)*, pages 1366–1373, May 2016.
- [158] M. Posa, T. Koolen, and R. Tedrake. Balancing and step recovery capturability via sums-of-squares optimization. In *Robotics: Science and Systems*, 2017.
- [159] I. Poulakakis and J.W. Grizzle. The spring loaded inverted pendulum as the hybrid zero dynamics of an asymmetric hopper. *Automatic Control, IEEE Transactions on*, 54(8):1779–1793, Aug 2009.
- [160] Ioannis Poulakakis, Evangelos Papadopoulos, and Martin Buehler. On the stability of the passive dynamics of quadrupedal running with a bounding gait. *The International Journal of Robotics Research*, 25(7):669–687, 2006.
- [161] J. Pratt, C.-M. Chew, A. Torres, P. Dilworth, and G. Pratt. Virtual model control: An intuitive approach for bipedal locomotion. *The International Journal of Robotics Research*, 20(2):129–143, 2001.
- [162] J. Pratt, J. Carff, S. Drakunov, and A. Goswami. Capture point: A step toward humanoid push recovery. In *2006 6th IEEE-RAS International Conference on Humanoid Robots*, pages 200–207, Dec 2006.
- [163] J. Pratt, T. Koolen, T. de Boer, J. Rebula, S. Cotton, J. Carff, M. Johnson, and P. Neuhaus. Capturability-based analysis and control of legged locomotion, part 2: Application to M2V2, a lower-body humanoid. *The International Journal of Robotics Research*, 31(10):1117–1133, 2012.
- [164] Hartmut Prautzsch, Wolfgang Boehm, and Marco Paluszny. *Bézier and B-spline techniques*. Springer-Verlag, 2002.
- [165] Marc H Raibert. *Legged robots that balance*. MIT press, 1986.

- [166] A. Ramezani, J.W. Hurst, K. Akbai Hamed, and J.W. Grizzle. Performance analysis and feedback control of ATRIAS, a three-dimensional bipedal robot. *Journal of Dynamic Systems, Measurement, and Control* December, *ASME*, 136(2), December 2013.
- [167] Ghost Robotics. <https://www.ghostrobotics.io/>.
- [168] N. Sadati, G.A. Dumont, K. Akbari Hamed, and W.A. Gruver. Two-level control scheme for stabilisation of periodic orbits for planar monopodal running. *Control Theory Applications, IET*, 5(13):1528–1543, Sept 2011.
- [169] N. Sadati, G. A. Dumont, K. Akbari Hamed, and Gruver W. A. *Hybrid Control and Motion Planning of Dynamical Legged Locomotion*. Wiley-IEEE Press, October 2012.
- [170] C. O. Saglam and K. Byl. Quantifying the trade-offs between stability versus energy use for underactuated biped walking. In *Intelligent Robots and Systems, IEEE/RSJ International Conference on*, pages 2550–2557, Sept 2014.
- [171] C. O. Saglam and K. Byl. Meshing hybrid zero dynamics for rough terrain walking. In *2015 IEEE International Conference on Robotics and Automation (ICRA)*, pages 5718–5725, May 2015.
- [172] C.O. Saglam and K. Byl. Switching policies for metastable walking. In *Decision and Control, IEEE 52nd Annual Conference on*, pages 977–983, Dec 2013.
- [173] I. Saha, R. Ramaithitima, V. Kumar, G. J. Pappas, and S. A. Seshia. Implan: Scalable incremental motion planning for multi-robot systems. In *2016 ACM/IEEE 7th International Conference on Cyber-Physical Systems (ICCPS)*, pages 1–10, April 2016.
- [174] B. Schlotfeldt, D. Thakur, N. Atanasov, V. Kumar, and G. J. Pappas. Anytime planning for decentralized multirobot active information gathering. *IEEE Robotics and Automation Letters*, 3(2):1025–1032, April 2018.
- [175] Mohammad Shahbazi, Robert Babuška, and Gabriel AD Lopes. Unified modeling and control of walking and running on the spring-loaded inverted pendulum. *IEEE Transactions on Robotics*, 32(5):1178–1195, 2016.
- [176] A.S. Shiriaev, L.B. Freidovich, and S.V. Gusev. Transverse linearization for controlled mechanical systems with several passive degrees of freedom. *IEEE Transactions on Automatic Control*, 55(4):893–906, April 2010.
- [177] N. Smit-Anseeuw, R. Gleason, R. Vasudevan, and C. D. Remy. The energetic benefit of robotic gait selection-A case study on the robot RAMone. *IEEE Robotics and Automation Letters*, 2(2):1124–1131, April 2017.

- [178] J Spletzer, Aveek K Das, Rafael Fierro, Camillo J Taylor, Vijay Kumar, and James P Ostrowski. Cooperative localization and control for multi-robot manipulation. In *Proceedings 2001 IEEE/RSJ International Conference on Intelligent Robots and Systems. Expanding the Societal Role of Robotics in the the Next Millennium (Cat. No. 01CH37180)*, volume 2, pages 631–636, 2001.
- [179] M. W. Spong and F. Bullo. Controlled symmetries and passive walking. *IEEE Transactions on Automatic Control*, 50(7):1025–1031, July 2005.
- [180] M. W. Spong, J. K. Holm, and D. Lee. Passivity-based control of bipedal locomotion. *Robotics Automation Magazine, IEEE*, 14(2):30–40, June 2007.
- [181] Olaf Sporns and Gerald M. Edelman. Solving Bernstein’s Problem: A proposal for the development of coordinated movement by selection. *Child Development*, 64(4): 960–981, 1993.
- [182] K. Sreenath, H.-W. Park, I. Poulakakis, and J. W. Grizzle. Compliant hybrid zero dynamics controller for achieving stable, efficient and fast bipedal walking on MABEL. *The International Journal of Robotics Research*, 30(9):1170–1193, August 2011.
- [183] K. Sreenath, H.-W. Park, I. Poulakakis, and J.W. Grizzle. Embedding active force control within the compliant hybrid zero dynamics to achieve stable, fast running on MABEL. *The International Journal of Robotics Research*, 32(3):324–345, 2013.
- [184] Koushil Sreenath and Vijay Kumar. Dynamics, control and planning for cooperative manipulation of payloads suspended by cables from multiple quadrotor robots. In *Proceedings of Robotics: Science and Systems*, Berlin, Germany, June 2013.
- [185] B. Stellato, G. Banjac, P. Goulart, A. Bemporad, and S. Boyd. OSQP: an operator splitting solver for quadratic programs. *Mathematical Programming Computation*, 12(4):637–672, 2020.
- [186] D. E. Stewart and J. C. Trinkle. An implicit time-stepping scheme for rigid body dynamics with inelastic collisions and coulomb friction. *International Journal for Numerical Methods in Engineering*, 39(15):2673–2691, 1996.
- [187] Andrea Tagliabue, Mina Kamel, Roland Siegwart, and Juan Nieto. Robust collaborative object transportation using multiple mavs. *The International Journal of Robotics Research*, 38(9):1020–1044, 2019.
- [188] R. Tedrake, T.W. Zhang, and H.S. Seung. Stochastic policy gradient reinforcement learning on a simple 3D biped. In *Intelligent Robots and Systems. Proceedings 2004 IEEE/RSJ International Conference on*, volume 3, pages 2849–2854 vol.3, Sept 2004.
- [189] E. Todorov, T. Erez, and Y. Tassa. MuJoCo: A physics engine for model-based control. In *2012 IEEE/RSJ International Conference on Intelligent Robots and Systems*, pages 5026–5033, Oct 2012.

- [190] Marco Tranzatto, Takahiro Miki, Mihir Dharmadhikari, Lukas Bernreiter, Mihir Kulkarni, Frank Mascarich, Olov Andersson, Shehryar Khattak, Marco Hutter, Roland Siegwart, et al. Cerberus in the darpa subterranean challenge. *Science Robotics*, 7(66): eabp9742, 2022.
- [191] E. Tuci, M. H. M. Alkilabi, and O. Akanyeti. Cooperative object transport in multi-robot systems: A review of the state-of-the-art. *Frontiers in Robotics and AI*, 5:59, 2018.
- [192] M. Turpin, N. Michael, and V. Kumar. Trajectory planning and assignment in multi-robot systems. In *Workshop on the Algorithmic Foundations of Robotics*, Boston, MA, June 2012.
- [193] Matthew Turpin, Nathan Michael, and Vijay Kumar. Capt: Concurrent assignment and planning of trajectories for multiple robots. *The International Journal of Robotics Research*, 33(1):98–112, 2014.
- [194] Unitree. <http://www.unitree.cc/>.
- [195] J.G. VanAntwerp and R.D. Braatz. A tutorial on linear and bilinear matrix inequalities. *Journal of Process Control*, 10(4):363–385, August 2000.
- [196] S. Veer, Rakesh, and I. Poulakakis. Input-to-state stability of periodic orbits of systems with impulse effects via Poincaré analysis. *IEEE Transactions on Automatic Control*, 64(11):4583–4598, Nov 2019.
- [197] Octavio Villarreal, Victor Barasuol, Patrick Wensing, and Claudio Semini. MPC-based controller with terrain insight for dynamic legged locomotion. *arXiv preprint arXiv:1909.13842*, 2019.
- [198] Octavio Villarreal, Victor Barasuol, Patrick M Wensing, Darwin G Caldwell, and Claudio Semini. MPC-based controller with terrain insight for dynamic legged locomotion. In *2020 IEEE International Conference on Robotics and Automation (ICRA)*, pages 2436–2442, 2020.
- [199] M. Vukobratović, B. Borovac, and D. Surla. *Dynamics of Biped Locomotion*. Springer, 1990.
- [200] A. Wächter and L. T. Biegler. On the implementation of an interior-point filter line-search algorithm for large-scale nonlinear programming. *Mathematical programming*, 106(1):25–57, 2006.
- [201] Y. Wang and S. Boyd. Fast model predictive control using online optimization. *IEEE Transactions on Control Systems Technology*, 18(2):267–278, March 2010.

- [202] Jad Wehbeh, Shatil Rahman, and Inna Sharf. Distributed model predictive control for uavs collaborative payload transport. In *2020 IEEE/RSJ International Conference on Intelligent Robots and Systems (IROS)*, pages 11666–11672, 2020.
- [203] P. M. Wensing, A. Wang, S. Seok, D. Otten, J. Lang, and S. Kim. Proprioceptive actuator design in the MIT Cheetah: Impact mitigation and high-bandwidth physical interaction for dynamic legged robots. *IEEE Transactions on Robotics*, 33(3):509–522, June 2017.
- [204] Patrick M Wensing and David E Orin. Improved computation of the humanoid centroidal dynamics and application for whole-body control. *International Journal of Humanoid Robotics*, 13(01):1550039, 2016.
- [205] E. R. Westervelt, J. W. Grizzle, and D. E. Koditschek. Hybrid zero dynamics of planar biped walkers. *IEEE Transactions on Automatic Control*, 48(1):42–56, Jan 2003.
- [206] E. R. Westervelt, J. W. Grizzle, C. Chevallereau, J. H. Choi, and B. Morris. *Feedback Control of Dynamic Bipedal Robot Locomotion*. Taylor & Francis/CRC, 2007.
- [207] David Williams and Oussama Khatib. The virtual linkage: A model for internal forces in multi-grasp manipulation. In *1993 Proceedings IEEE International Conference on Robotics and Automation*, pages 1025–1030, 1993.
- [208] A. W. Winkler, F. Farshidian, D. Pardo, M. Neunert, and J. Buchli. Fast trajectory optimization for legged robots using vertex-based ZMP constraints. *IEEE Robotics and Automation Letters*, 2(4):2201–2208, Oct 2017.
- [209] Z. Yan, N. Jouandeau, and A. A. Cherif. A survey and analysis of multi-robot coordination. *International Journal of Advanced Robotic Systems*, 10(12):399, 2013.
- [210] Chenyu Yang, Guo Ning Sue, Zhongyu Li, Lizhi Yang, Haotian Shen, Yufeng Chi, Akshara Rai, Jun Zeng, and Koushil Sreenath. Collaborative navigation and manipulation of a cable-towed load by multiple quadrupedal robots. *arXiv preprint arXiv:2206.14424*, 2022.
- [211] Hyunsoo Yang and Dongjun Lee. Hierarchical cooperative control framework of multiple quadrotor-manipulator systems. In *2015 IEEE international conference on robotics and automation (ICRA)*, pages 4656–4662, 2015.
- [212] H. Ye, A. N. Michel, and L. Hou. Stability theory for hybrid dynamical systems. *Automatic Control, IEEE Transactions on*, 43(4):461–474, Apr 1998.
- [213] H. Zhao, J. Horn, J. Reher, V. Paredes, and A. D. Ames. Multicontact locomotion on transfemoral prostheses via hybrid system models and optimization-based control. *IEEE Transactions on Automation Science and Engineering*, 13(2):502–513, 2016.

- [214] Huihua Zhao, Jonathan Horn, Jacob Reher, Victor Paredes, and Aaron D Ames. First steps toward translating robotic walking to prostheses: a nonlinear optimization based control approach. *Autonomous Robots*, pages 1–18, 2016.
- [215] K. Zhou and J. C. Doyle. *Essentials of Robust Control*. Prentice Hall, October 1997.
- [216] K. Zhou, K. Glover, B. Bodenheimer, and J. Doyle. Mixed \mathcal{H}_2 and \mathcal{H}_∞ performance objectives I: Robust performance analysis. *IEEE Transactions on Automatic Control*, 39(8):1564–1574, Aug 1994.